SYNTHESIS AND CHARACTERIZATION OF NANOSIZED HYBRID POLYMER MODIFIER (HPM) FOR IMPROVED MECHANICAL AND THERMAL BEHAVIOUR OF COMPOSITES

By

DILLI RAM DHAKAL

Bachelor of Science in Physics
Tribhuvan University
Kathmandu, Nepal
2007

Master of Science in Physics
Tribhuvan University
Kathmandu, Nepal
2012

Master of Science in Materials Science and Engineering
Oklahoma State University
Stillwater, OK
2018

Submitted to the Faculty of the
Graduate College of the
Oklahoma State University
in partial fulfillment of
the requirements for
the Degree of
DOCTOR OF PHILOSOPHY
May, 2022

SYNTHESIS AND CHARACTERIZATION OF NANOSIZED HYBRID POLYMER MODIFIER (HPM) FOR IMPROVED MECHANICAL AND THERMAL BEHAVIOUR OF COMPOSITES

Dissertation Approved:

Dr. Ranji Vaidyanathan

Dissertation Adviser

Dr. Raman P. Singh

Dr. Do Young Kim

Dr. Frank D. Blum

ACKNOWLEDGEMENTS

First and foremost, I would like to express my sincere gratitude to my Ph.D. advisor, Prof. Ranji Vaidyanathan, for his continuous support of my whole Ph.D. study. A patient guide, his inspiration, encouragement, and direction to allow me to develop into the independent thinker and researcher I am today. His remarkable ideas lead me into the field of composite materials. I am truly indebted to him for helping me in my professional development. Besides my advisor, I would like to thank the rest of my Ph.D. committee members, Prof. Raman Singh, Prof. Do Young Kim, and Prof. Frank D Blum, for their time and insightful comments. Especially, I am indebted to Dr. Bhishma Sedai for his advice, support, encouragement, and motivation. In the same regard, my lab coworkers, Mr. Pralhad Lamichhane, Mr. Siddhesh Chaudari, and Mr. Ishan N. Jayalath have been integral to my success. I also would like to thank Mr. Seduraman Mathiravedu, and Mrs. Lynsey Baxter for their help. A special thanks goes to Prof. Kaan kalkan and Mr. Nishan Khatri for helping me with Raman spectroscopy. I want to acknowledge the funding support from MITO Material Solutions via National Science Foundation SBIR grant # 1926906 and Oklahoma Center for Advancement of Science and Technology Oklahoma Applied Research Support program grant # AR19-011 for the financial support during the completion of this project. I am thankful to the School of Material Science and Engineering at Oklahoma State University for providing this great opportunity.

Most importantly, I would like to thank my parents, other family members, and friends for their love and encouragement, and most of all for my loving, supportive, encouraging, and motivating wife, Ishwori Kafle Dhakal, and daughter, Sayana Dhakal, whose unconditional support, and strength during my Ph.D. study is so appreciated.

Name: DILLI RAM DHAKAL

Date of Degree: MAY, 2022

Title of Study: SYNTHESIS AND CHARACTERIZATION OF NANOSIZED HYBRID POLYMER MODIFIER (HPM) FOR IMPROVED MECHANICAL AND THERMAL BEHAVIOUR OF COMPOSITES

Major Field: MATERIALS SCIENCE AND ENGINEERING

Abstract: Lightweight carbon fiber-reinforced polymer composites are replacing metallic components in the aerospace and automotive industries due to their improved strength-to-weight ratios and fatigue resistance. Despite their attractive properties, these composites, however, crack and delaminate due to low-velocity impact causing a drastic drop in their mechanical properties. Some of the approaches evaluated to overcome these issues include surface modification of the carbon fibers and the addition of nanoparticles such as graphene, graphene oxide etc. The addition of these nanoparticles shows improved resistance to crack propagation and reduced delamination in these composites. One carbon-based nano-additive additive, graphene oxide (GO), can achieve excellent dispersion with organic solvents in polymer matrices due to the presence of specific functional groups compatible with most composite matrix systems. However, the presence of oxygen within these functional groups makes GO moisture sensitive and results in the loss of several vital properties such as electrical conductivity and mechanical properties compared to pristine graphene. Prior research from our group has demonstrated successful grafting of GO with other molecules such as polyhedral oligomeric silsesquioxane (POSS) to optimize the thermal stability of GO. Due to the robust cage-like structure of POSS, dispersion of these hybrid nanoparticles within polymer matrices could result in an overall enhancement in the mechanical as well as thermal behavior of the composite materials. In this work, a hybrid polymer modifier (HPM) has been developed by hybridizing methacryl polyhedral oligomeric silsesquioxanes (MAPOSS) to GO via a facile redox reaction system with cerium (IV) ammonium nitrate/nitric acid (Ce(IV)/HNO_3) and GO sheets' hydroxyl groups as the redox couple, and characterized with different characterization techniques. XRF analysis showed that 10.2 mass% of silicon was added to GO due to the MAPOSS grafting. Furthermore, Raman analysis confirmed the increased structural distortion of GO induced by the incorporation of MAPOSS ($(I_D/I_G)_{HPM}$ = 1.43, $(I_D/I_G)_{GO}$ = 1.30).The dispersion of HPM was studied in thermoset resin system Epoxy and presented. In addition, the effect of HPM on polymer and carbon fiber reinforced polymer composite were studied. The result confirmed that the addition of HPM at very low wt.% can enhance the viscoelastic, mechanical, and thermal properties of composites.

TABLE OF CONTENTS

Chapter Page

Chapter Page

LIST OF TABLES

LIST OF FIGURES

Figure Page

Figure Page

Figure Page

CHAPTER I

INTRODUCTION

Lightweight carbon fiber-reinforced polymer composites are replacing metallic components in the aerospace and automotive industries due to their improved strength-to-weight ratios and fatigue resistance. Despite their attractive properties, these composites, however, crack and delaminate due to low-velocity impact causing a drastic drop in their mechanical properties. Some of the approaches evaluated to overcome these issues include surface modification of the carbon fibers and the addition of nanoparticles such as carbon-based nanomaterials (graphene, graphene oxide, carbon nanotubes, etc.). The addition of these nanoparticles shows improved resistance to crack propagation and reduced delamination in these composites. One carbon-based nano-additive additive, graphene oxide (GO), can achieve excellent dispersion with organic solvents in polymer matrices due to the presence of specific functional groups compatible with most composite matrix systems. However, the presence of oxygen within these functional groups makes GO moisture sensitive and results in the loss of several vital properties such as electrical conductivity and mechanical properties compared to pristine graphene. Prior research from our group has demonstrated successful grafting of GO with other

molecules such as polyhedral oligomeric silsesquioxane (POSS) to optimize the thermal stability of GO. Due to the robust cage-like structure of POSS, dispersion of these hybrid nanoparticles within polymer matrices could result in an overall enhancement in the mechanical as well as thermal behavior of the composite materials. In this chapter, the modification and incorporation of GO/POSS hybrid nanoparticles in polymer matrix composites, the degree of enhancement of mechanical properties, and potential challenges are summarized. Based on the review of past research and results, specific challenges have been identified, and a series of hypotheses on which further research work could be based are stated.

1.1 Background and Classification

New aerospace platforms such as the Boeing Dreamliner, Airbus (B787, A380, and A350 platforms), and new jetfighters (F-35, F-22) require materials with a high strength to weight ratio [1]. For example, almost 50% of the Boeing Dreamliner is manufactured out of carbon fiber-reinforced composite materials [2]. When this aircraft was introduced in 2008, Boeing claimed that it would lead to a 32% savings in maintenance costs and 20% less fuel compared to comparable aircraft [2]. In the automobile industry, the current push for zero emissions (electric vehicles) or reduced weight components used in the Toyota Siena, Ford, Volkswagen liftgate, and BMW MX-3 require composites that can reduce the automobile's overall weight while also reducing the fuel consumption [3]. However, the exact weight savings due to composites or fuel savings in automobiles is still a matter of research. In the case of airframes, it has been shown that using composites in place of aluminum can save up to 19% weight [4]. A similar need for composites in wind energy [5] can be observed, although this review focuses on composites used in the aerospace and automotive industries.

Nature is full of composites; wood and bone are well-known natural composites [4]. Prehistoric people mixed small, chopped straws with mud, increasing the strength and toughness of mud walls that allowed the mud blocks to resist crack propagation. This fundamental idea of composites has led to high-strength lightweight components for the aerospace, wind energy, and automobile industries. Composites are made of two or more components: the matrix, the reinforcement, and the interface. In general, each part of the composite material is combined in a way that the synergetic properties are more beneficial than the individual components. The matrix and reinforcement material will depend on the application. Based on the matrix material, composites are classified into the following four broad categories [5]:

- Polymer Matrix Composites
- Carbon Matrix Composites
- Metal Matrix Composites
- Ceramic Matrix Composites

In this work, polymer matrix composites and reinforcement techniques are the primary focus. An overview of the classification of engineered composite materials is presented in the chart below:

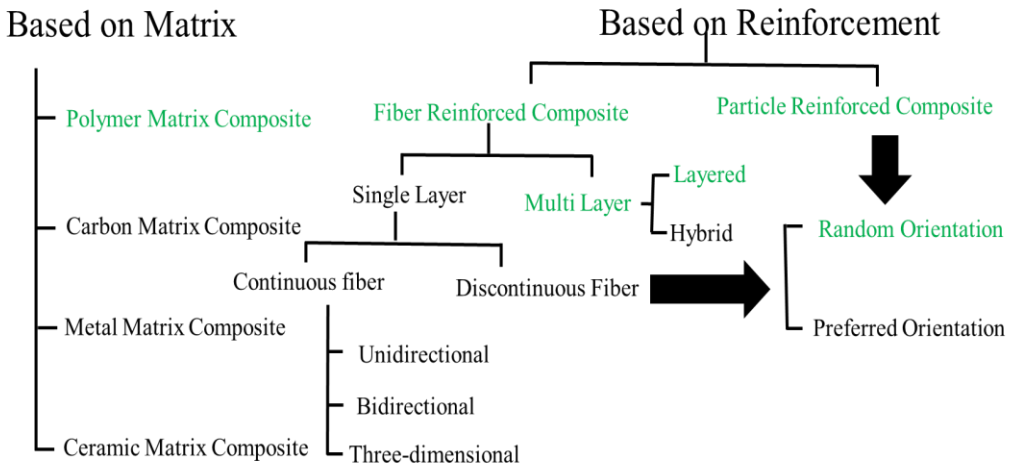

Fig. 1.1. Engineered Composite Material Classification [5].

1.2 Composites Market

The following is a brief discussion of the composites market, which shows the current state, growth possibility, and industrial importance. The composites market is projected to

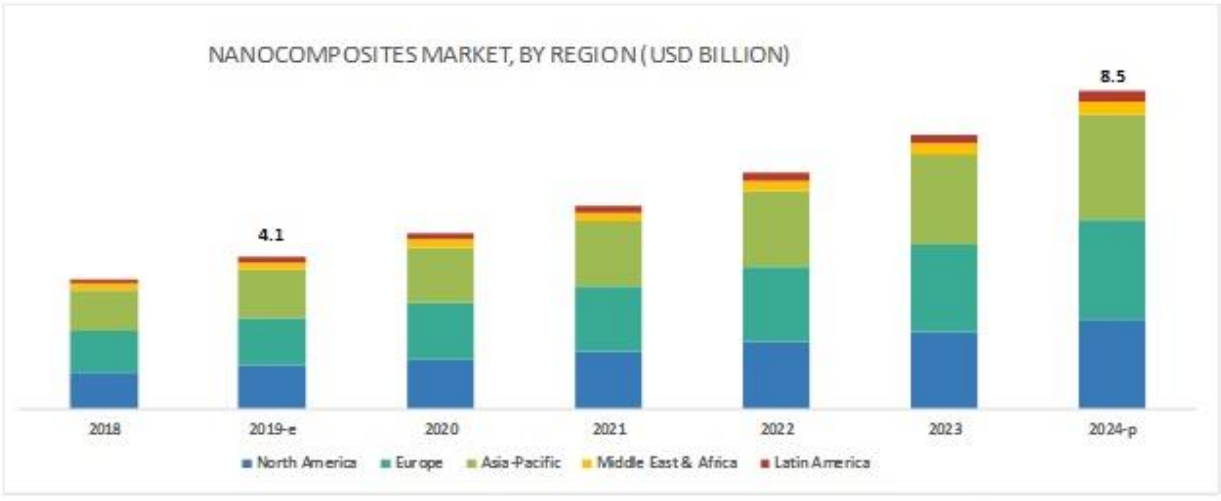

Fig. 1.2: Nanocomposite market by region [6].

grow to $ 112.8 billion by 2025 and is projected to have a compounded annual growth rate (CAGR) of 8.8% between 2020 and 2025 [6]. An analyst from Grand View Research reported that the Global composite market size is projected to grow to $ 160.54 billion by 2027 at a CAGR of 7.6% [7].

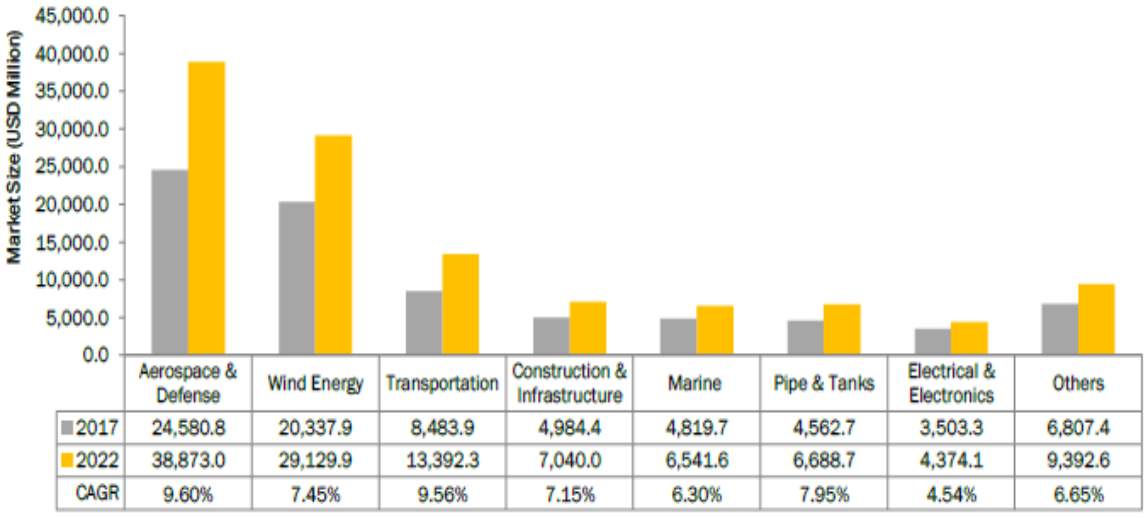

	Aerospace & Defense	Wind Energy	Transportation	Construction & Infrastructure	Marine	Pipe & Tanks	Electrical & Electronics	Others
2017	24,580.8	20,337.9	8,483.9	4,984.4	4,819.7	4,562.7	3,503.3	6,807.4
2022	38,873.0	29,129.9	13,392.3	7,040.0	6,541.6	6,688.7	4,374.1	9,392.6
CAGR	9.60%	7.45%	9.56%	7.15%	6.30%	7.95%	4.54%	6.65%

Fig. 1.3: Composite market analysis based on different industries [7].

Another report on the nanocomposite market showed a high demand for nanocomposites from the packaging, aerospace & defense, automotive, and electronics & semiconductor industries. The nanocomposite market is expected to grow from $4.1 billion in 2019 to $8.5 billion by 2024 at a CAGR of 16%, as shown in Figure 1.2[8]. A variety of reinforcement fibers (glass, carbon, natural, basalt, and aramid) and polymer matrices (thermoset and thermoplastic) are used in composites depending on the industry: aerospace & defense, transportation, wind energy, marine, pipe & tanks, and sporting goods. Figure 1.3, from MarketsandMarkets, shows the potential market size by end-use areas for composites, with aerospace and defense being the fastest growing segments [9].

1.3 Polymer Matrix Composites

Based on the resin used, polymer matrix composites can be divided into thermoset composites and thermoplastic composites. Thermoset composites have a more comprehensive range of applications than thermoplastic composites, as the former are more resistant to heat transfer. Thus, they have more uses in transportation, aerospace & defense applications that require heat-resistant materials. Thermoset composites are manufactured using thermoset resins such as epoxy, polyester, vinyl ester resins, and polyurethane, as well as specialty resins such as polyimides and bismaleimides [4].

Various nano-additives or nanomaterials are used to improve the toughness of polymer composites. The new class of materials created as a result of introducing nano-additives into polymer composites is typically described as polymer nanocomposites. However, a major issue with polymer nanocomposites is the agglomeration of the nanoparticles [10], as they can act as stress raisers, or areas of stress concentration, acting as crack initiators and causing failure of the composite. In the case of carbon nanofillers, the π-π interaction is usually the cause of agglomeration. Graphene sheets are also susceptible to restacking and aggregation. Though the single-layer graphene can be produced, it is not easy to retain the single-layer state once it has been dispersed in the polymer matrix.

1.4 Fiber-reinforced Polymer Composites:

Classification of fiber-reinforced composites are illustrated below in Figure 1.4:

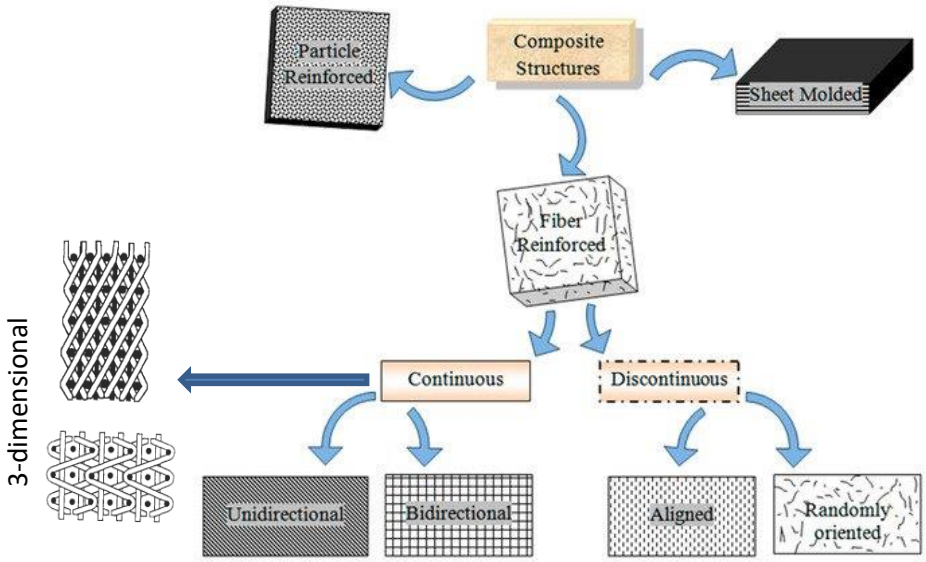

Fig. 1.4. Classification of fiber-reinforced composites [11].

There are several types of reinforcement classifications based on fiber orientation, as shown above in Figure 1.4. These can be listed as continuous unidirectional, continuous bidirectional, continuous 3-dimensional, discontinuous aligned, or discontinuous randomly oriented. The fiber reinforcement effectively affects the crack-bridging mechanisms in a composite material, improving the toughness and overall composite performance. Another challenge in fiber-reinforced polymer composites is the mismatch in the thermal expansion coefficient between the fiber and the matrix, which could introduce micro-cracks while the composites are cooling down after curing. It is also desirable to have tailored chemical or physical entanglement in the fiber matrix interfacial area because it could lead to better fiber-matrix bonding and toughening in composites.

1.5 Polyhedral Oligomeric Silsesquioxane (POSS) and its Importance in Polymer Composites

Polyhedral oligomeric silsesquioxane or POSS is a special type of nanomaterial that Dr. Joseph Lichtenhan, and coworkers developed while he was at the Materials and Manufacturing Directorate at the Air Force Research Laboratory at Edwards Air Force Base, CA [12]. He subsequently started Hybrid Plastics in Hattiesburg, MS, to develop applications for POSS in the composites industry. POSS is a class of molecule that has a unique silicon cage with eight organic moieties that have both organic and inorganic features. It has a nanosized cage structure comparable to polymeric segments with empirical formula $R_n(SiO1.5)_n$, where R represents organic functional groups like alkyl, alkylene, acrylate, or epoxide, etc. [13-15]. This is shown in Figure 1.5. Due to its organic and inorganic structure, it is compatible with a number of composite resin systems. The siloxane (Si-O-Si) moiety imparts thermal stability, chemical resistance, rigidity, and flame

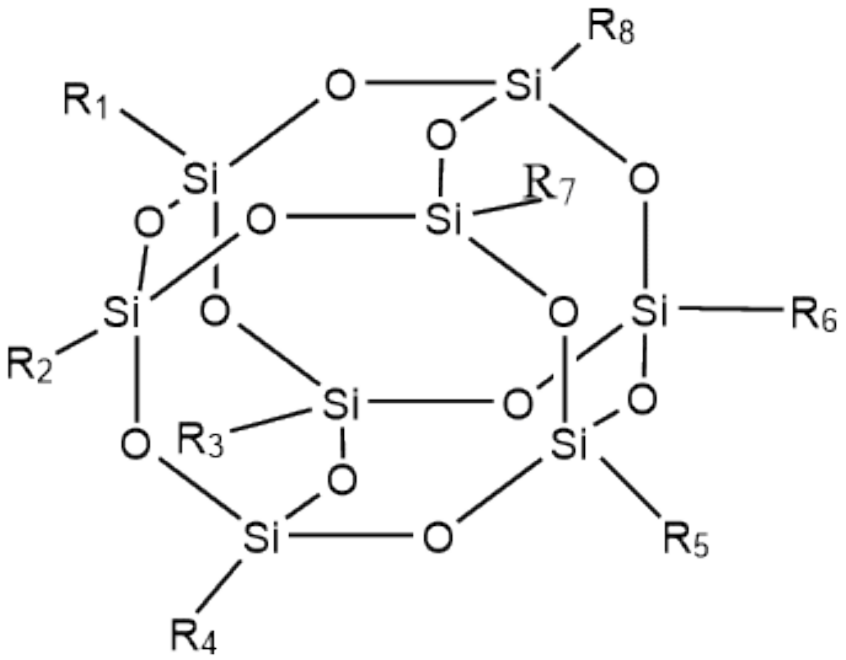

Fig. 1.5: POSS Structure.

retardant properties to POSS and, therefore, to the matrix resin it is added to. The organic groups can be either inert or reactive. They impart reactivity, processability, and ductility to POSS. POSS can have a wide range of properties based on the attached organic group. POSS can be blended into a polymer matrix by either chemical or physical mixing. Additionally, the organic groups attached to the Si cage can be modified with different substituents leading to better solubility in common solvents [13, 16]. Therefore, a range of properties can be introduced to POSS by altering the organic groups. It has been used for various polymer composite applications due to its hybrid nature [17-19].

1.6 Carbon-Based Nanomaterials

The natural state of graphene is in the form of a stack of multiple sheets, held together by van der Waals attraction. Graphene-based products are available in different forms: graphene, graphene oxide (GO), reduced graphene oxide (rGO), and monolayer graphene. The structure of graphene and GO is shown in Figure 1.6.

The properties of graphene are influenced by the number of layers and their functionality. However, the applications of graphene are limited due to the difficulty of dispersing graphene in solvents. This issue is directly related to the van der Waals interaction and π- π stacking between graphene sheets [20, 21].

Graphene oxide (GO), obtained from the oxidation and exfoliation of graphite, contains oxygen-containing carbonyl, hydroxyl, and epoxy functional groups. The presence of a functional group imparts several advantages to GO over pristine graphenes, such as 1) flexibility of further modification, 2) excellent dispersion in polymer matrices and solvents, and 3) excellent interfacial interaction between the functional groups and the polymer matrix. However, GO has poor thermal stability and electrical conductivity compared to graphene [22, 23]. Several studies have been reported related to the recovery of these properties [24]. However, the steps to recover these properties were found to be expensive and time-consuming. The general structure of graphene and graphene oxide are illustrated in figure 1.6.

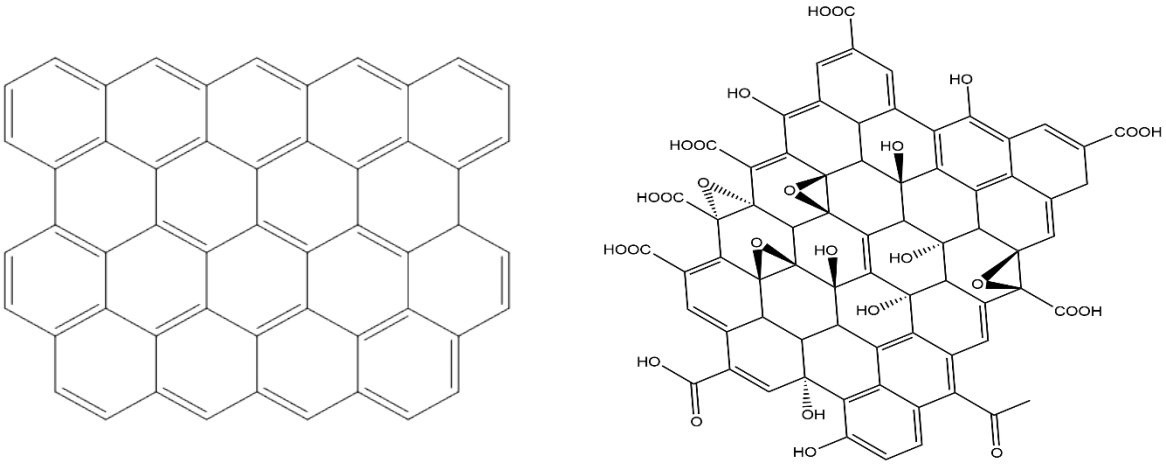

Fig. 1.6: Structure of graphene and graphene oxide.

1.7 Redox free radical polymerization:

Producing polymers with minimal energy consumption is one of the major challenges in the polymer industry [25]. Fortunately, in the 1940's, researchers from Germany and Great Britain discovered a redox initiation reaction with the capability to accelerate the process in polymerization at low temperatures (usually < 100 °C) with low energy consumption (

usually < 80 KJ/mol) [25, 26]. At present, about 50% of polymers and synthetic rubbers are manufactured via the free radical polymerization process. Hence, chain growth free radical polymerizations (FRP) have always been a significant interest in the polymer research community.

In a redox reaction, mixing the reducing agent with oxidizing agent leads to redox polymerization. In this process, a reactive species is generated, allowing polymer chain growth. A typical redox-free radical reaction involves three significant steps: initiation, propagation, and termination. Initiation consists of the generation of free radicals by the electron transfer mechanism. In propagation, free radical attracts the available double bonds leading to chain growth. In the termination step, the chain growing process is halted by three different mechanisms - first is termination by coupling with other radicals, known as mutual termination, the second is termination due to coupling with free radical, known as oxidative termination, and the last is disproportionation and chain transfer reaction where a species simultaneously redox and oxidized, yielding two different products.

The redox reaction can be operated in an aqueous solution at a mild temperature with low energy consumption and "greener" compared to other chemical reactions. It is widely accepted in the hybrid polymerization process. Past research has shown that the hydroxyl groups on GO surface serve as great reducing agents if coupled with Ce(IV) salts to initiate the polymerization [27]. The reaction scheme of those research groups is presented in Figure 1.7.

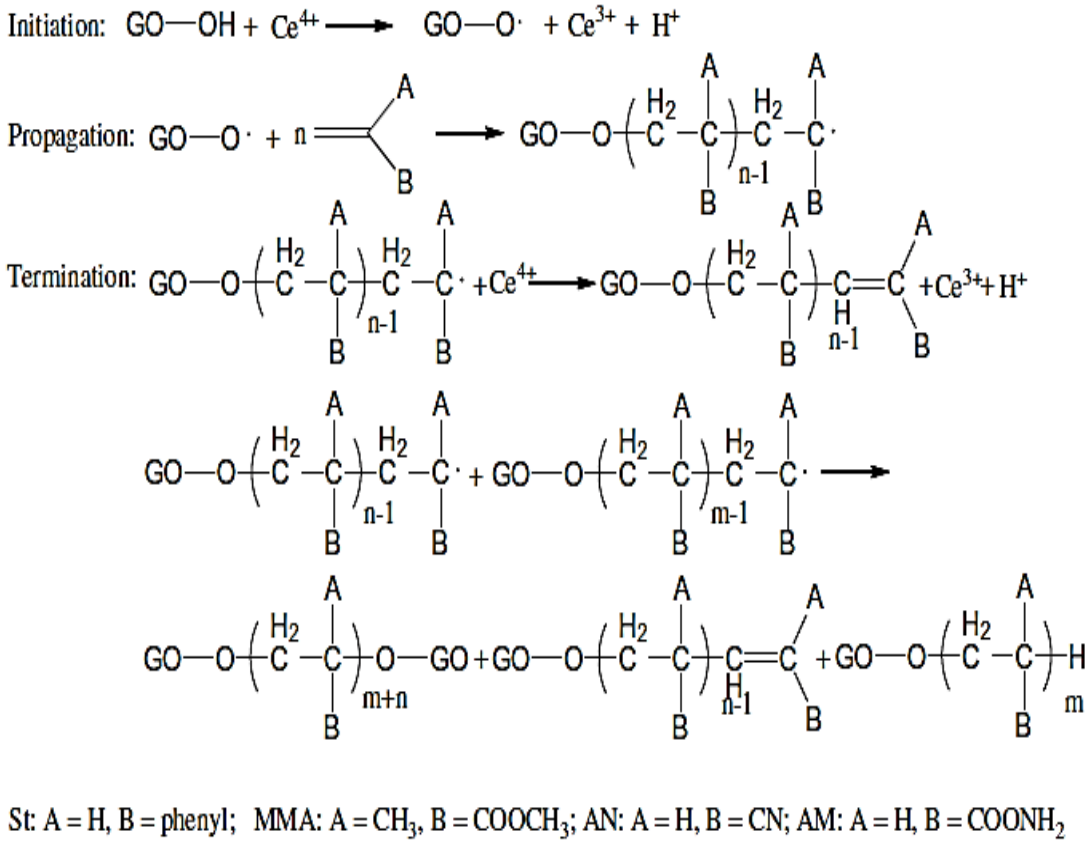

Fig. 1.7: Polymerization mechanism of monomers on the surface of GO using a Ce (IV) redox free radical initiation system [27].

1.8 Literature Review

Hybridizing GO by grafting with other functional groups has been found to reduce the agglomeration of GO and improve its dispersion. The presence of a hydrophilic functional group causes GO to more effectively disperse in polar solvents, opening the platform for chemical modification with higher possibilities of new materials with excellent properties [21, 28-31].

The presence of functional groups in GO imparts several advantages to graphene. Several studies have reported improved quasi-static [25], fatigue [26], and electrical properties [27] for graphene-based polymer composites. Some of these studies have concluded that GO is the most effective form of graphene for composite reinforcement and scale-up [32-36].

The most common synthesis methods of GO-based hybrid nano-materials are in situ polymerization [37, 38], hydrothermal method [39, 40], electrochemical co-deposition [41], microwave-assisted method [42, 43], vacuum impregnation [44] and sol-gel technique [45]. GO serves as either a functional component or substrate in a GO-based composite [46, 47]. Of all the above methods, in situ polymerization is more controllable, scalable, and effective in grafting monomers to GO and rGO. This method is also more common for scaled-up hybrid GO nanocomposite production without chain destruction [21, 48]. The “wrinkled” surface of reduced graphene is often considered to be a favorable medium for creating a robust interface that can interlock with the matrix. The atomically smooth surface has been shown to have low interfacial strength in strain-dependent Raman spectroscopy measurements [24].

Furthermore, restacking the sheets after chemical or thermal reduction demonstrates poor dispersion in solvents used in polymer processing, which could result in agglomeration, similar to CNT composites. However, the latter concern has been partially alleviated using surfactants or polymer blending before reduction [24]. The functional groups (epoxide, hydroxyl, carboxyl, and carbonyl) present on the basal planes and edges of GO facilitate dispersion in water or protic solvents. Moreover, the groups may further improve matrix affinity and allow for additional surface chemistry tailoring if desired. GO is preferred over other expensive fillers, like CNT, due to its larger aspect ratio and extraordinary mechanical and thermal properties [49-52].

Mishra et al. studied the effects of different types of POSS in epoxy resins. They investigated fracture toughness of epoxy composites as a function of POSS loading for

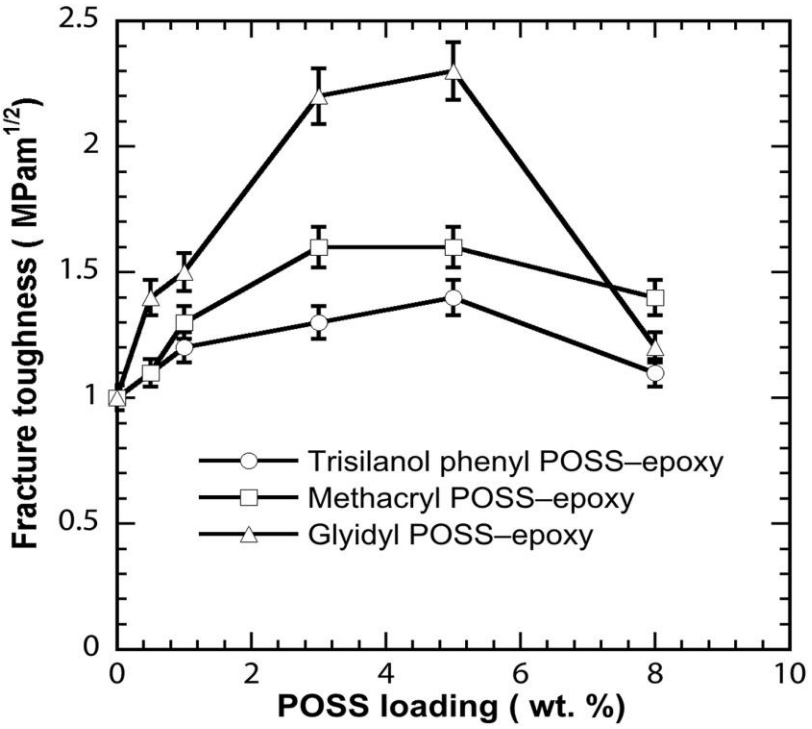

Fig. 1.8: K_{ic} for different loading of POSS of different functional groups [53].

trisilanol poss-epoxy, methacryl poss-epoxy, and glycidyl POSS. Their study (Figure 1.8) showed that the fracture toughness in terms of critical stress intensity factor (K_{ic}) improved (at 5%wt loading) by 230%, 160%, and 130% due to the presence of glycidyl, methacryl, and trisilanol POSS, respectively [53]. Figure 1.9 shows the flexural strength of these composites

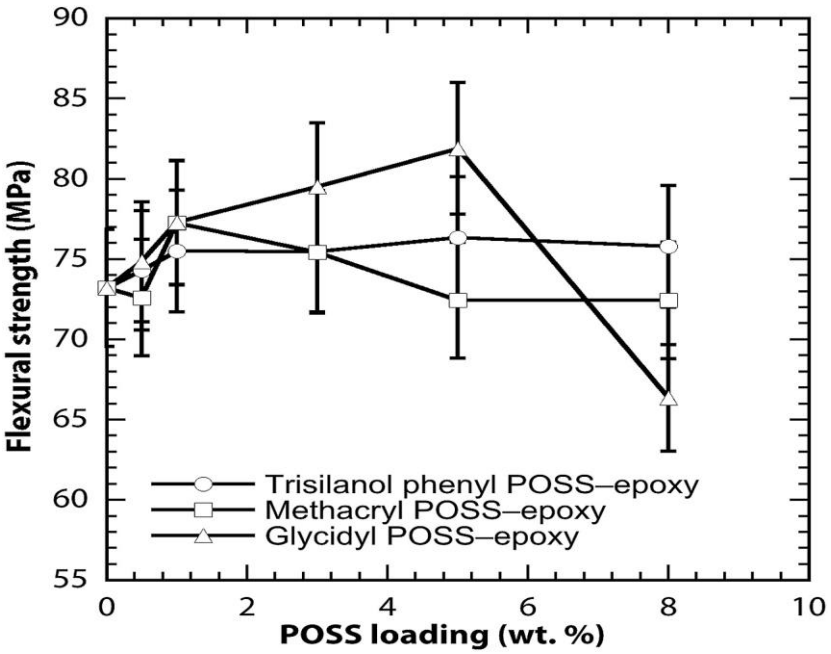

Fig. 1.9: Flexural strength of POSS–epoxy nanocomposites with different POSS content [53].

as a function of the POSS content. It was observed that the flexural strength was maximized for glycidyl POSS, whereas the other two POSS molecules did not show any significant change in the flexural strength.

Ahmadi-Moghadam, B. and F. Taheri studied the effect of a different form of carbon-based nano additives (GO), (GNP), Amino functionalized GNP (G-NH_2), and silane functionalized GNP (G-Si)) for the interlaminar fracture toughness (Mode I, Mode II, and Mode III) of glass/epoxy composites. The result, presented in Figure 1.10, showed remarkable improvement in Mode I fracture toughness with functionalized GNP [54].

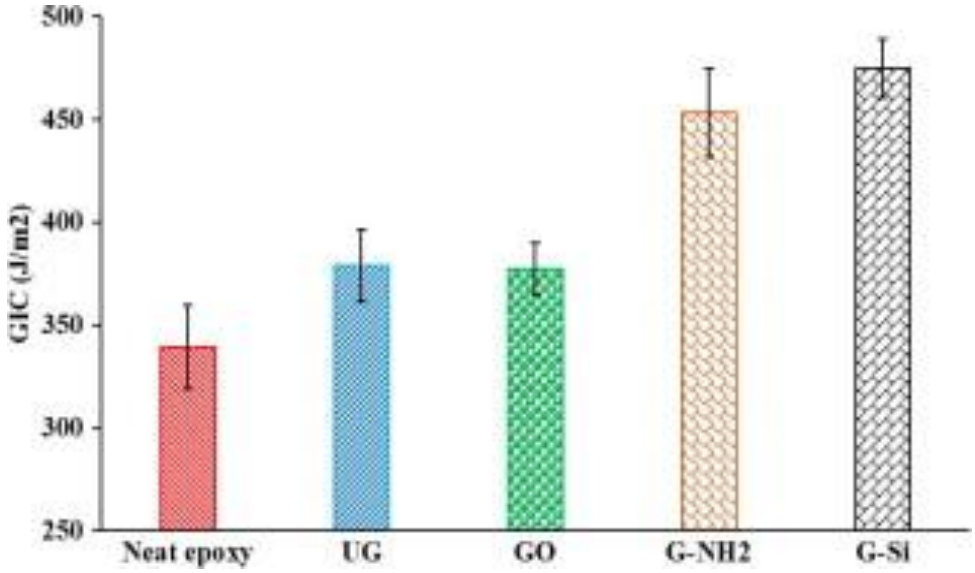

Fig. 1.10: Mode I critical energy release rates of FRP plates adhered by the neat resin and various GNP-reinforced resins [54].

Zhu, Imam, et al. claimed that the addition of carbon-nano tube (CNT) as nano additives traps free radicals, leading to reduced interaction between fiber and matrix, hence the mechanical properties [55]. In the same study, they added a nanotube with an extra initiator to promote the local interaction, and the result showed the improvement in shear strength up to 45% at 0.1% loading (Figure 1.11). From their work, it can be inferred that the interaction between fiber, matrix, and nano additives is crucial for improvement in mechanical properties.

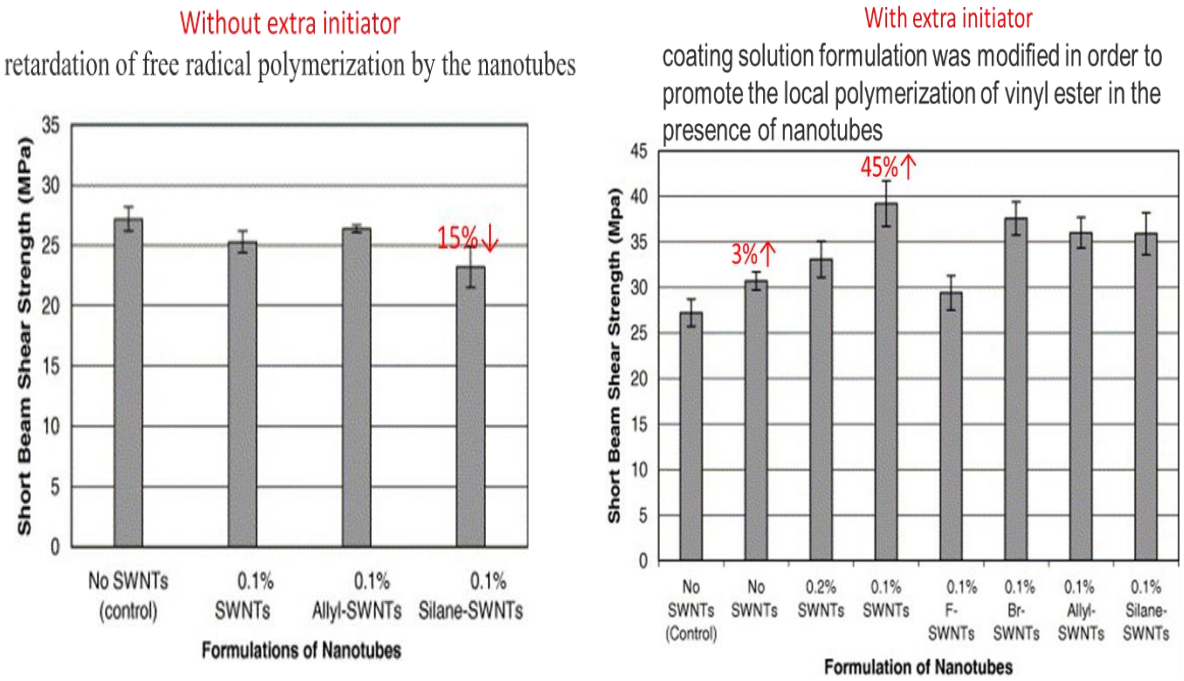

Fig. 1.11: Effect of different forms of carbon-nano tubes with and without extra initiator [55].

Degirmenci M. et al. investigated a novel method effective in the photopolymerization of vinyl monomers using GO. Their study showed that the ceric-ion-photo initiator redox method is highly effective in synthesizing photoinitiator functionality polymers [56]. A similar study published by Wang B. et al. reported a convenient redox polymerization method for covalent grafting of poly(N-isopropyl acrylamide) and poly (acrylic acid) on the GO surface. The polymerization reaction was initiated by an aqueous cerium ammonium nitrate solution at moderate temperatures (room temperature to 80 °C). The effectiveness of polymerization was based on the formation of redox centers on GO upon reaction with cerium ammonium nitrate [57]. Another study by Ma L. et al. described the synthesis and characterization of polymer grafted GO sheets using a Ce (IV)/HNO_3 redox system. Their study concluded that the regular and periodic structure of GO disappears by the redox system, yielding a thoroughly exfoliated structure [27]. They reported a 99% grafting ratio of polystyrene on GO via Ce (IV)/HNO3 redox system, as shown in Figure 1.12.

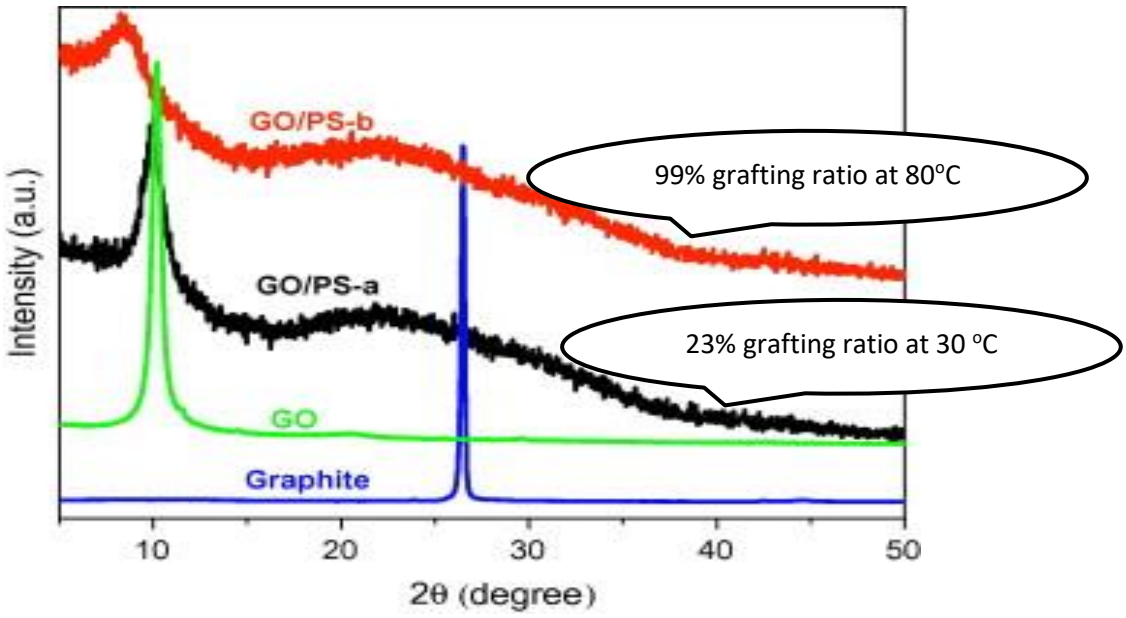

Fig. 1.12: XRD curves of graphite, GO and GO/polystyrene composites [27].

Xue Y. et al. reported chemical grafting of amine-functionalized POSS to graphene oxide (GO) [58]. Their results suggested that POSS-g-GO is soluble in many organic solvents, enabling it to be used in several composite systems. In addition, the use of POSS-g-

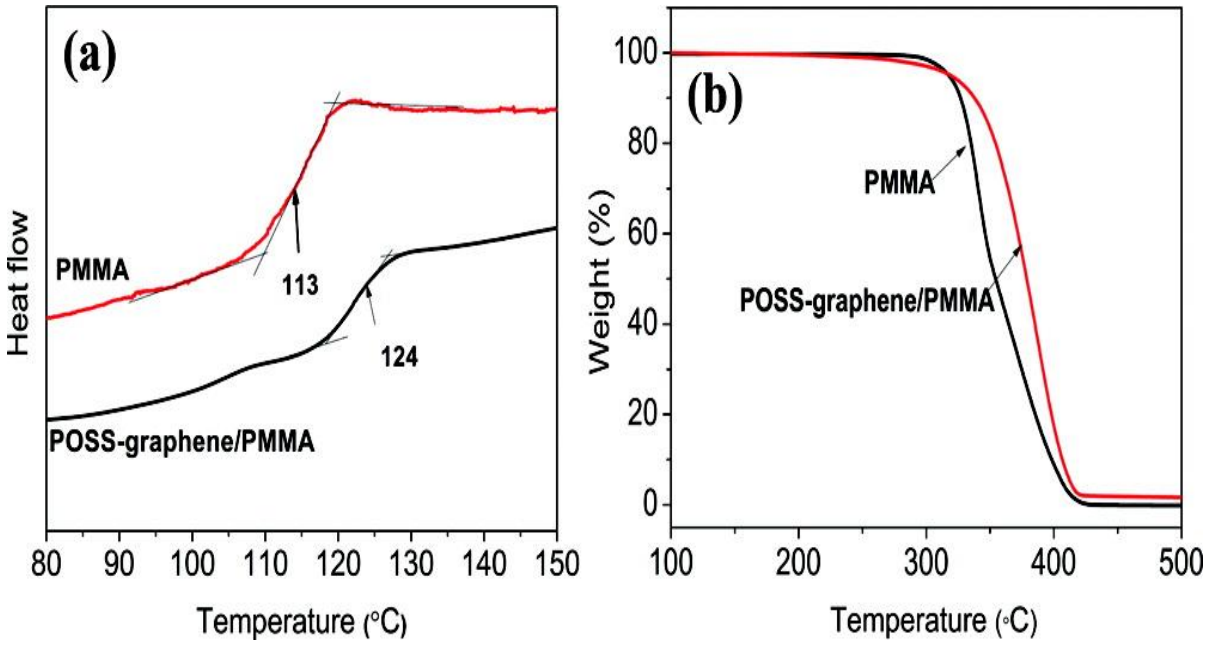

Fig. 1.13 (a) DSC (b) TGA of pure PMMA and a POSS-graphene/PMMA composite [58].

GO as a nano-filler in PMMA showed higher thermal stability for PMMA, increasing its glass transition temperature (T_g) by 11 °C. In this study, Xue et al. also reported the super hydrophobic properties with water/air, increasing the contact angle from ~30° to ~157°, showing a more hydrophobic character, which also suggests that the modification improved the compatibility of GO with the matrix resin. Figure 1.13 shows the DSC and TGA data for pure PMMA and POSS-graphene/PMMA composite, showing an increase in the thermal stability [58]. Figure 1.14 shows the SEM of the films and the contact angle measurements of pure GO and the modified POSS-GO films respectively [58].

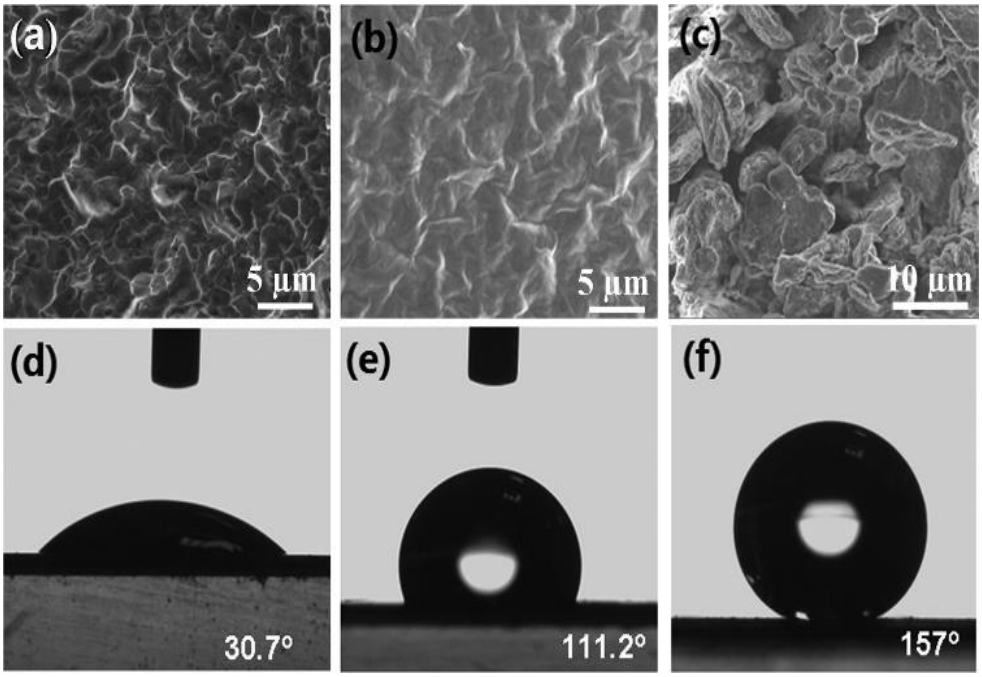

Fig. 1.14: SEM images of (a) a GO film, (b) the as-synthesized POSS-graphene film, and (c) a rough POSS-graphene film prepared from POSS-graphene particles. The corresponding water droplet and air/water contact angles for (d) the GO film, (e) the as-synthesized POSS-graphene film, and (f) the rough POSS-graphene film prepared from POSS-graphene particles [58].

The grafting of different types of POSS with GO results in composite properties that cannot be obtained through other methods. Interestingly, these properties are obtained at low levels of addition of the hybrid nano-additive. For example, Wang et al. studied the effect of octaaminophenyl POSS grafted GO nanoparticles on the fire retardancy of epoxy resins. They concluded that the reinforcement of POSS (2-wt.%) and POSS-Graphene (2-wt %) improved the degradation temperature onset by 24 ℃ and 43 ℃ of the epoxy composite at 5% weight loss. It should be noted that either 5 or 10% weight loss is typically used to characterize degradation temperature for composite materials. The superior fire-retardant property of POSS-graphene could be due to a) the formation of a more stable form of graphene while compared to neat GO and b) increased char yield because of the silica layers on the surface [59].

Multiple researchers have reported the grafting of POSS on GO to enhance the mechanical and thermal properties of composites to which they are added. For example, Valentini, L., et al., reacted amino-functionalized POSS (POSS-NH_2) with GO [60] and confirmed the improved hydrophobic behavior by an increased water contact angle from 51° to 86°. The same group developed a novel method to deposit POSS vapor into GO and demonstrated a carbon/silicon nanomaterial having photoconductivity response. They reported ~ 8×10^{-5}Amp current for ~ 250 s exposure in visible light [61, 62].

Antoniou, K.S., et al. reviewed the synthesis and properties of carbon nanostructures containing organic-inorganic cage-like polyhedral oligomeric silsesquioxane (POSS) nanoparticles. They reported that the physical and chemical functionalization of carbon nanomaterials such as graphene, graphene oxide, carbon nanotubes, and fullerene with POSS

improves the solubility of carbon nanostructures, enhance thermal, mechanical and flame retardancy behaviors in polymers, and alters the electronic properties [63].

Yu, W., et al. found that OapPOSS-GO increased the thermal degradation temperature by 319.3 °C compared to pure GO. They also reported that incorporating OapPOSS-GO into the epoxy matrix at ~0.1% reduces the dielectric constant and dielectric loss by 9% and 49% respectively [64]. Qu, L. et al. reported a significant improvement in the epoxy composite fire retardancy when reinforced with octa (propyl glycidyl ether) POSS functionalized GO. They concluded that the addition of functionalized GO lengthens the heat path leading to a reduction in peak heat release rate and total smoke released by 49.7% and 41%, respectively [65].

1.9 Challenges related to impact damage in polymer composites:

As discussed previously, with the increase in polymer composite applications, issues such as delamination due to low-velocity impact, which affects their fatigue performance, are critical [60, 61]. Hence, there is a need for improving the impact resistance of polymer composites, which could be accomplished by improving their interlaminar fracture toughness (IFT). The fundamental factors determining the initiation and development of fracture in fiber-reinforced composites are loading speed, stress concentration, temperature, and thermal shock [66].

For various fiber/epoxy composites, the modulus of fiber (E_f) and matrix (E_m) are significantly different, leading to a mismatch in their ability to withstand impact. D. Liu studied the mismatch coefficient of carbon, Kevlar©, and glass fiber with epoxy resin. The

study reported that the carbon/epoxy composite (CFRP) has the highest mismatch in these properties, leading to easier delamination in CFRP composites [67].

Kumar et al. analyzed low-speed drop weight impact on hemp and basalt fiber reinforced polymer laminate composites [68]. When compared to the hybrid (hemp & basalt)/epoxy composite, their study showed that hemp/epoxy composite is more susceptible to delamination upon impact. The researchers concluded that an opportunity exists to create a better fiber-matrix interaction mechanism in fiber-reinforced polymer composites.

1.10 Hypothesis and proposed work:

Based on this literature review on polymer composites where hybrid nano-additives have been added, limited results have been reported in the use of POSS-w-GO/polymer (epoxy, vinyl ester, polyester, etc.) composites for improving their delamination resistance. Grafting POSS molecules with GO and investigating their effect on mechanical and thermal properties of the polymer matrix could provide new insights. Additionally, there is also a need to develop techniques to scale up these processes to develop POSS-GO molecules that have good compatibility with different resin matrices. The following are possible hypotheses to be investigated.

I. *The low thermal stability of GO can be optimized by hybridizing POSS on GO.*

From among different carbon-based nano-additives, GO is a good potential candidate for incorporation into polymer matrices due to its compatibility with different resin matrices. However, the thermal stability of GO is limited. Therefore, it is hypothesized that the low thermal stability of GO can be improved by the hybridizing POSS (due to its inorganic Si cage) on the basal or edge plane. The hybrid nature of POSS could also be exploited to react with GO to create nanoparticles that disperse well in resin matrices.

II. The hybridization of POSS into GO can be achieved by redox polymerization.

The chemical route of grafting determines the overall quality and yield of nano-additives. It is hypothesized that the optimum hybridization of POSS into GO can be achieved by redox polymerization initiated by cerium ammonium nitrate in an aqueous solution at a temperature below 100 °C.

III. *By hybridizing POSS on GO, the dispersion of nano-additives can be improved.*

The presence of POSS cages between the GO layers could inhibit the van der Waals' forces of attraction and can prevent the restacking of GO sheets. It is hypothesized that the POSS cages between the GO layers could result in improved dispersion of the nanoparticles in polymer matrices, thus improving the mechanical and thermal properties of polymer matrix composites.

IV. POSS-w-GO will provide improved resistance to interlaminar crack propagation.

The delamination of fiber-reinforced polymer composites due to low-velocity impact needs to be minimized. It is hypothesized that the effective grafting of POSS into GO layers will cause the modified GO to be more chemically and mechanically interactive with the fiber surface. This could ultimately lead to better resistance to crack initiation and propagation.

The proposed plan of work is summarized as follows:

1. Design and assemble components of a redox reaction system for synthesis of functionalized graphene oxide under an inert nitrogen atmosphere at mild temperatures.
2. Synthesis and scale-up the product from milli grams up to 20 g of methacryl POSS hybridized graphene oxide.
3. Characterize the hybrid nanomaterial (GO-g-MAPOSS) by Fourier transform infrared (FTIR), Raman, X-ray diffraction (XRD), X-ray fluorescence (XRF) Spectroscopy, Transmission electron microscopy (TEM) and Thermogravimetric analysis (TGA) to confirm the hybridization of MAPOSS on GO.

4. Investigate the effect of hybrid nanomaterial in polymer matrix composites (PMC), and carbon fiber-reinforced polymer (CFRP) composites on their mechanical properties.

REFERENCES:

1. Air Force SBIR\STTR. *New Composite Materials Will Promote Bigger Fuel Savings And Better Fatigue Resistance In Aircraft*. 2016, April 1st [cited August, 2021; Available from: https://www.afsbirsttr.af.mil/News-Media/Success-Stories/Article/1480873/new-composite-materials-will-promote-bigger-fuel-savings-and-better-fatigue-res/.
2. CompositesWorld. *Aviation Outlook: Fuel pricing ignites demand for composites in commercial transports*. 2006, June 30th [cited August 2021; Available from: https://www.compositesworld.com/articles/aviation-outlook-fuel-pricing-ignites-demand-for-composites-in-commercial-transports.
3. Chad Schell, G.J.L., Blake Marshall,. *Composites*. 2020, June [cited August, 2021; Available from: Advanced Manufacturing Office (AMO) Peer Review presented at Washington DC https://manufacturing.energy.gov.
4. Chawla, K.K., *Composite materials: science and engineering,Third Edition,* Springer Science & Business Media, New york 2012, ISBN 978-0-387-74364-6 ISBN 978-0-387-7436503(eBook), DOI 10.1007/978-0-787-74365-3.
5. Park, S.-J. and M.-K. Seo, *Interface science and composites*. Vol. 18. 2011: Academic Press.
6. MARKETSANDMARKETS. *Composites Market by Fiber Type (Glass Fiber Composites, Carbon Fiber Composites, Natural Fiber Composites), Resin Type (Thermoset Composites, Thermoplastic Composites), Manufacturing Process, End-use Industry and Region - Global Forecast to 2025*. 2020 [cited 2020 November, 2020]; Available from: https://www.marketsandmarkets.com/Market-Reports/composite-market-

200051282.html?gclid=EAIaIQobChMIpc7Xjonx7AIVEPfjBx24yAalEAAYASAAEgI-wPD_BwE.

7. GrabdViewResearch. *Composites Market Size Worth $160.54 Billion By 2027 | CAGR: 7.6%*. 2020 [cited 2020 November, 2020]; Available from: https://www.grandviewresearch.com/press-release/global-composites-market.

8. MARKETSANDMARKETS. *Nanocomposites Market by Type (Carbon Nanotubes, Nanoclay Metal Oxide, Nanofiber, Graphene), Resin Type, Application (Packaging, Automotive, Electrical & Semiconductors, Coatings, Aerospace & Defense, Energy), Region - Global Forecast to 2024*. 2021 [cited 2021 02/26/2021]; Available from: https://www.marketsandmarkets.com/Market-Reports/nanocomposites-market-141476334.html#utm_source=Mailgun-260221&utm_medium=NA.

9. MARKETSANDMARKETS. *"COMPOSITES MARKET - GLOBAL FORECAST TO 2022*. 2017 [cited 2020 November, 202].

10. Gudarzi, M.M. and F. Sharif, *Enhancement of dispersion and bonding of graphene-polymer through wet transfer of functionalized graphene oxide.* Express Polymer Letters, 2012. **6**(12).

11. Rajak, D.K., D.D. Pagar, P.L. Menezes, and E. Linul, *Fiber-reinforced polymer composites: Manufacturing, properties, and applications.* Polymers, 2019. **11**(10): p. 1667.

12. Lichtenhan, J.D., T.S. Haddad, J.J. Schwab, M.J. Carr, K.P. Chaffee, and P.T. Mather, *The next generation of silicon-based plastics: Polyhedral oligomeric silsesquioxane (POSS) nanocomposites.* American Chemical Society, Polymer Preprints, Division of Polymer Chemistry, 1998. **39**(1): p. 489-490.

13. Król-Morkisz, K. and K. Pielichowska, *Thermal decomposition of polymer nanocomposites with functionalized nanoparticles*, in *Polymer Composites with Functionalized Nanoparticles*. 2019, Elsevier. p. 405-435.

14. Kuo, S.-W. and F.-C. Chang, *POSS related polymer nanocomposites.* Progress in polymer science, 2011. **36**(12): p. 1649-1696.

15. Pielichowski, K., J. Njuguna, B. Janowski, and J. Pielichowski, *Polyhedral oligomeric silsesquioxanes (POSS)-containing nanohybrid polymers*, in *Supramolecular Polymers Polymeric Betains Oligomers*. 2006, Springer. p. 225-296.

16. Raftopoulos, K.N. and K. Pielichowski, *Segmental dynamics in hybrid polymer/POSS nanomaterials.* Progress in Polymer Science, 2016. **52**: p. 136-187.

17. Zhao, J., Y. Fu, and S. Liu, *Polyhedral oligomeric silsesquioxane (POSS)-modified thermoplastic and thermosetting nanocomposites: a review.* Polymers and Polymer Composites, 2008. **16**(8): p. 483-500.

18. Gnanasekaran, D., K. Madhavan, and B. Reddy, *Developments of polyhedral oligomeric silsesquioxanes (POSS), possnanocomposites and their applications: A review.* 2009.

19. Ayandele, E., B. Sarkar, and P. Alexandridis, *Polyhedral oligomeric silsesquioxane (POSS)-containing polymer nanocomposites.* Nanomaterials, 2012. **2**(4): p. 445-475.

20. Huang, X., Z. Yin, S. Wu, X. Qi, Q. He, Q. Zhang, Q. Yan, F. Boey, and H. Zhang, *Graphene-based materials: synthesis, characterization, properties, and applications.* small, 2011. **7**(14): p. 1876-1902.

21. Norhayati, H., M. Zuhailimuna, H. Mohd Zobir, M.I. Illyas, M. Azmi, K. Azlan, A.B. Suriani, M. Mazidah, and J. AdilaMohamad, *A Brief Review On Recent Graphene Oxide-Based Material Nanoco Mposites: Synthesis And Applications.* 2016.

22. Mathur, R.B., B.P. Singh, and S. Pande, *Carbon nanomaterials: synthesis, structure, properties and applications*. 2016: CRC Press.

23. Tang, J., H. Zhou, Y. Liang, X. Shi, X. Yang, and J. Zhang, *Properties of graphene oxide/epoxy resin composites.* Journal of Nanomaterials, 2014. **2014**.

24. Pei, S. and H.-M. Cheng, *The reduction of graphene oxide.* Carbon, 2012. **50**(9): p. 3210-3228.

25. Braun, D., *Origins and development of initiation of free radical polymerization processes.* International Journal of Polymer Science, 2009.

26. Garra, P., C. Dietlin, F. Morlet-Savary, F. Dumur, D. Gigmes, J.-P. Fouassier, and J. Lalevée, *Redox two-component initiated free radical and cationic polymerizations: Concepts, reactions and applications.* Progress in Polymer Science, 2019. **94**: p. 33-56.

27. Ma, L., X. Yang, L. Gao, M. Lu, C. Guo, Y. Li, Y. Tu, and X. Zhu, *Synthesis and characterization of polymer grafted graphene oxide sheets using a Ce (IV)/HNO3 redox system in an aqueous solution.* carbon, 2013. **53**: p. 269-276.

28. Liu, J., G. Liu, and W. Liu, *Preparation of water-soluble β-cyclodextrin/poly (acrylic acid)/graphene oxide nanocomposites as new adsorbents to remove cationic dyes from aqueous solutions.* Chemical Engineering Journal, 2014. **257**: p. 299-308.

29. Chauke, V.P., A. Maity, and A. Chetty, *High-performance towards removal of toxic hexavalent chromium from aqueous solution using graphene oxide-alpha*

cyclodextrin-polypyrrole nanocomposites. Journal of Molecular Liquids, 2015. **211**: p. 71-77.

30. Mkhoyan, K.A., A.W. Contryman, J. Silcox, D.A. Stewart, G. Eda, C. Mattevi, S. Miller, and M. Chhowalla, *Atomic and electronic structure of graphene-oxide.* Nano letters, 2009. **9**(3): p. 1058-1063.

31. Lin, Z., Y. Liu, Z. Li, and C.-p. Wong,Lin, Z., Y. Liu, Z. Li, and C.-p. Wong, *Novel preparation of functionalized graphene oxide for large scale, low cost, and self-cleaning coatings of electronic devices*. in *2011 IEEE 61st Electronic Components and Technology Conference (ECTC)*. 2011. IEEE.

32. Potts, J.R., D.R. Dreyer, C.W. Bielawski, and R.S. Ruoff, *Graphene-based polymer nanocomposites.* Polymer, 2011. **52**(1): p. 5-25.

33. Sengupta, R., M. Bhattacharya, S. Bandyopadhyay, and A.K. Bhowmick, *A review on the mechanical and electrical properties of graphite and modified graphite reinforced polymer composites.* Progress in polymer science, 2011. **36**(5): p. 638-670.

34. Rafiee, M.A., J. Rafiee, Z. Wang, H. Song, Z.-Z. Yu, and N. Koratkar, *Enhanced mechanical properties of nanocomposites at low graphene content.* ACS nano, 2009. **3**(12): p. 3884-3890.

35. Rafiee, M.A., W. Lu, A.V. Thomas, A. Zandiatashbar, J. Rafiee, J.M. Tour, and N.A. Koratkar, *Graphene nanoribbon composites.* ACS nano, 2010. **4**(12): p. 7415-7420.

36. Wang, Y., Z. Shi, J. Fang, H. Xu, and J. Yin, *Graphene oxide/polybenzimidazole composites fabricated by a solvent-exchange method.* Carbon, 2011. **49**(4): p. 1199-1207.

37. Gui, D., C. Liu, F. Chen, and J. Liu, *Preparation of polyaniline/graphene oxide nanocomposite for the application of supercapacitor.* Applied surface science, 2014. **307**: p. 172-177.

38. Wang, H., Q. Hao, X. Yang, L. Lu, and X. Wang, *A nanostructured graphene/polyaniline hybrid material for supercapacitors.* Nanoscale, 2010. **2**(10): p. 2164-2170.

39. Xu, X., J. Shen, N. Li, and M. Ye, *Facile synthesis of reduced graphene oxide/CoWO4 nanocomposites with enhanced electrochemical performances for supercapacitors.* Electrochimica Acta, 2014. **150**: p. 23-34.

40. Zhao, X., J. Zhang, J. Zhang, C. Gong, X. Gu, Z. Ma, J. Zhou, L. Yu, and Z. Zhang, *Construction of spongy antimony-doped tin oxide/graphene nanocomposites using commercially available products and its excellent electrochemical performance.* Journal of Power Sources, 2015. **294**: p. 223-231.

41. Li, Y., D. Wang, W. Li, and Y. He, *Photoelectric conversion properties of electrochemically codeposited graphene oxide–ZnO nanocomposite films.* Journal of Alloys and Compounds, 2015. **648**: p. 942-950.

42. Xu, G., F. Jiang, Z.-a. Ren, and L.-w. Yang, *Polyhedral MnO nanocrystals anchored on reduced graphene oxide as an anode material with superior lithium storage capability.* Ceramics International, 2015. **41**(9): p. 10680-10688.

43. She, X., X. Zhang, J. Liu, L. Li, X. Yu, Z. Huang, and S. Shang, *Microwave-assisted synthesis of Mn3O4 nanoparticles@ reduced graphene oxide nanocomposites for high performance supercapacitors.* Materials research bulletin, 2015. **70**: p. 945-950.

44. Mehrali, M., S.T. Latibari, M. Mehrali, H.S.C. Metselaar, and M. Silakhori, *Shape-stabilized phase change materials with high thermal conductivity based on paraffin/graphene oxide composite.* Energy conversion and management, 2013. **67**: p. 275-282.

45. He, H.-Y., *Photoinduced superhydrophilicity and high photocatalytic activity of ZnO–reduced graphene oxide nanocomposite films for self-cleaning applications.* Materials Science in Semiconductor Processing, 2015. **31**: p. 200-208.

46. Luo, L., Y. Yang, A. Zhang, M. Wang, Y. Liu, L. Bian, F. Jiang, and X. Pan, *Hydrothermal synthesis of fluorinated anatase TiO2/reduced graphene oxide nanocomposites and their photocatalytic degradation of bisphenol A.* Applied Surface Science, 2015. **353**: p. 469-479.

47. Song, Y., K. Qu, C. Zhao, J. Ren, and X. Qu, *Graphene oxide: intrinsic peroxidase catalytic activity and its application to glucose detection.* Advanced Materials, 2010. **22**(19): p. 2206-2210.

48. Yan, X., X. Zhang, H. Liu, Y. Liu, J. Ding, Y. Liu, Q. Cai, and J. Zhang, *Fabrication of SDBS intercalated-reduced graphene oxide/polypyrrole nanocomposites for supercapacitors.* Synthetic metals, 2014. **196**: p. 1-7.

49. Gong, L., I.A. Kinloch, R.J. Young, I. Riaz, R. Jalil, and K.S. Novoselov, *Interfacial stress transfer in a graphene monolayer nanocomposite.* Advanced Materials, 2010. **22**(24): p. 2694-2697.

50. Stankovich, S., R.D. Piner, X. Chen, N. Wu, S.T. Nguyen, and R.S. Ruoff, *Stable aqueous dispersions of graphitic nanoplatelets via the reduction of exfoliated*

graphite oxide in the presence of poly (sodium 4-styrenesulfonate). Journal of Materials Chemistry, 2006. **16**(2): p. 155-158.

51. Wang, X., J. Jin, and M. Song, *Cyanate ester resin/graphene nanocomposite: curing dynamics and network formation.* European polymer journal, 2012. **48**(6): p. 1034-1041.

52. Yu, A., P. Ramesh, M.E. Itkis, E. Bekyarova, and R.C. Haddon, *Graphite nanoplatelet− epoxy composite thermal interface materials.* The Journal of Physical Chemistry C, 2007. **111**(21): p. 7565-7569.

53. Mishra, K., G. Pandey, and R.P. Singh, *Enhancing the mechanical properties of an epoxy resin using polyhedral oligomeric silsesquioxane (POSS) as nano-reinforcement.* Polymer Testing, 2017. **62**: p. 210-218.

54. Ahmadi-Moghadam, B. and F. Taheri, *Influence of graphene nanoplatelets on modes I, II and III interlaminar fracture toughness of fiber-reinforced polymer composites.* Engineering Fracture Mechanics, 2015. **143**: p. 97-107.

55. Zhu, J., A. Imam, R. Crane, K. Lozano, V.N. Khabashesku, and E.V. Barrera, *Processing a glass fiber reinforced vinyl ester composite with nanotube enhancement of interlaminar shear strength.* Composites Science and Technology, 2007. **67**(7-8): p. 1509-1517.

56. Degirmenci, M., S. Hicri, and H. Yilmaz, *Synthesis and characterization of a novel water-soluble mid-chain macrophotoinitiator of polyacrylamide by Ce (IV)/HNO3 redox system.* European polymer journal, 2008. **44**(11): p. 3776-3781.

57. Wang, B., D. Yang, J.Z. Zhang, C. Xi, and J. Hu, *Stimuli-responsive polymer covalent functionalization of graphene oxide by Ce (IV)-induced redox*

polymerization. The Journal of Physical Chemistry C, 2011. **115**(50): p. 24636-24641.

58. Xue, Y., Y. Liu, F. Lu, J. Qu, H. Chen, and L. Dai, *Functionalization of graphene oxide with polyhedral oligomeric silsesquioxane (POSS) for multifunctional applications.* The journal of physical chemistry letters, 2012. **3**(12): p. 1607-1612.

59. Wang, X., Y. Hu, L. Song, H. Yang, B. Yu, B. Kandola, and D. Deli, *Comparative study on the synergistic effect of POSS and graphene with melamine phosphate on the flame retardance of poly (butylene succinate).* Thermochimica acta, 2012. **543**: p. 156-164.

60. Valentini, L., S.B. Bon, O. Monticelli, and J.M. Kenny, *Deposition of amino-functionalized polyhedral oligomeric silsesquioxanes on graphene oxide sheets immobilized onto an amino-silane modified silicon surface.* Journal of Materials Chemistry, 2012. **22**(13): p. 6213-6217.

61. Valentini, L., S.B. Bon, M. Cardinali, O. Monticelli, and J.M. Kenny, *POSS vapor grafting on graphene oxide film.* Chemical Physics Letters, 2012. **537**: p. 84-87.

62. Valentini, L., M. Cardinali, J.M. Kenny, M. Prato, and O. Monticelli, *A photoresponsive hybrid nanomaterial based on graphene and polyhedral oligomeric silsesquioxanes.* European Journal of Inorganic Chemistry, 2012. **2012**(32): p. 5282-5287.

63. Antoniou, K.S., M. Karakassides, D. Gournis, and P. Rudolf, *Carbon nanostructures containing polyhedral oligomeric silsesquioxanes (POSS).* Chemistry, 2016. **20**(6): p. 662-673.

64. Yu, W., J. Fu, X. Dong, L. Chen, and L. Shi, *A graphene hybrid material functionalized with POSS: Synthesis and applications in low-dielectric epoxy composites.* Composites science and technology, 2014. **92**: p. 112-119.

65. Qu, L., Y. Sui, C. Zhang, P. Li, X. Dai, B. Xu, and D. Fang, *POSS-functionalized graphene oxide hybrids with improved dispersive and smoke-suppressive properties for epoxy flame-retardant application.* European Polymer Journal, 2020. **122**: p. 109383.

66. Maleque, M.A. and M.S. Salit, *Mechanical failure of materials*, in *Materials Selection and Design*. 2013, Springer. p. 17-38.

67. Liu, D., *Impact-induced delamination—a view of bending stiffness mismatching.* Journal of composite materials, 1988. **22**(7): p. 674-692.

68. Kumar, C.S., M. Fotouhi, M. Saeedifar, and V. Arumugam, *Acoustic emission based investigation on the effect of temperature and hybridization on drop weight impact and post-impact residual strength of hemp and basalt fibres reinforced polymer composite laminates.* Composites Part B: Engineering, 2019. **173**: p. 106962.

CHAPTER II

SYNTHESIS/CHARACTERIZATION OF HYBRID POLYMER MODIFIER

ABSTRACT

Epoxy resins are highly crosslinked thermoset polymers that exhibit good thermal stability, excellent chemical resistance, and enhanced modulus after curing. Despite the favorable properties of epoxy resins, their high crosslink density causes them to be inherently brittle and prone to cracking. There have been several studies on toughening epoxies focused on the addition of nanoparticles, including carbon-based nanomaterials like graphene, graphene oxide, carbon nanotubes, etc. Recent studies have focused on the potential of carbon-based nanomaterials as candidates to address the brittleness and cracking issues in epoxies. One additive in particular, graphene oxide (GO), has been shown to achieve excellent dispersion with organic solvents in polymer matrices due to the presence of specific functional groups compatible with the matrix. GO is more attractive for specific applications, however, the presence of oxygen on GO could make it prone to thermo-oxidative degradation and the loss of several other valuable properties of pristine

graphene. Past reports demonstrated the successful grafting of GO with suitable molecules like polyhedral oligomeric silsesquioxane (POSS) to optimize thermal stability. The robust cage-like structure of POSS supports the overall enhancement of the mechanical and thermal behaviors of epoxy-based composite material when dispersed within the polymer matrices. In this work, a hybrid polymer modifier (HPM) has been developed by grafting methacryl polyhedral oligomeric silsesquioxanes (MAPOSS) to GO via a facile redox reaction system with cerium (IV) ammonium nitrate/nitric acid (Ce(IV)/HNO_3) and GO sheets' hydroxyl groups as the redox couple. HPM was characterized with Fourier transform infrared (FTIR), X-ray diffraction (XRD), X-ray fluorescence (XRF) spectroscopy, Thermogravimetric analysis (TGA), and Transmission electron microscopy (TEM). XRF analysis showed that 10.2 mass% of silicon was added to GO due to the MAPOSS grafting. Furthermore, Raman analysis confirmed the increased structural distortion of GO induced by the incorporation of MAPOSS ($(I_D/I_G)_{HPM}$ = 1.43, $(I_D/I_G)_{GO}$ = 1.30).The dispersion of HPM was studied in thermoset resin system epoxy and presented in this paper. Since POSS and GO have individually been reported to be effective in enhancing the interlaminar toughness of fiber-reinforced composites, HPM is expected to improve these properties while overcoming issues such as dispersion and degradation in mechanical properties beyond a certain limit.

2.1 Introduction:

Thermosets, especially epoxy resins, are polymers used in many structural applications because of their temperature-stability, chemical inertness, and attractive mechanical properties [1]. Due to their high crosslink density, thermosets are inherently brittle and prone to impact damage [2]. Introduction of a reinforcing secondary phase for epoxy

have been evaluated using carbon-based nano-fillers such as carbon nanotubes [3, 4], graphene [5, 6], graphene oxide (GO) [7-9], and other nanofillers [10]. Adding inorganic fillers to the polymer matrix can improve their electrical and thermal conductivity [11, 12], mechanical properties such as modulus, impact strength, and elongation at break [13-15]. Adding nanoparticles as a secondary phase can enhance mechanical, thermal and electrical properties polymers, but nanoparticle agglomeration is a serious challenge that needs to be overcome [16]. In the case of carbon nanofillers, this drawback is directly connected with the van der Waals interaction and π- π stacking between the graphene sheets [17-19]. While single-layer graphene can be produced using highly advanced techniques, it is difficult to retain a single layer state once it is dispersed in the polymer matrix.

Graphene oxide (GO), obtained from oxidation and exfoliation of graphite, is a versatile nanofiller owing to its compatibility with polymer matrices. The presence of several oxygen-containing functional groups such as carbonyl, hydroxyl, and epoxy impart numerous advantages to the graphene, such as (1) flexibility for further modification of these groups, (2) improved dispersion in polymer matrices and solvents, and (3) ability to facilitate interfacial interaction between the functional groups and the polymer matrix. The presence of a hydrophilic functional group makes GO more dispersible in polar solvents. However, as discussed above, the dispersion of GO nanosheets can be difficult due to the aggregation and forces between sheets. One of the potential approaches to overcome this particle agglomeration is the surface modification of GO nanosheets. The presence of various functional groups on the surface of GO opens the platform for chemical modification to produce new hybrid materials with compatible properties and

lower probability of agglomeration [18, 20-23]. Surface modification can be achieved in two ways: the first method is based on reaction or surface absorption with small molecules such as silane coupling agents, and the second process consists of grafting polymeric molecules via covalent bonding to the existing functional groups. The second procedure is more desirable because one can select the desired species of the grafting monomer and tailor the grafting conditions to a specific matrix [9].

Recent studies have reported improved thermal and mechanical properties of polymer composites with the incorporation of polyhedral oligomeric silsesquioxane or POSS [24-27]. The physical and chemical functionalization of carbon nanomaterials such as graphene, graphene oxide, and carbon nanotubes with POSS has been developed toward the fabrication of novel hybrid nanostructures [24]. POSS is a three-dimensional nanostructured material with a diameter of 1-3 nm and a unique cage structure having both inorganic and organic moieties. POSS has a nanosized cage structure compatible to polymeric segments with an empirical formula $R_n(SiO_{1.5})_n$, where R represents organic functional groups like alkyl, alkylene, acrylate, or epoxide [25-27]. The siloxane (Si-O-Si), the inorganic moiety, imparts thermal stability, chemical resistance, rigidity, and flame retardant properties to POSS. Eight groups of an external organic group give POSS many benefits like compatibility with polymer matrix, active sites for further reactions, and a degree of compatibility to the molecule. The robust cage-like structure of POSS supports the overall enhancement of the mechanical and thermal behaviors of epoxy-based composite material when dispersed within the polymer matrices. POSS has been widely used for polymer composite applications owing to its hybrid nature [28-30].

The functionalization of GO with POSS resulting in multifunctional hybrid GO has been accomplished by several researchers. Xue, Y. et al. reported chemical grafting of amine functionalized POSS to graphene oxide (GO). Their study showed that POSS-g-GO is highly soluble in many organic solvents [31]. Yu, W. et al. synthesized a hybrid material OapPOSS-GO by functionalizing GO with octa-aminophenyl polyhedral oligomeric silsesquioxanes (OapPOSS). Their study showed that the OapPOSS-GO increased the initial thermal degradation temperature by 319.3 ℃ compared to GO [32]. Similarly, Wang et. al. studied simultaneous reduction and surface functionalization of GO with octa-aminophenyl polyhedral oligomeric silsesquioxanes (OapPOSS) [33]. Valentini, L., et al., reacted amino-functionalized polyhedral oligomeric silsesquioxanes (POSS-NH_2) with GO sheets to graft POSS-NH_2 onto a GO layer immobilized onto a layer of 3-aminopropyltriethoxysilane, self-assembled onto Si substrate [34]. An investigation on the effect of POSS grafted GO nanoparticles in fire retardancy of epoxy resins was also reported Qu et al. [35]. They concluded that the addition of functionalized GO lengthens the heat path leading to a reduction in peak heat release rate and total smoke released by 49.7% and 41.0 %, respectively [35, 36].

The work presented here describes the redox reaction mechanism for grafting of methacryl POSS (MAPOSS) on GO basal and edge plane in the presence of aqueous Ce(IV)/HNO_3. The material, MAPOSS grafted GO (GO-g-MAPOSS), also defined as hybrid polymer modifier (HPM), is characterized, and confirmed by Fourier transform infrared (FTIR), X-ray Diffraction (XRD), Raman spectroscopy, X-ray fluorescence (XRF), and Transmission electron microscopy (TEM) analysis. In addition, the improved thermal stability of HPM is confirmed with Thermogravimetric analysis (TGA). The

dispersion of dry and wet forms of synthesized GO-g-MAPOSS in EPON 862 is investigated under optical microscopy. Dispersions were prepared using five different common processes, and a comparative analysis between wet and dry HPM on EPON 862 is presented.

2.2 Materials and Methodology:

2.2.1 Materials

A 2.5% graphene oxide dispersion in water was purchased from Graphenea Inc. (Cambridge, MA). Nitric acid, acetonitrile, and cerium ammonium nitrate (CAN) were purchased from Alpha Aesar (Haverhill, MA). Methacryl POSS (MAPOSS) cage mixture was purchased from Hybrid Plastics (Hattiesburg, MS). Epoxy resin EPON 862 was purchased from Hexion LLC (Columbus, OH). Acetone was purchased from BDH VWR Analytical (Radnor, PA). All the reagents and chemicals were used without further modifications.

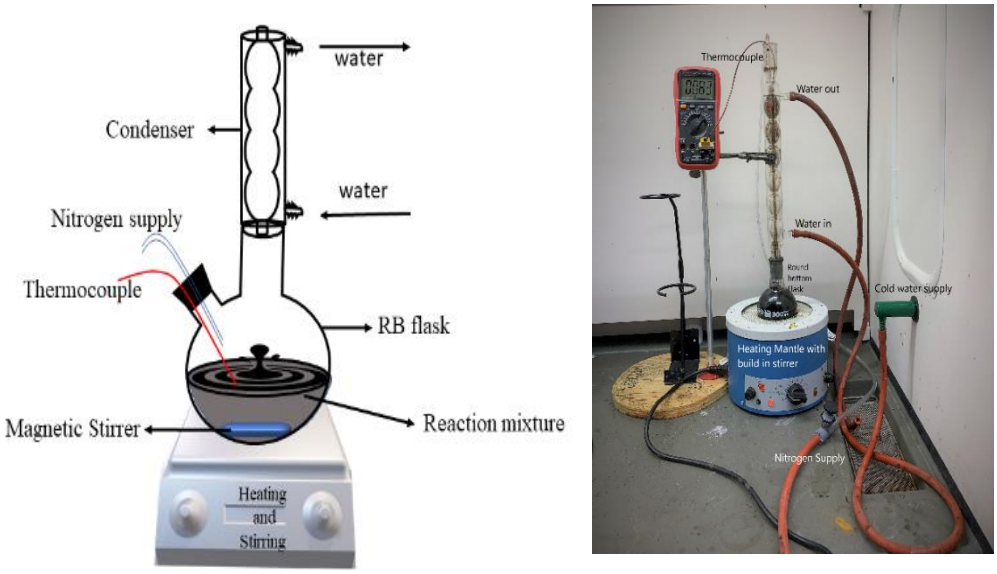

Fig. 2.1: Schematic representation (left) and lab set-up (right) of redox reaction reactor set up.

2.2.2 Redox Reaction System Set-up

To functionalize the GO with MAPOSS, a chemical reactor capable of handling redox reaction was designed and successfully assembled. The schematic representation of customized chemical reactor is shown in Figure 2.1.

2.2.3 Grafting of MAPOSS on GO via Redox reaction

Methacryl POSS (MAPOSS) was hybridized on the surface of graphene oxide (GO) layers using a redox polymerization method. The proposed polymerization mechanism is shown in Fig.2.2. In a typical synthesis reaction, 1.25% (w/v) of GO

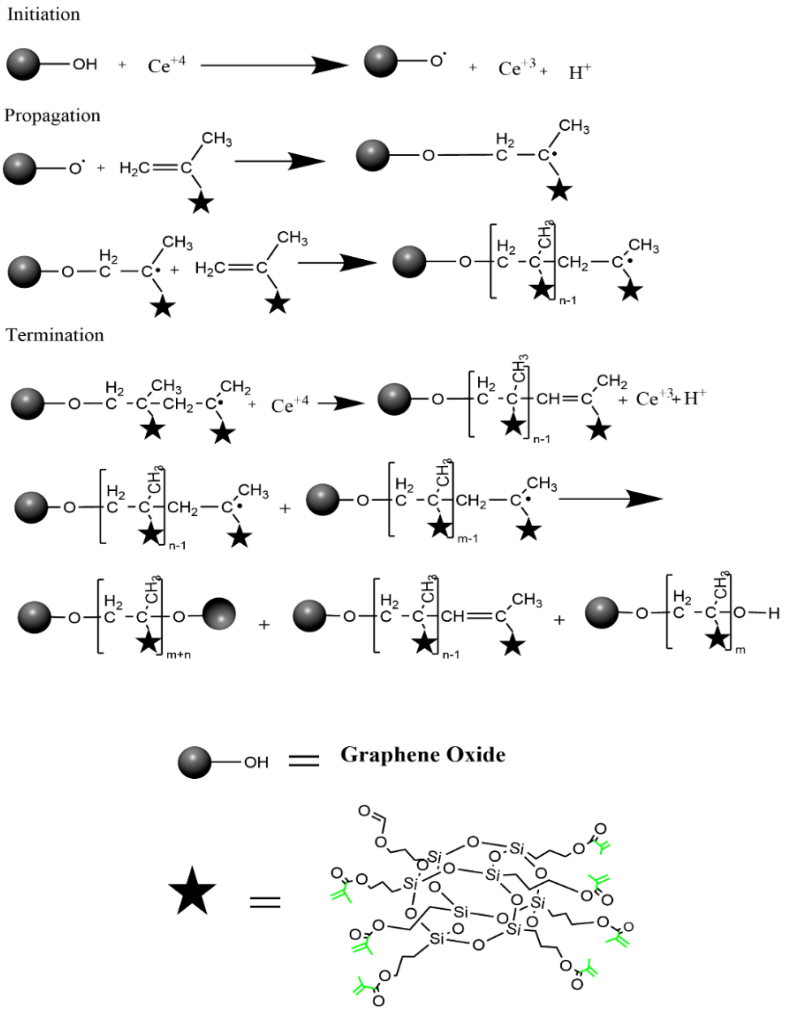

Fig. 2.2. Polymerization mechanism of MAPOSS on the surface of GO using a Ce (IV) redox initiation system

dispersion in 200 mL of water was prepared and mixed mechanically in a round bottom flask. Then, 0.5 g of CAN was dissolved in 50 mL of 1 N nitric acid solution prepared in water. The CAN mixture was then added into the GO dispersion in the round bottom flask. This mixture was stirred gently for 1 h at 80 ^{o}C under an N_2 atmosphere. A solution of 2.5 g of MAPOSS measured and dissolved in 250 ml of acetonitrile was then added to the reaction mixture drop by drop by maintaining constant stirring at 80 °C under nitrogen flow. The MAPOSS and GO ratio was 1:1. The reaction mixture was refluxed at 80 °C for 24 h in the dark and an inert nitrogen atmosphere. After 24 h, the mixture was filtered, washed three times with 1500 mL of acetone, and the final product GO-g-MAPOSS (described as MEGO) was obtained as a wet cake. The polymerization mechanism for GO sheets with MAPOSS in presence of CAN/HNO_3 is outlined in Fig. 2.2. The initiation starts with the generation of free radicals on GO sheets via a redox reaction with Ce (IV)/HNO_3. In the second step, called propagation, the free radical on GO sheets attack the C = C double bond of MAPOSS. This process generates the free radicals on MAPOSS arms and chain propagation occurs. The third and last step is called termination, where the growing chains are halted. Chain termination may occur in three different ways as shown in Fig.2.2. First is termination by coupling with other radicals, known as mutual termination. The second is termination due to coupling with free radical Ce (IV), known as oxidative termination, and the last is disproportionation and chain transfer reaction where a species is simultaneously redoxed and oxidized, yielding two different products. The schematic representation of initiation, propagation and

termination are shown in figure 2.3, 2.4 and 2.5.

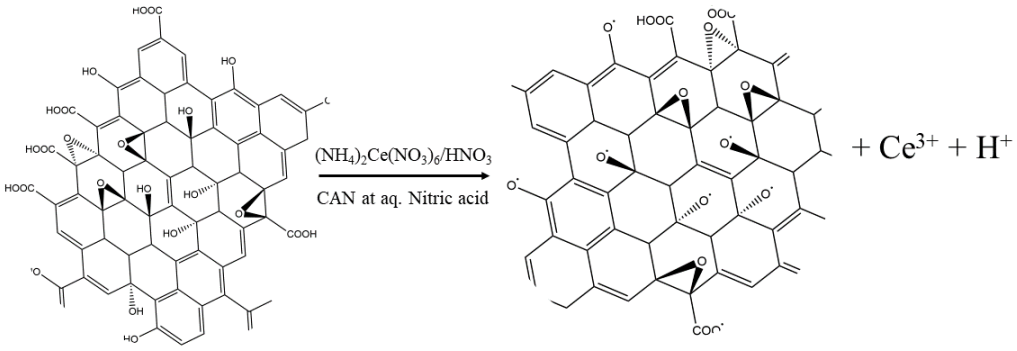

Fig. 2.3: Initiation - Generation of free radicals on GO sheets via a redox reaction with Ce (IV)/HNO_3.

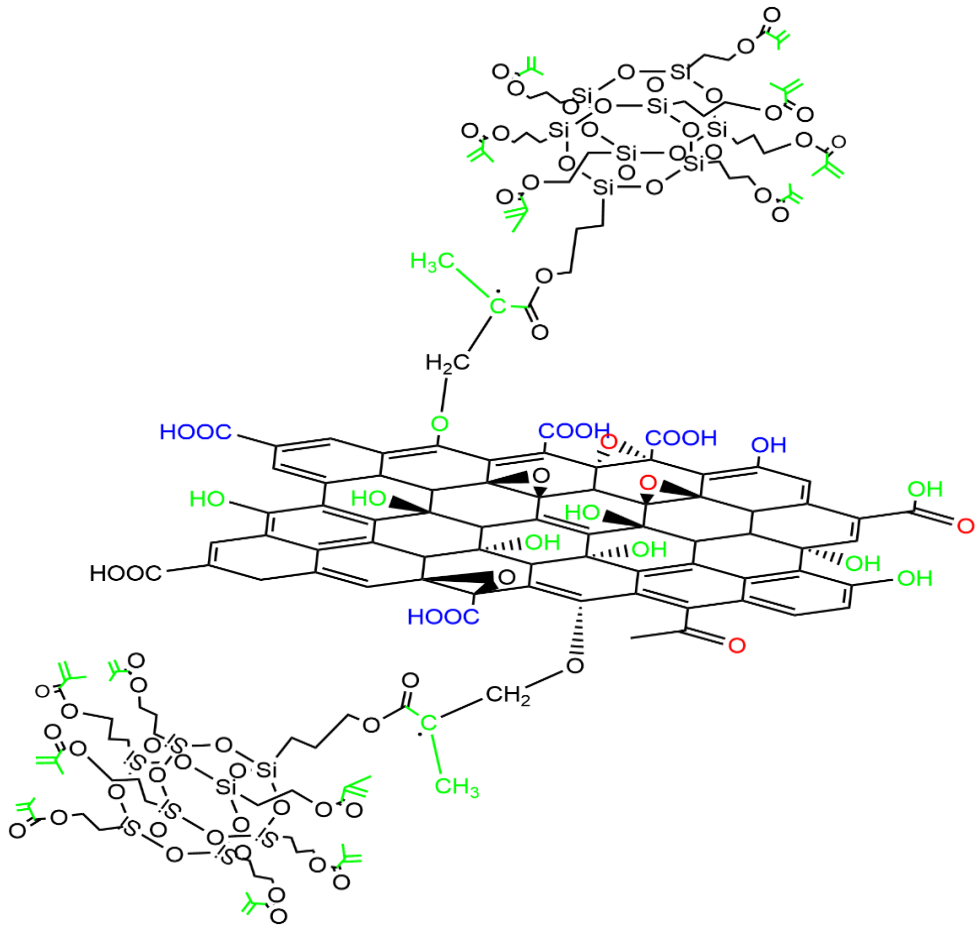

Fig.2.4: Propagation- the free radical on GO sheets attack the C = C of MAPOSS.

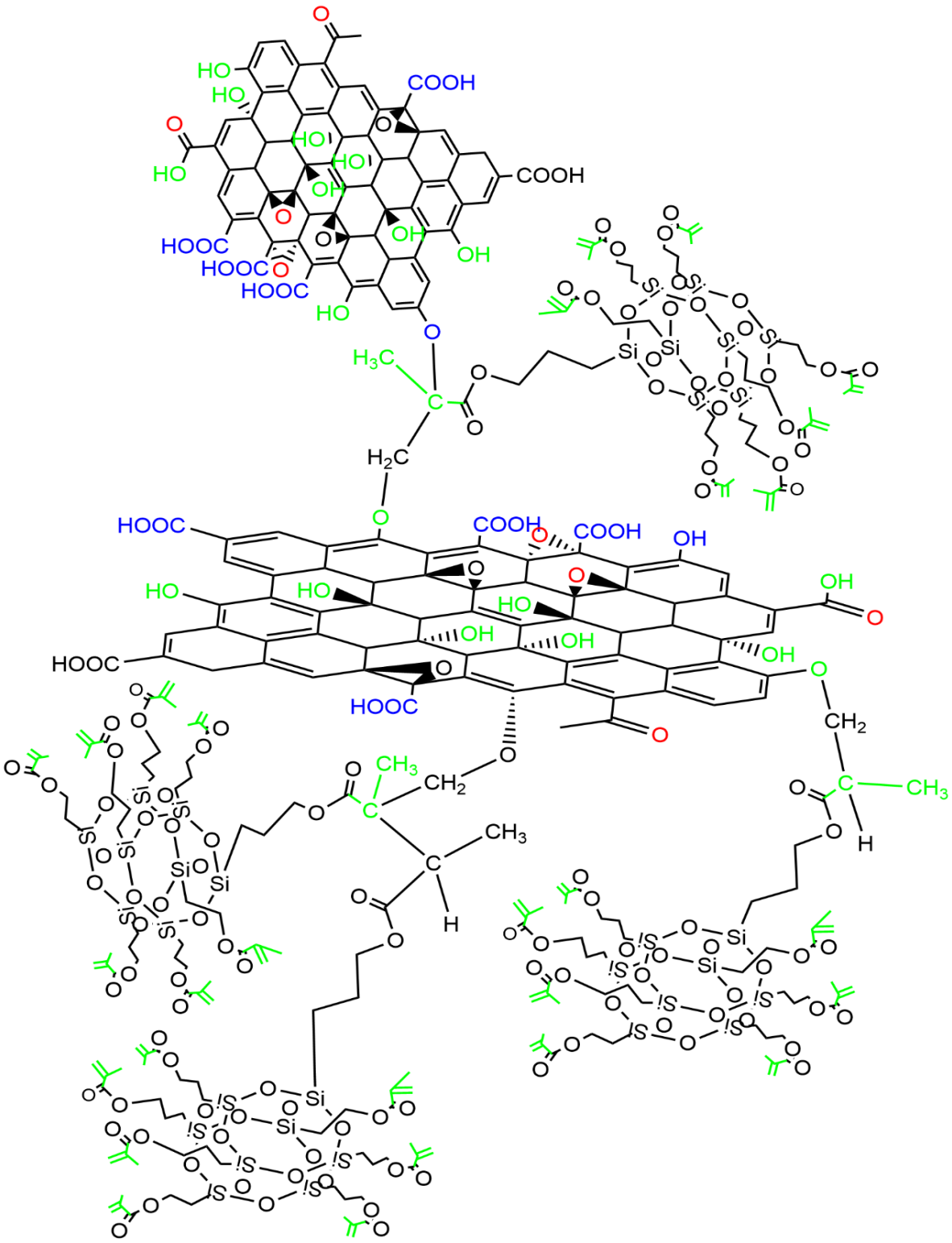

Fig.2.5: Termination - the growing chains are halted.

2.2.4 Estimation of yield product mass

From the fresh wet MEGO cake, two 1 g samples were taken and kept in a vacuum oven at 65 ℃ for 12 h and dried completely. The estimation of yield product mass of the reaction was obtained from the dry weight of both the samples.

2.2.5 Preparation of dry and wet MEGO

The freshly prepared MEGO cake was weighed and divided into two equal parts. Half of the cake was dried under a vacuum oven at room temperature such that the acetone: MEGO = 3:1 (Wet MEGO), while the remaining half of the cake was dried under vacuum overnight completely to obtain a “dry” (solvent free) product (Dry MEGO).

2.2.6 Dispersion of MEGO

Both wet and dry MEGO were dispersed into a polymer resin with five different mixing methods.

2.2.6.1 Shear Mixing

Shear mixing is the easiest and most common mixing method in polymer industries. The desired amount of wet or dry MEGO was taken and mixed with the polymer resin with a shear mixer for 2 h. After the mixing process, the dispersion was kept in a chamber under negative pressure for an additional 2 h to remove the air bubbles.

2.2.6.2 Speed Mixing

A high-speed mixer (DAC 150.1 FVZ-K) manufactured by Hauschild, Germany and marketed by FlackTek, SC was used for the high-speed mixing. It operates based on a dual asymmetric centrifugal mixing technology, which does not generate heat or create air bubbles, and does not involve any physical contact with the material. In this work, wet or dry MEGO was mixed with polymer resin in the high-speed mixer at 3500 rpm for 5 min.

2.2.6.3 Ultra-sonication

Hand-mixed dry or wet MEGO with the resin was kept in a probe sonicator for 30 min. The conditions used were amplitude 40, run time 30 s, and off-time 10 s. Ultrasonication was carried out in an ice bath for avoiding the overheating of the resin. Ultrasonication produces high-energy sound waves for dispersing nanoparticles which helps to exfoliate the filler effectively.

2.2.6.4 Three-roll Mill

The hand-mixed MEGO was mixed with resin using a three-roll mill system. Three-roll mill has three rollers, out of which the first one is called feed, and the last one is called apron rollers. The feed and apron rollers rotate in the same direction while the central one rotates in the opposite direction. Samples were poured into the feed roller and collected at the apron. For both dry and wet MEGO, a 3% masterbatch was prepared by repeating the mixing process seven times.

2.2.6.5 Three-roll Milling followed by ultra-sonication.

To observe the synergistic effect of the two dispersion techniques, ultra-sonication was conducted on the three-roll milled 3% master batch of both wet and dry MEGO in the desired resin system. The ultra-sonication conditions for the three-roll mill master batch were the same as mentioned previously.

2.3. Characterization

2.3.1: Fourier Transform Infrared (FTIR) spectroscopy

Fourier transform infrared spectroscopy in attenuated total reflection (ATR) mode was used to confirm the grafting of MAPOSS to GO. The IR spectra of hybrid polymer modifier samples were collected using a Nicolet iS50 Spectrometer Thermo Scientific Inc. (Waltham, MA) equipped with a diamond crystal (45° angle) as an ATR accessory. Each sample was run using 64 scans versus the background that was also collected using 64 scans to generate a single beam spectrum at 4 cm^{-1} resolution in the range of 500 to 4000 cm^{-1}. The data spacing was 0.482 cm^{-1}.

2.3.2: Raman Spectroscopy

The Raman spectroscopy measurements were conducted using WITec alpha 300R Raman spectrometer with a 532 nm laser, spot size 5 μm, 20X objective lens of 0.40 numerical aperture, and 600 lines/mm grating and 100 μm confocal aperture (fiber) diameter.

2.3.3: Transmission Electron Microscopy

A JEOL JEM-2100 Scanning Transmission Electron Microscope (TEM) with LaB_6 filament gun operating at an accelerating voltage up to 200KV was used to obtain the TEM image of GO and MEGO.

2.3.4: X-ray diffraction (XRD) spectroscopy

For the identification of phase in MEGO, x-ray diffraction spectroscopy was performed. The XRD spectrum was collected using Bruker AXS D8 Discover X-ray Diffractometer with general area detector diffraction system (GADDS) Vantec 500 2D detector. The wavelength of X-ray used is 1.54056 Å. The scanning time was set to 90 s with the range of diffraction angle (2θ) from 5 to 40 degrees.

2.3.5: X-ray fluorescence (XRF) spectroscopy

The principle of XRF spectroscopy is to measures the fluorescent X-ray discharge from a sample due to excitement by incident X-rays. Rigaku ZXS Primus IV x-ray fluorescence spectrometer was used for the accurate quantitative determination of elements from beryllium (Be) through uranium (U) in dry MEGO and GO palate samples. Pallets of the 1-inch diameter of each sample were prepared using hydraulic pressure for XRF spectroscopy.

2.3.6: Thermogravimetric analysis (TGA)

Thermogravimetric analysis of GO, MAPOSS, and MEGO were performed using a high-resolution Thermogravimetric analyzer (TA Q-50, TA instruments, New Castle, DE). The samples were heated at a rate of 20 °C/min from room temperature to 950 °C under both

air and Nitrogen atmosphere. During the test, 40 ml/min of continuous air or nitrogen flow was maintained.

2.3.7 Optical Microscopy

An Olympus SZX9 stereo microscope integrated with a digital camera and image processing software was used to analyze the particle size of both dry and wet MEGO dispersed in desired resin systems with five different dispersion techniques. The 0.1% MEGO dispersion in EPON 862 was analyzed under a stereomicroscope for all techniques.

Advanced microscopy like SEM/ TEM are costly, time consuming and not suitable for liquid phase samples. But optical microscopy is an easy and cost-effective method to understand the dispersion in uncured resin, which could be a key information to decide the future mechanical and thermal analysis tests of polymer composites. Though, optical microscopy is not a standard method, it could be very useful to analyze the dispersion with less effort and cost.

2.4. Results and Discussion

2.4.1: Fourier Transform Infrared (FTIR) Spectroscopy

The FTIR spectra of pure GO, MAPOSS, and GO-g-MAPOSS (MEGO) are shown in Fig. 2.6. The GO spectrum shows a broad band around 3500 cm^{-1} corresponding to O-H stretching vibrations of the hydrogen-bonded group along with other expected resonances. Additional peaks for C=O stretch of -COOH group at 1715 cm^{-1}, absorbed water and unoxidized graphitic domain stretch at 1614 cm^{-1}, and C-O stretch at 1038 cm^{-1} were observed [2, 37]. Modified GO (MEGO) showed a band around 3500 cm^{-1} corresponding to –OH stretching vibration, which is a characteristic signal of hydroxyethyl methacrylate (HEMA). The new peaks observed around 2950 cm^{-1} and

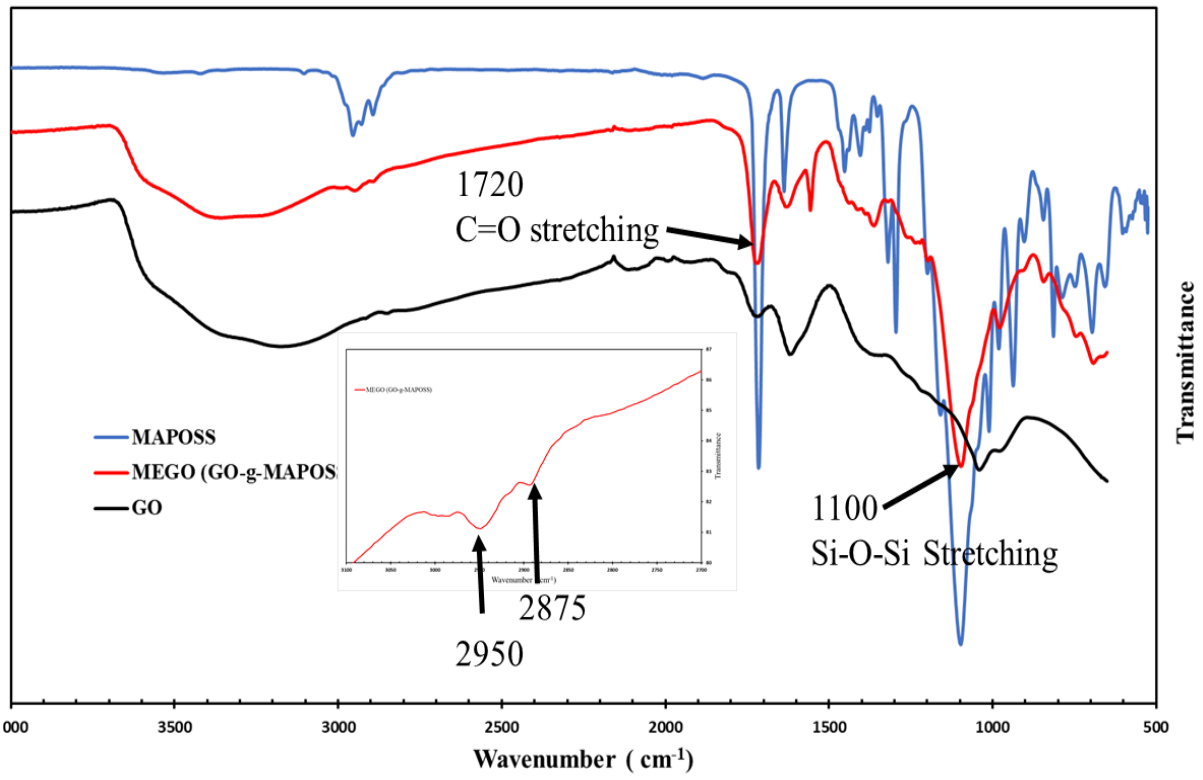

Fig. 2.6. FTIR Spectra of GO, MEGO and MAPOSS.

2875 cm^{-1} are corresponding to isobutyl group stretching vibrations [38]. The peak around 1720 cm^{-1} is attributed to the C=O stretching vibration. The symmetric deformation and bending vibration of Si-O-Si are represented by the peaks around 1300 cm^{-1} and 820 $cm^{-1,}$ respectively, which are characteristic signals of MAPOSS. The peak located at 1450 cm^{-1} is a characteristic vibration of methyl methacrylate (MMA). The peak around 1100 cm^{-1} is attributed to the Si-O-Si stretching vibration band [39]. The distinct peaks observed in MEGO, between 2750 and 3000 cm^{-1} derived from the isobutyl group and peak around 1100 cm^{-1} associated with Si-O-Si stretching, clearly explain the successful grafting between GO and MAPOSS. Thus, the infrared spectroscopy results confirmed the successful grafting of MAPOSS on GO. In addition, 3 different batch (1 g, 5 g and 20 g) production were successfully carried out and the FTIR spectra of each batch were compared (Figure 2.7). Each and every peak observed for 1g batch were exactly presented on 5 g and 20 g batch production confirming the successful scale-up of MEGO up to 20g production with proposed method.

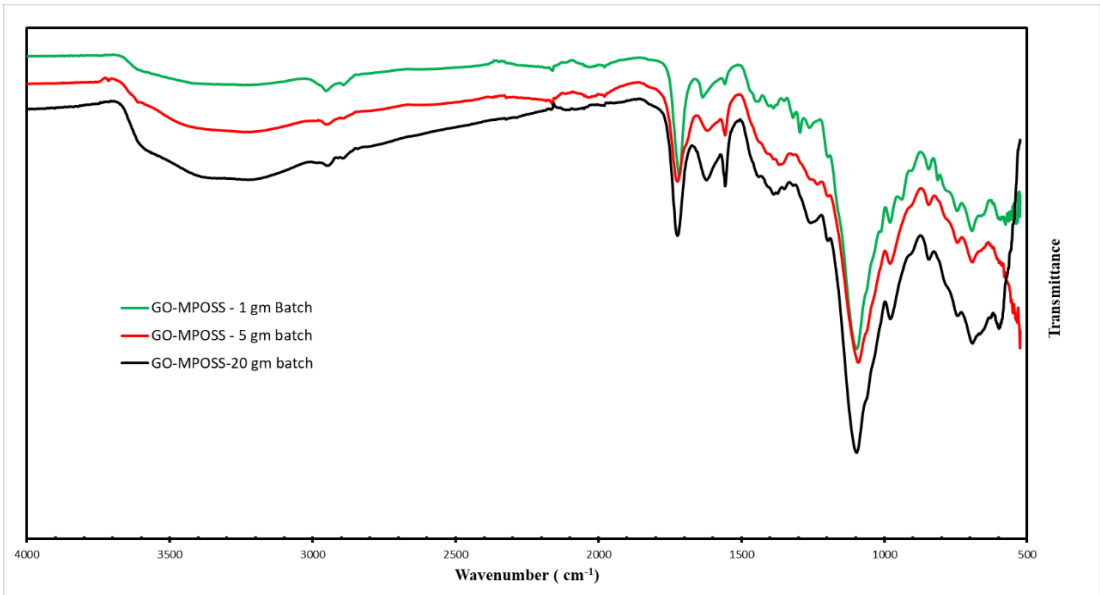

Fig. 2.7. FTIR Spectra of 1g, 5 g and 20 g batch production of MEGO.

2.4.2: X-ray diffraction (XRD) Spectroscopy

The exfoliation of carbon-based nanomaterial in polymer matrix directly correlates with the interlaminar spacing and its randomness in orientation. One major objective of this research is to increase the interlaminar distance as well as enhance the randomness so that

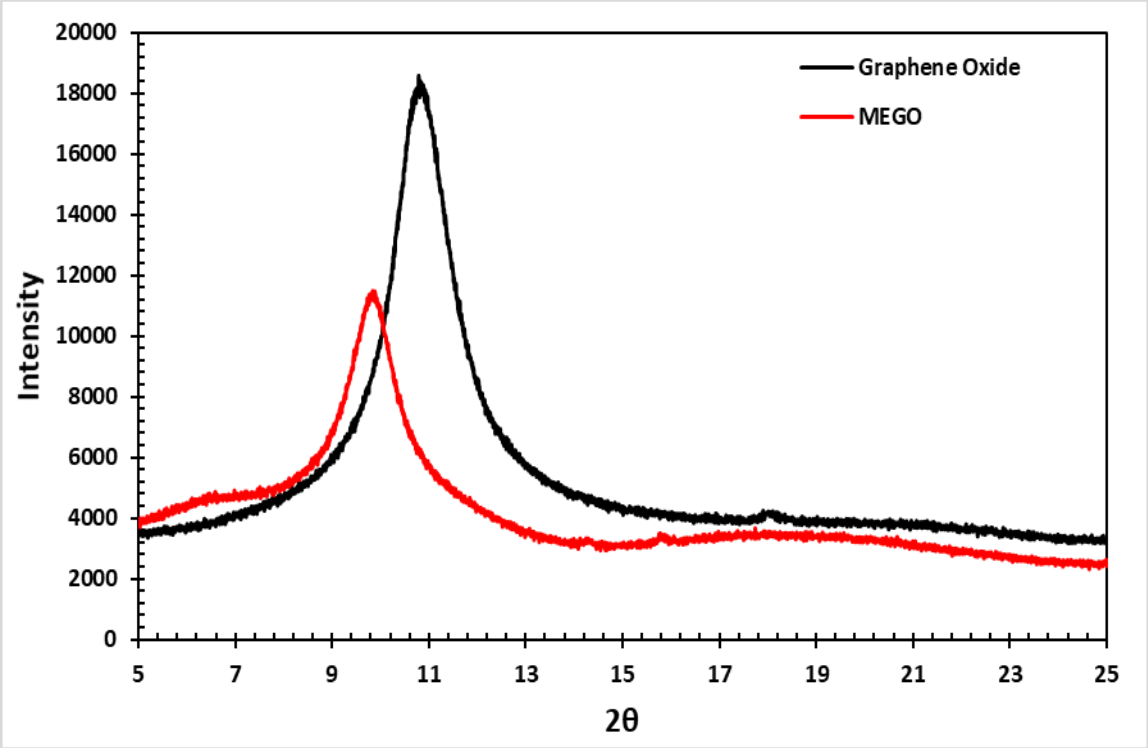

Fig. 2.8. XRD Spectroscopy of Graphene Oxide and MEGO

the van der Waal's force of attraction can be reduced between each GO layer. This could help to reduce the agglomeration of the GO additive. Powder X-ray diffraction of GO and MEGO is shown in Fig. 2.8. The peak of graphene oxide at 10.79^{o} represents interlayer spacing of 8.2 Å. The modified GO, i.e., MEGO (GO-g-MAPOSS), shows the XRD peak shift by 0.95^{o} towards the left, representing the interlayer spacing of 9.0 Å with an increase of 0.8 Å. The peak intensity of MEGO is also reduced by 7094 units inferring the increase in randomness in orientation. The shift in peak position and decreased intensity of MEGO indicates that the chemical modification of GO [40] that corresponds

with the increase in interlaminar spacing and randomness in orientation. The modification of graphene oxide (GO) to MEGO has thus been confirmed by the XRD spectra.

2.4.3: X-ray fluorescence (XRF) spectroscopy

The elemental composition of GO and MEGO was determined by using x-ray fluorescence spectroscopy and shown in Table 2.1. The graphene oxide consists of mainly carbon (45.5 mass %) and oxygen (50.2 mass %) with traces of sulphur, manganese, aluminum, etc. In contrast, MEGO depicted new elements silicon (10.2 mass %) and cerium (0.717 mass %) mainly due to the grafting of MAPOSS in the presence of cerium ammonium nitrate (CAN). From the same process, the mass % of oxygen has

Table 2.1. Elemental composition of GO and MEGO

	Graphene Oxide		
	Component	Mass %	Elementary line
1	Carbon (C)	45.5	K- Alpha
2	Oxygen (O)	50.2	K- Alpha
3	Sulphur (S)	2.78	K- Alpha
4	Manganese (Mn)	0.973	K- Alpha
5	Aluminum (Al)	0.237	K- Alpha
6	Others	0.31	

	MEGO (GO-w-MAPOSS)		
	Component	Mass %	Elementary line
1	Carbon (C)	44.8	K- Alpha
2	Oxygen (O)	43.7	K- Alpha
3	Silicon (Si)	10.2	K- Alpha
4	Cerium (Ce)	0.717	L- Alpha
5	Sulphur (S)	0.365	K- Alpha
6	Manganese (Mn)	0.0698	K- Alpha
7	Others	0.1482	

reduced from 50.2% to 43.7%, while the mass % of carbon reduced by less than 1 %. Overall, the successful incorporation of MAPOSS on GO was confirmed.

2.4.4 Raman spectroscopy

Raman spectroscopy was carried out to investigate the GO & MEGO structures and could partially indicate the hybridization of POSS on GO. Figure 2.9 depicts the Raman spectra of GO and MEGO with D-band (around 1350 cm^{-1}) and G-band (around 1600 cm^{-1}), which are typical characteristics peaks of graphitic materials. The D peak is ascribed to the lattice defect of sp^3 C-atom, and the G peak represents the in-plane stretching vibration due to sp^2 C-atom. Generally, I_D/I_G ratio of Raman spectra is used for investigating the degree of disorder in carbon-based materials. The I_D/I_G ratio of observed

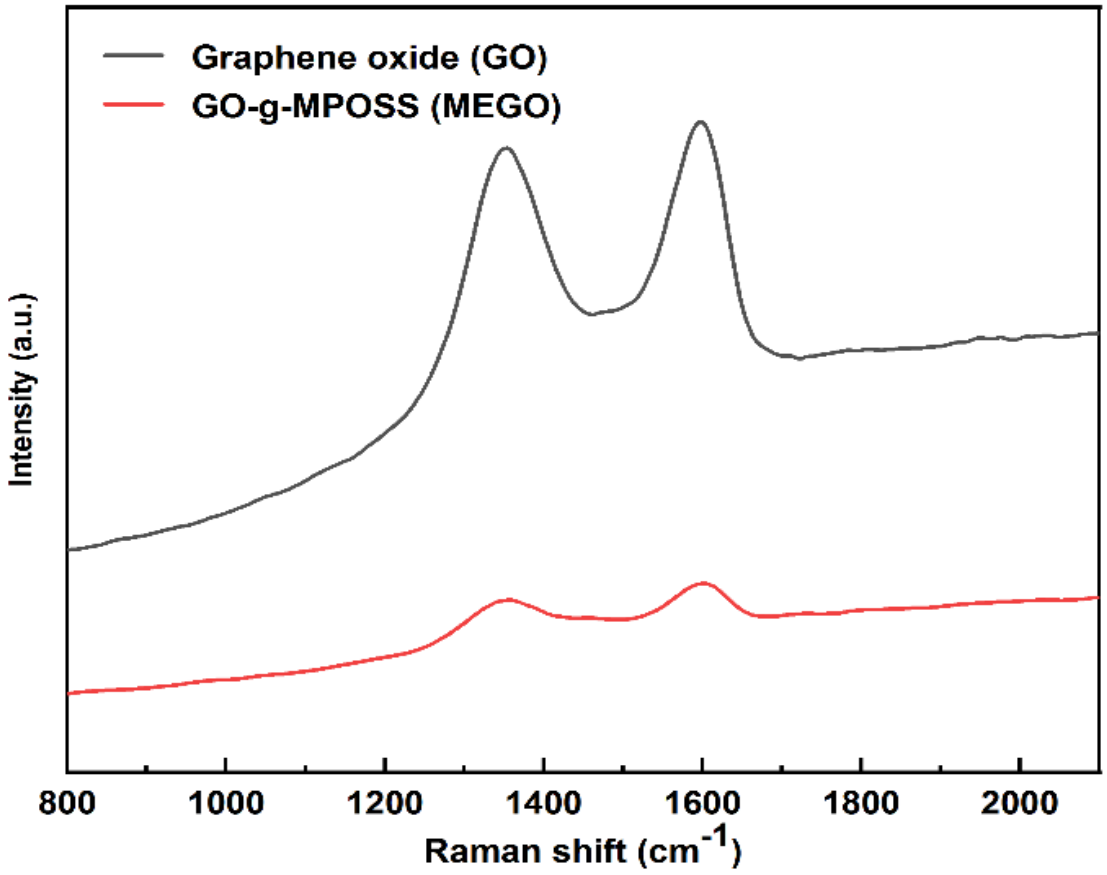

Fig. 2.9: Obtained Raman spectra of GO & MEGO.

spectra was calculated by using the area under the Gaussian fitted curve for D-band and G-band. Table 2.2 and 2.3 displays all statistical information for the fitted curve for D

and G band of MEGO and GO respectively. The increased I_D/I_G ratio of MEGO (1.43) in comparison to that of GO (1.30) confirms the increased structural distortion induced by

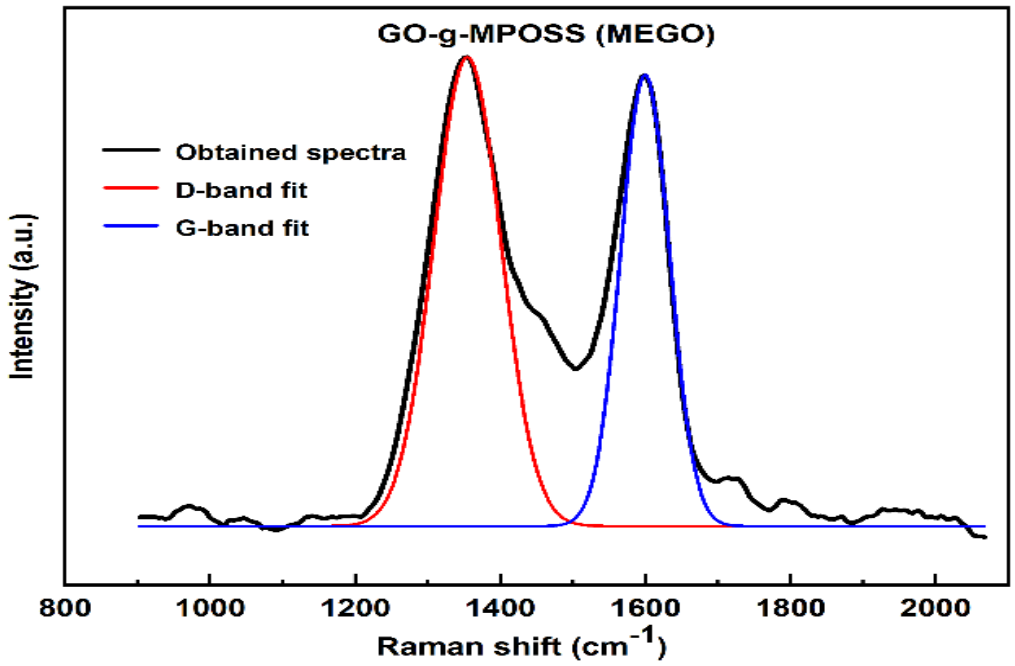

Fig. 2.10: D & G bands fitted raman spectra with baseline correction for MEGO.

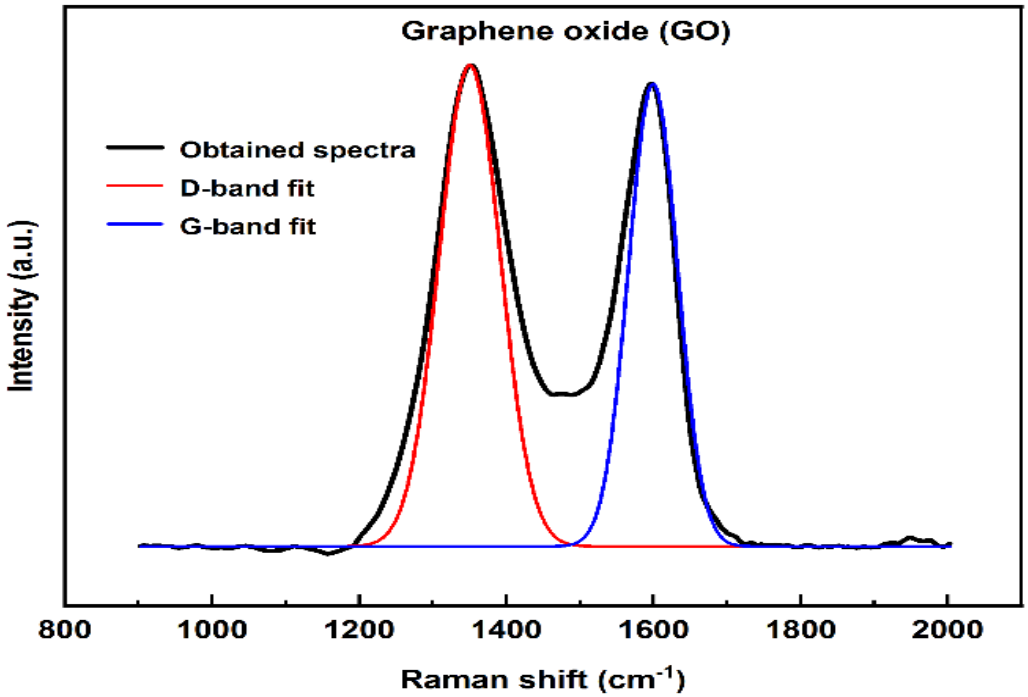

Fig. 2.11: D & G bands fitted raman spectra with baseline correction for GO.

the incorporation of MAPOSS. These results concur with previously reported results by other groups [35, 41].

Table 2.2: Statistical data for D and G - band fit for Raman spectra of MEGO.

Model	**Gaussian fit for MEGO**	
Equation	$Y = Y_o + \frac{A}{w \times \sqrt{\frac{\pi}{4 \times \ln(2)}}} \times e^{\frac{-4\ln(2) \times (x - x_c)^2}{w^2}}$	
Plot	D-band fit	G-band fit
$\boldsymbol{Y_o}$	-2.65 ± 1.14	-2.65 ± 1.14
$\boldsymbol{x_c}$	1354.39 ± 1.65	1599.33 ± 1.44
$\boldsymbol{A}$	16101.30 ± 571.17	11250.24 ± 464.40
$\boldsymbol{w}$	109.51 ± 4.10	79.54 ± 3.53
Reduced Chi-Sqr	240.69	
R-Square (COD)	0.87	
Adj. R-Square	0.87	

Table 2.3: Statistical data for D and G - band fit for Raman spectra of GO.

Model	**Gaussian fit for GO**	
Equation	$Y = Y_o + \frac{A}{w \times \sqrt{\frac{\pi}{4 \times \ln(2)}}} \times e^{\frac{-4\ln(2) \times (x - x_c)^2}{w^2}}$	
Plot	D-band fit	G-band fit
$\boldsymbol{Y_o}$	-0.82± 6.87	-0.82 ± 6.87
$\boldsymbol{x_c}$	1350.24 ± 1.56	1599.33 ± 1.43
$\boldsymbol{A}$	83772.94 ± 3128.05	64412.05 ± 2697.81
$\boldsymbol{w}$	97.97 ± 3.87	78.38 ± 3.52
Reduced Chi-Sqr	8154.05	
R-Square (COD)	0.87	
Adj. R-Square	0.87	

2.4.5 Transmission Electron Microscopy (TEM)

Changes in the microstructure of the GO are expected due to the modifications. TEM analysis was carried out to investigate the microstructure of GO and MEGO. Fig. 5a shows the TEM micrograph of GO, where a very thin and wrinkled surface of GO with sharp edges can be clearly observed. Such wrinkled structures in GO are attributed to the presence of oxygen-containing functional groups [9, 42]. When compared with GO, the micrograph of MEGO (Fig. 5b) displays distinct and dark circular patches with irregular edges. This is due to the grafting of MAPOSS to GO, which supports the previous results.

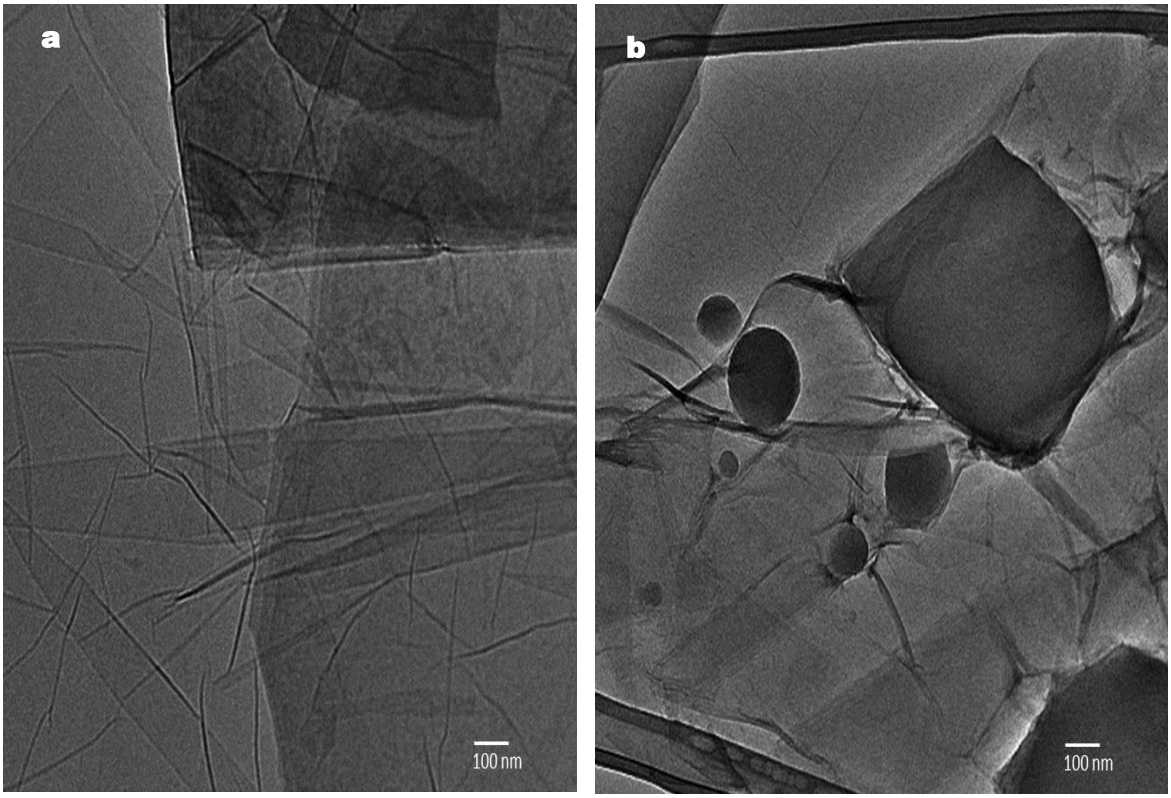

Fig. 2.12. TEM images of (a) GO (b) MEGO.

2.4.6 Thermogravimetric Analysis (TGA)

Thermal decomposition behaviors are inherent structural properties of materials. TGA is a convenient method to identify the thermal stability of different materials and can be used to calculate the amount of grafted entities on parent materials. Derivative thermogravimetric (DTG) is a thermal analysis mode, where the rate of material weight change upon heating is plotted against temperature. Such a plot can simplify the differentiation of the weight versus temperature thermogram peaks which may occur close to one another. TGA/DTG helps to understand the thermal stability of MEGO, GO and MAPOSS, and estimate the amount of grafted MAPOSS on GO. Fig. 2.13 and 2.14 shows the thermal stability of nanofillers MEGO, GO, and MA-POSS under Air and Nitrogen atmosphere, respectively.

TGA/DTG curve of GO presents three step degradations in both air and nitrogen atmosphere. The degradation at about 110°C is mainly due to the loss of water and loosely bonded molecules, while the rapid weight loss in the range 110 – 400 °C corresponds to the pyrolysis of the oxygen-containing functional groups [43]. The degradation of the carbon backbone occurs at 400 – 850 °C producing ~2% char yield. Both air and nitrogen atmosphere shows quite similar weight loss process up to 600 °C, after which the carbon combustion becomes more rapid for air, compared to N_2 because of difference in inertness of combustion atmosphere.

The thermogravimetric profile of MAPOSS showed that the thermal degradation (T_d) at 5% weight loss is about 335 °C at both air and nitrogen atmosphere. The two-step weight loss of MEGO includes 335 – 500 °C (decomposition of all eight methacrylate substituents) and 500 – 850 ºC (breakdown of the Si_8O_8 cage). This infers that the higher

thermal stability of MAPOSS is due to the existence of the Si-O-Si cage at the core [44, 45]. In addition, the weight loss up to 900 °C is 65% and 55% for Air and N_2 atmosphere, respectively. Each result infers that the higher thermal stability of MAPOSS is due to the existence of the Si-O-Si cage at the core[44].

Compared with pure GO, functionalized GO with MAPOSS (MEGO) exhibits better thermal stability with a four-step weight loss process. The first step, up to 110 °C relates to the loss of water and loosely bonded molecules, 110 – 350 °C is mainly due to the loss of oxygen-containing functional group, 350 – 520 °C corresponds to the degradation of grafted methacrylate substituents of MAPOSS, and the final weight loss from 520 – 850 °C corresponds to the Si-O-Si cage breakdown and carbon combustion. From the comparison of the TGA/DTG curves of MEGO and GO, it can be surmised that the grafting of MAPOSS on GO was successful in significantly improving the thermal stability of MEGO.

The char yield at higher temperatures is of significance when it comes to the flame retardancy of MEGO as well as resin blends containing MEGO. The ability of a material to form a large amount of char suppresses its flammability. The residual weight of MEGO was about 16% and 22% at 850 °C for air and nitrogen atmosphere respectively, which suggests that MEGO has better thermal stability than GO (residual weight ~ 2% for both atmospheres).

Table 2.4: Onset degradation temperature (T_d) at 10% wt. loss and char yield at 900 °C

Sample	T_d at 10% in °C		Char Yield %	
	Air	Nitrogen	Air	Nitrogen
GO	153	143.3	1.62	2.51
MEGO	201	216.4	16.06	21.6

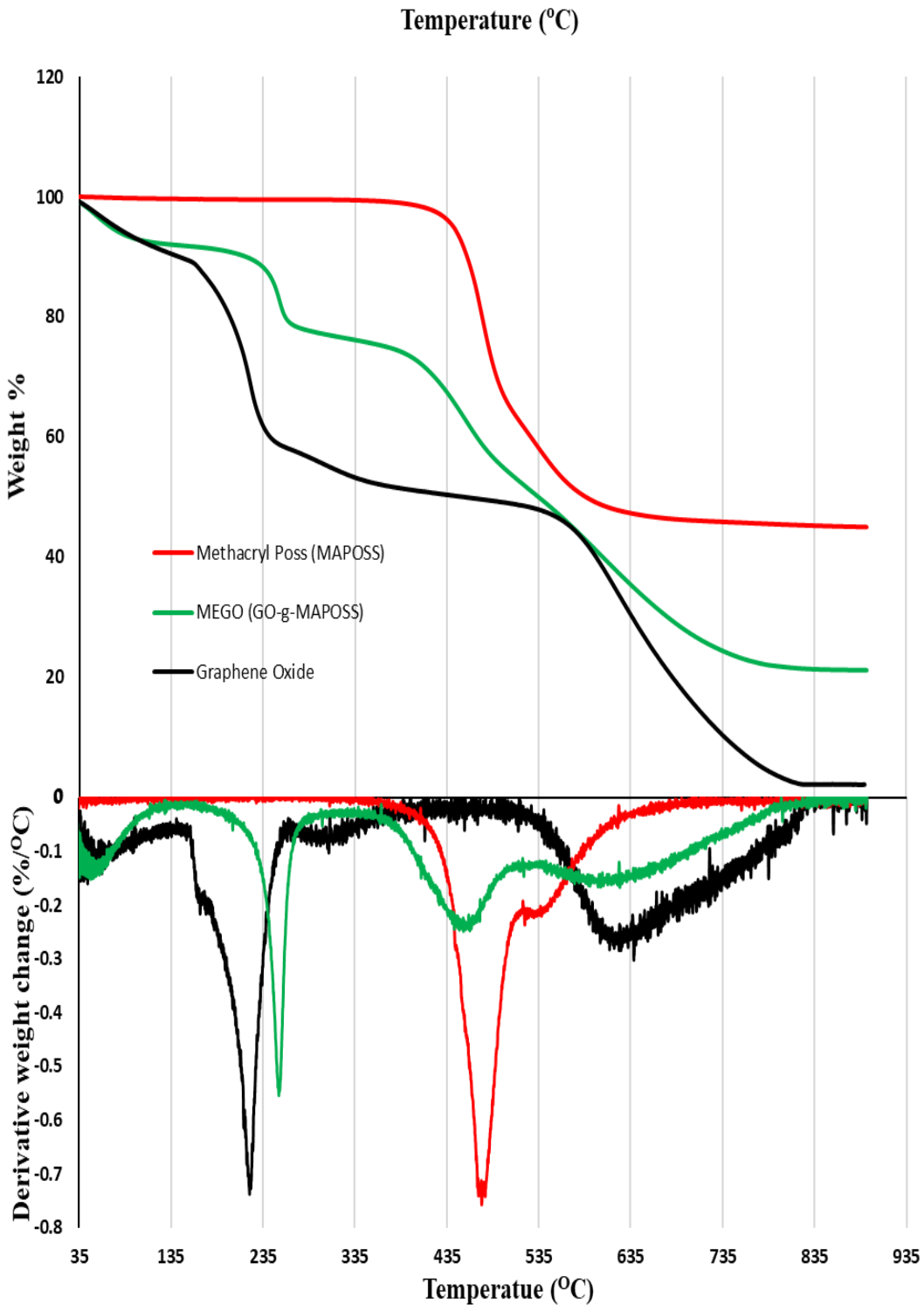

Fig. 2.13. TGA/DTG curves of GO, MAPOSS and MEGO under N_2 atmosphere.

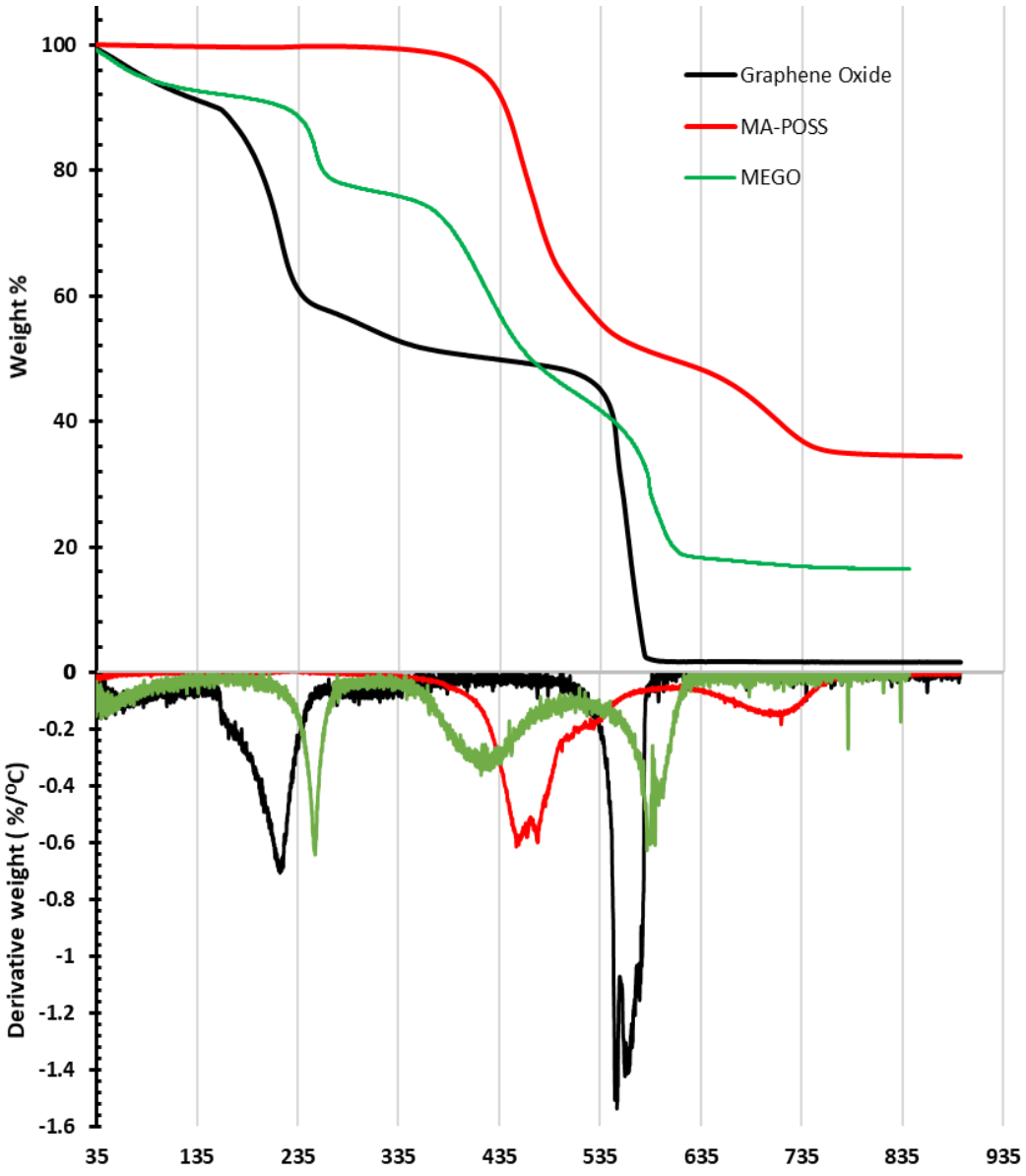

Fig. 2.14: TGA/DTG curves for GO, MAPOSS and MEGO under air atmosphere.

2.4.7 Particle size analysis in a resin system

The mechanical properties of polymer matrix composites with nano-additives are controlled by the dispersion of the nano-additives. This is due to the fact that the agglomeration of nano-additives can result in stress concentrations leading to premature failure. Previous research by Mishra et al. suggested that there was a limit to the amount of GO or POSS individually that could be added to epoxy matrices [46]. The dispersion of MEGO in EPON 862 was examined using five different dispersion methods and the results are shown in Table 2. The terminology used in the dispersion analysis table are defined as follows:

a) Particle size range – Difference between smallest and largest particle in the dispersion

b) Number density – Number of particles observed in the field of view. Category of number density is defined as:

   High: number of particles in the field of view greater than 25.

   Medium: number of particles in the field of view between 10 and 25.

   Low: number of particles in the field of view less than 10.

c) Air bubble: Minimum or no presence of air bubble is desired for better dispersion.

The dispersion analysis under an optical microscope is displayed in Fig. 2.15 – 2.20, and the analyzed data are summarized in Table 2.5. The tabulated result suggests that a three-roll mill (3R) and three-roll mill followed by ultra-sonication (3R+S) dispersion of wet MEGO in EPON 862 shows promising dispersion method for further mechanical

analysis. Also, for all dispersion methods, dispersion of wet MEGO leads to better dispersion in epoxy than dry powder MEGO.

Table 2.5: Summarized result of wet and dry GO/MEGO with different dispersion

GO dispersion in EPON 862	Particle size range(μm)		Number density		Air bubble(μm)	
	Wet	Dry	Wet	Dry	Wet	Dry
Three-roll mill	17.4-221.3	260-1490	High	Medium	No	No

MEGO dispersion in EPON 862	Particle size range(μm)		Number density		Air bubble(μm)	
	Wet	Dry	Wet	Dry	Wet	Dry
Shear Mixing	19.9-70.8	21.9 -77.7	High	High	No	No
Speed Mixing	25.3-48.3	24.5-68.9	High	High	25.3-31.6	No
Ultrasonication	19.5-49.46	25.5-64.1	High	High	No	No
Three-roll milling	20.5-44.5	16.2-99.2	Medium	High	138.37	No
Three-roll mill followed by Ultrasonication	14.1-29.9	15.43-62.92	low	High	No	No

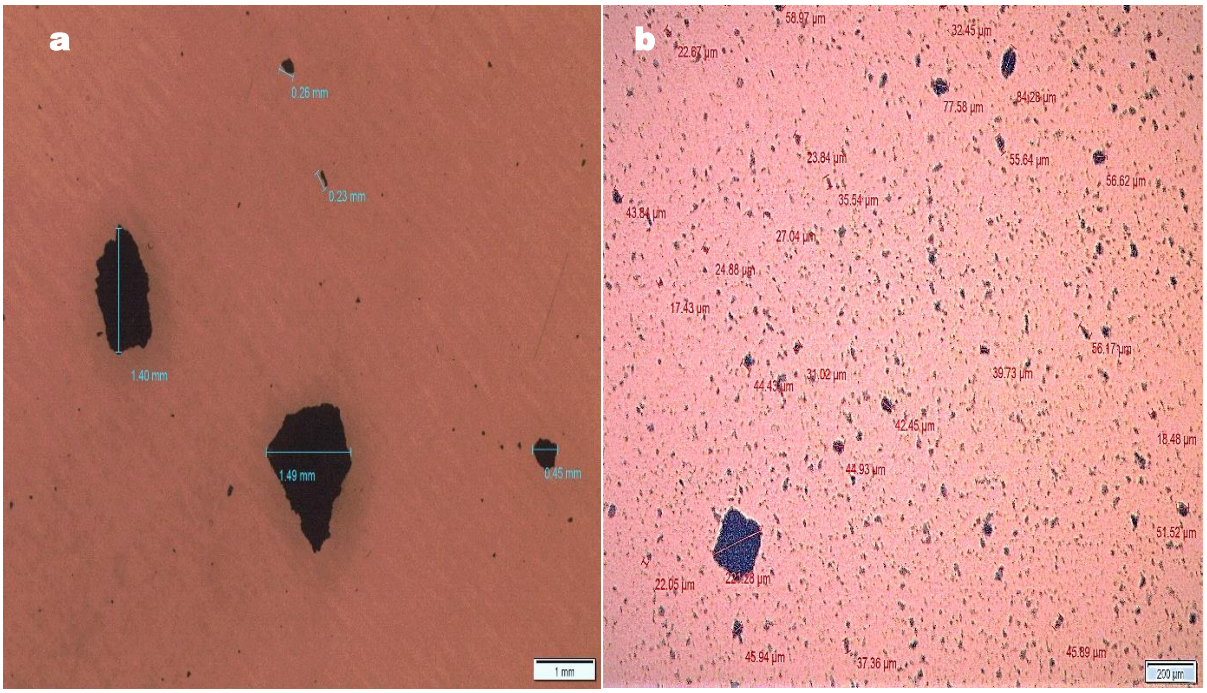

Fig.2.15. Optical microscopy of 0.1% dispersion of dry (a) and wet (b) GO in EPON 862 by three-roll mill.

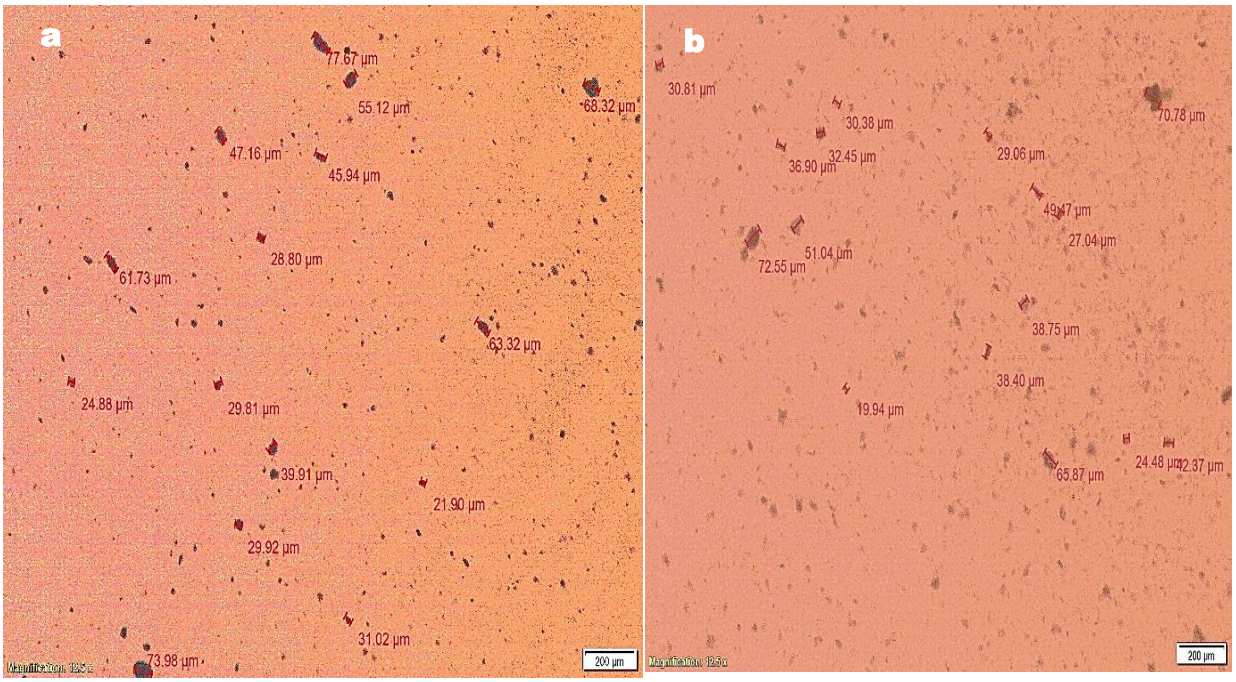

Fig.2.16. Optical microscopy of 0.1% dispersion of dry (a) and wet (b) MEGO in EPON 862 by shear mixing followed by negative vacuum pressure.

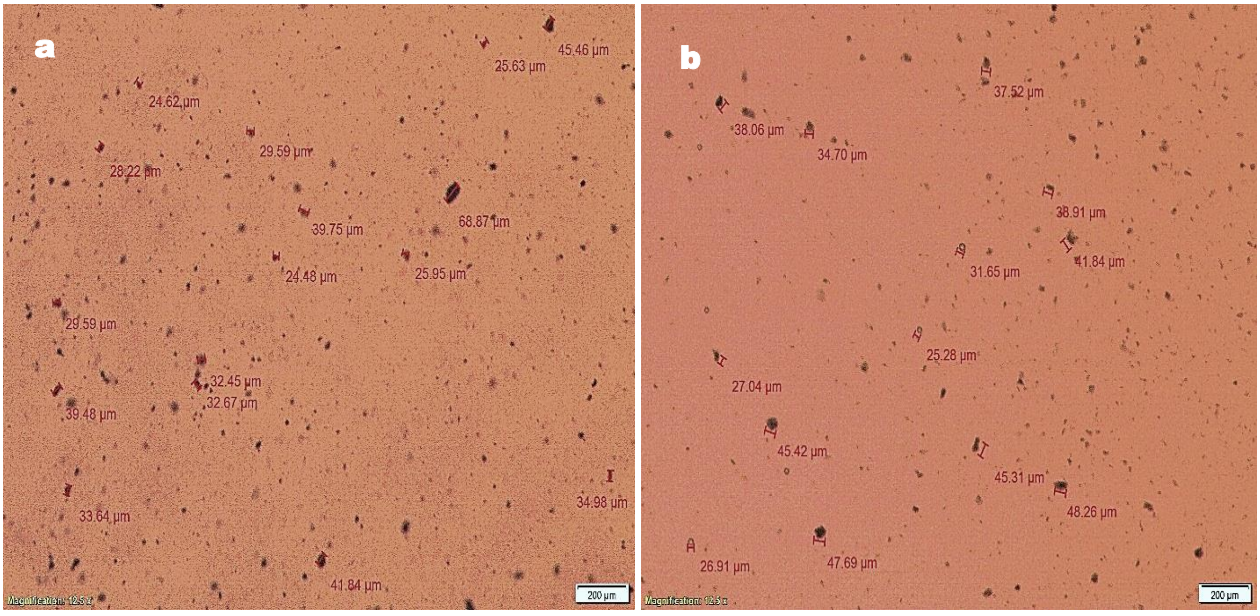

Fig.2.17. Optical microscopy of 0.1% dispersion of dry (a) and wet (b) MEGO in EPON 862 by the speed mixing method.

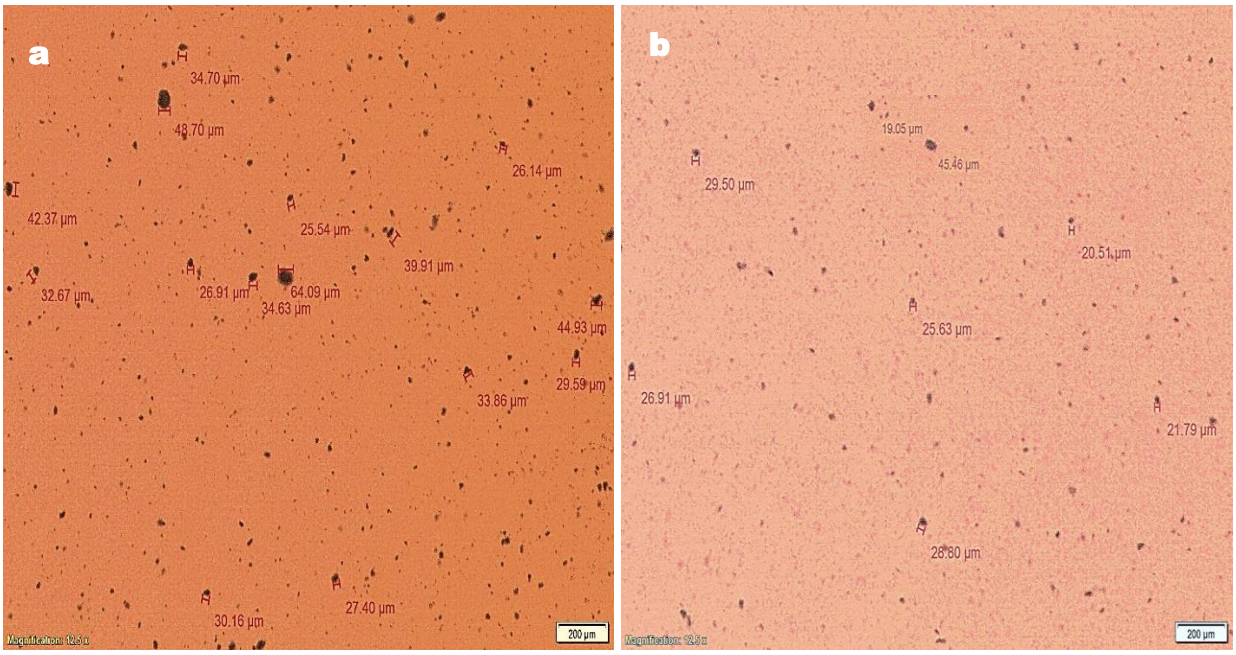

Fig.2.18. Optical microscopy of 0.1% dispersion of dry (a) and wet (b) MEGO in EPON 862 by ultra-sonication method.

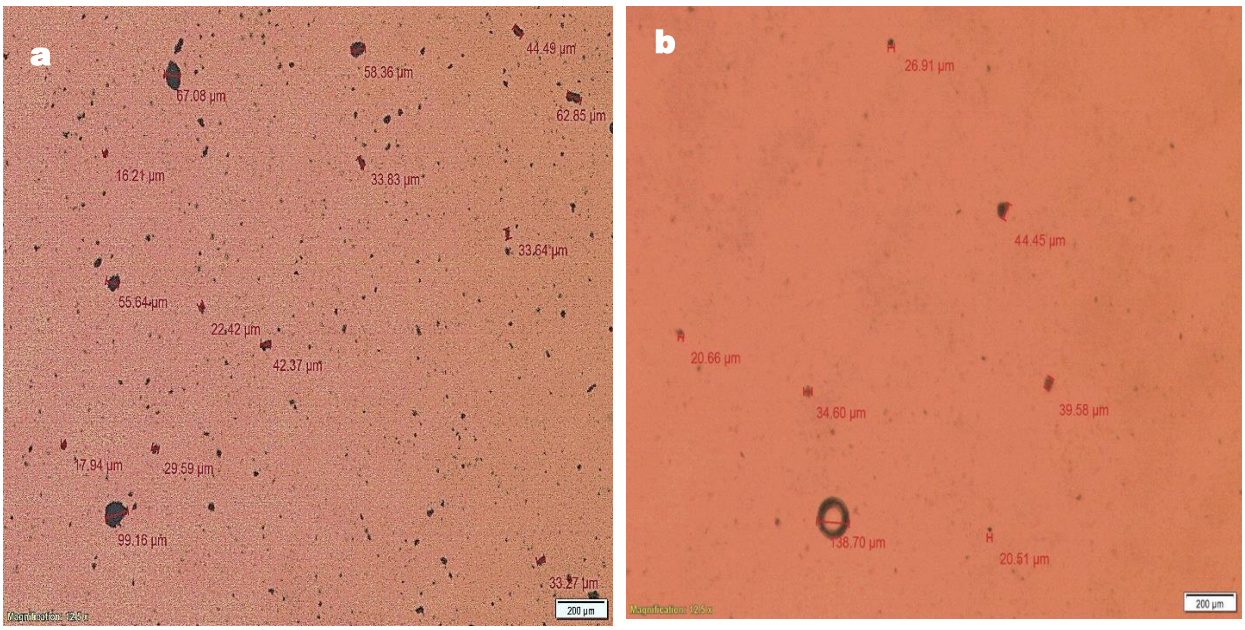

Fig.2.19. Optical microscopy of 0.1% dispersion of dry (a) and wet (b) MEGO in EPON 862 by three roll-mill method.

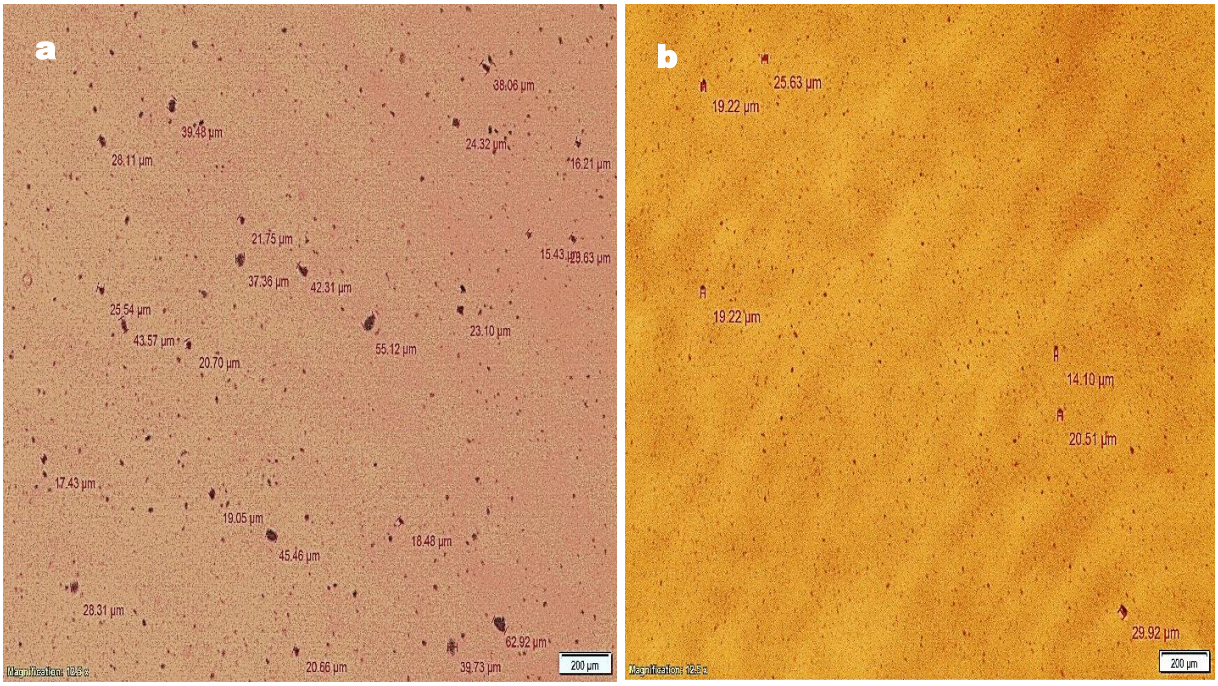

Fig.2.20. Optical microscopy of 0.1% dispersion of dry (a) and wet (b) MEGO in EPON 862 by three-roll mill followed by ultra-sonication.

2.5. Conclusions:

A simple and scalable process was developed for the modification of GO by grafting MAPOSS. Analysis of FTIR and XRD spectra confirmed the reaction between MAPOSS and GO. The XRD peak was reduced by 0.95°, inferring that the modification of GO with MAPOSS increased the interlaminar distance of GO by 0.8 Å. The decrease in intensity of the peak in the XRD spectrum confirms the increase in random orientation of the hybrid material. XRF result showed that 10.2 mass % of silicon was added to GO because of MAPOSS grafting. The increased ratio of I_D/I_G ($(I_D/I_G)_{GO} = 1.30$, $(I_D/I_G)_{MEGO} = 1.43$) in Raman spectroscopy is totally in agreement with the FTIR, XRD and XRF results. In addition, TEM images also support the hybridization of MAPOSS on GO. TGA curves showed a significant improvement in thermal stability and char yield (2% increased to 22%) after the hybridization. The particle size distribution studies indicated that the wet hybrid material showed better dispersion than dry MEGO. The use of the three-roll mill followed by ultra-sonication, showed excellent dispersion of MEGO in EPON 862 resin. This dispersion method could be a potential method to enhance the mechanical and thermal properties of polymer nanocomposites. These results emphasize an efficient way for further investigating GO/polymer composite and may lead to a better approach to enhance mechanical and thermal properties of polymer composites. As a continued part of this work, the methods of two dispersion three-roll mill and three-roll mill followed by ultra-sonication for wet MEGO will be considered for composite fabrication.

REFERENCES:

1. Pascault, J., H. Sautereau, J. Verdu, and R. Williams, *Are cured thermosets inhomogeneous?* Thermosetting Polymers. New York: Marcel Dekker, 2002.
2. He, S., N.D. Petkovich, K. Liu, Y. Qian, C.W. Macosko, and A. Stein, *Unsaturated polyester resin toughening with very low loadings of GO derivatives.* Polymer, 2017. **110**: p. 149-157.
3. Nadler, M., J. Werner, T. Mahrholz, U. Riedel, and W. Hufenbach, *Effect of CNT surface functionalisation on the mechanical properties of multi-walled carbon nanotube/epoxy-composites.* Composites Part A: Applied Science and Manufacturing, 2009. **40**(6-7): p. 932-937.
4. Hernández-Pérez, A., F. Avilés, A. May-Pat, A. Valadez-González, P. Herrera-Franco, and P. Bartolo-Pérez, *Effective properties of multiwalled carbon nanotube/epoxy composites using two different tubes.* Composites Science and Technology, 2008. **68**(6): p. 1422-1431.
5. Fang, M., K. Wang, H. Lu, Y. Yang, and S. Nutt, *Covalent polymer functionalization of graphene nanosheets and mechanical properties of composites.* Journal of Materials Chemistry, 2009. **19**(38): p. 7098-7105.
6. Wang, X., W. Xing, P. Zhang, L. Song, H. Yang, and Y. Hu, *Covalent functionalization of graphene with organosilane and its use as a reinforcement in epoxy composites.* Composites science and technology, 2012. **72**(6): p. 737-743.
7. Li, Z., R. Wang, R.J. Young, L. Deng, F. Yang, L. Hao, W. Jiao, and W. Liu, *Control of the functionality of graphene oxide for its application in epoxy nanocomposites.* Polymer, 2013. **54**(23): p. 6437-6446.

8. Ji, X., L. Cui, Y. Xu, and J. Liu, *Non-covalent interactions for synthesis of new graphene based composites.* Composites Science And Technology, 2015. **106**: p. 25-31.

9. Pour, Z.S. and M. Ghaemy, *Polymer grafted graphene oxide: for improved dispersion in epoxy resin and enhancement of mechanical properties of nanocomposite.* Composites Science and Technology, 2016. **136**: p. 145-157.

10. Rezić, I., T. Haramina, and T. Rezić, *Metal nanoparticles and carbon nanotubes—perfect antimicrobial nano-fillers in polymer-based food packaging materials*, in *food packaging*. 2017, Elsevier. p. 497-532.

11. Wong, C. and R.S. Bollampally, *Thermal conductivity, elastic modulus, and coefficient of thermal expansion of polymer composites filled with ceramic particles for electronic packaging.* Journal of applied polymer science, 1999. **74**(14): p. 3396-3403.

12. Bauhofer, W. and J.Z. Kovacs, *A review and analysis of electrical percolation in carbon nanotube polymer composites.* Composites science and technology, 2009. **69**(10): p. 1486-1498.

13. Shen, C., Y. Zhou, R. Dou, W. Wang, B. Yin, and M.-b. Yang, *Effect of the core-forming polymer on phase morphology and mechanical properties of PA6/EPDM-g-MA/HDPE ternary blends.* Polymer, 2015. **56**: p. 395-405.

14. Ferri, J.M., O. Fenollar, A. Jorda-Vilaplana, D. García-Sanoguera, and R. Balart, *Effect of miscibility on mechanical and thermal properties of poly (lactic acid)/polycaprolactone blends.* Polymer International, 2016. **65**(4): p. 453-463.

15. Huang, A., X. Peng, and L.-S. Turng, *In-situ fibrillated polytetrafluoroethylene (PTFE) in thermoplastic polyurethane (TPU) via melt blending: Effect on rheological behavior, mechanical properties, and microcellular foamability.* Polymer, 2018. **134**: p. 263-274.

16. Gudarzi, M.M. and F. Sharif, *Enhancement of dispersion and bonding of graphene-polymer through wet transfer of functionalized graphene oxide.* Express Polymer Letters, 2012. **6**(12).

17. Huang, X., Z. Yin, S. Wu, X. Qi, Q. He, Q. Zhang, Q. Yan, F. Boey, and H. Zhang, *Graphene-based materials: synthesis, characterization, properties, and applications.* small, 2011. **7**(14): p. 1876-1902.

18. Norhayati, H., M. Zuhailimuna, H. Mohd Zobir, M.I. Illyas, M. Azmi, K. Azlan, A.B. Suriani, M. Mazidah, and J. AdilaMohamad, *A Brief Review On Recent Graphene Oxide-Based Material Nanoco Mposites: Synthesis And Applications.* 2016.

19. Noh, Y.J., H.-I. Joh, J. Yu, S.H. Hwang, S. Lee, C.H. Lee, S.Y. Kim, and J.R. Youn, *Ultra-high dispersion of graphene in polymer composite via solvent freefabrication and functionalization.* Scientific reports, 2015. **5**(1): p. 1-7.

20. Liu, J., G. Liu, and W. Liu, *Preparation of water-soluble β-cyclodextrin/poly (acrylic acid)/graphene oxide nanocomposites as new adsorbents to remove cationic dyes from aqueous solutions.* Chemical Engineering Journal, 2014. **257**: p. 299-308.

21. Chauke, V.P., A. Maity, and A. Chetty, *High-performance towards removal of toxic hexavalent chromium from aqueous solution using graphene oxide-alpha*

cyclodextrin-polypyrrole nanocomposites. Journal of Molecular Liquids, 2015. **211**: p. 71-77.

22. Mkhoyan, K.A., A.W. Contryman, J. Silcox, D.A. Stewart, G. Eda, C. Mattevi, S. Miller, and M. Chhowalla, *Atomic and electronic structure of graphene-oxide.* Nano letters, 2009. **9**(3): p. 1058-1063.
23. Lin, Z., Y. Liu, Z. Li, and C.-p. Wong,Lin, Z., Y. Liu, Z. Li, and C.-p. Wong, *Novel preparation of functionalized graphene oxide for large scale, low cost, and self-cleaning coatings of electronic devices*. in *2011 IEEE 61st Electronic Components and Technology Conference (ECTC)*. 2011. IEEE.
24. Antoniou, K.S., M. Karakassides, D. Gournis, and P. Rudolf, *Carbon nanostructures containing polyhedral oligomeric silsesquioxanes (POSS).* Chemistry, 2016. **20**(6): p. 662-673.
25. Król-Morkisz, K. and K. Pielichowska, *Thermal decomposition of polymer nanocomposites with functionalized nanoparticles*, in *Polymer Composites with Functionalized Nanoparticles*. 2019, Elsevier. p. 405-435.
26. Kuo, S.-W. and F.-C. Chang, *POSS related polymer nanocomposites.* Progress in polymer science, 2011. **36**(12): p. 1649-1696.
27. Pielichowski, K., J. Njuguna, B. Janowski, and J. Pielichowski, *Polyhedral oligomeric silsesquioxanes (POSS)-containing nanohybrid polymers*, in *Supramolecular Polymers Polymeric Betains Oligomers*. 2006, Springer. p. 225-296.

28. Zhao, J., Y. Fu, and S. Liu, *Polyhedral oligomeric silsesquioxane (POSS)-modified thermoplastic and thermosetting nanocomposites: a review.* Polymers and Polymer Composites, 2008. **16**(8): p. 483-500.

29. Gnanasekaran, D., K. Madhavan, and B. Reddy, *Developments of polyhedral oligomeric silsesquioxanes (POSS), possnanocomposites and their applications: A review.* 2009.

30. Ayandele, E., B. Sarkar, and P. Alexandridis, *Polyhedral oligomeric silsesquioxane (POSS)-containing polymer nanocomposites.* Nanomaterials, 2012. **2**(4): p. 445-475.

31. Xue, Y., Y. Liu, F. Lu, J. Qu, H. Chen, and L. Dai, *Functionalization of graphene oxide with polyhedral oligomeric silsesquioxane (POSS) for multifunctional applications.* The journal of physical chemistry letters, 2012. **3**(12): p. 1607-1612.

32. Yu, W., J. Fu, X. Dong, L. Chen, and L. Shi, *A graphene hybrid material functionalized with POSS: Synthesis and applications in low-dielectric epoxy composites.* Composites science and technology, 2014. **92**: p. 112-119.

33. Wang, X., L. Song, H. Yang, W. Xing, B. Kandola, and Y. Hu, *Simultaneous reduction and surface functionalization of graphene oxide with POSS for reducing fire hazards in epoxy composites.* Journal of Materials Chemistry, 2012. **22**(41): p. 22037-22043.

34. Valentini, L., S.B. Bon, O. Monticelli, and J.M. Kenny, *Deposition of amino-functionalized polyhedral oligomeric silsesquioxanes on graphene oxide sheets immobilized onto an amino-silane modified silicon surface.* Journal of Materials Chemistry, 2012. **22**(13): p. 6213-6217.

35. Qu, L., Y. Sui, C. Zhang, P. Li, X. Dai, B. Xu, and D. Fang, *POSS-functionalized graphene oxide hybrids with improved dispersive and smoke-suppressive properties for epoxy flame-retardant application.* European Polymer Journal, 2020. **122**: p. 109383.

36. Valentini, L., M. Cardinali, J.M. Kenny, M. Prato, and O. Monticelli, *A photoresponsive hybrid nanomaterial based on graphene and polyhedral oligomeric silsesquioxanes.* European Journal of Inorganic Chemistry, 2012. **2012**(32): p. 5282-5287.

37. Galande, C., A.D. Mohite, A.V. Naumov, W. Gao, L. Ci, A. Ajayan, H. Gao, A. Srivastava, R.B. Weisman, et al., *Quasi-molecular fluorescence from graphene oxide.* Scientific reports, 2011. **1**(1): p. 1-5.

38. Yu, B., K. Wang, Y. Hu, F. Nan, J. Pu, H. Zhao, and P. Ju, *Tribological properties of synthetic base oil containing polyhedral oligomeric silsesquioxane grafted graphene oxide.* RSC advances, 2018. **8**(42): p. 23606-23614.

39. Guo, D., J. Chen, L. Wen, P. Wang, S. Xu, J. Cheng, X. Wen, S. Wang, C. Huang, et al., *A superhydrophobic polyacrylate film with good durability fabricated via spray coating.* Journal of Materials Science, 2018. **53**(22): p. 15390-15400.

40. De Silva, K.K.H., H.-H. Huang, and M. Yoshimura, *Progress of reduction of graphene oxide by ascorbic acid.* Applied Surface Science, 2018. **447**: p. 338-346.

41. Ye, Y., D. Zhang, J. Li, T. Liu, J. Pu, H. Zhao, and L. Wang, *One-step synthesis of superhydrophobic polyhedral oligomeric silsesquioxane-graphene oxide and*

its application in anti-corrosion and anti-wear fields. Corrosion Science, 2019. **147**: p. 9-21.

42. Zhang, C., T. Li, H. Song, Y. Han, Y. Dong, Y. Wang, and Q. Wang, *Improving the thermal conductivity and mechanical property of epoxy composites by introducing polyhedral oligomeric silsesquioxane-grafted graphene oxide.* Polymer Composites, 2018. **39**(S3): p. E1890-E1899.

43. Farivar, F., P.L. Yap, K. Hassan, T.T. Tung, D.N. Tran, A.J. Pollard, and D. Losic, *Unlocking thermogravimetric analysis (TGA) in the fight against "Fake graphene" materials.* Carbon, 2021. **179**: p. 505-513.

44. Qiang, X., F. Chen, X.Y. Ma, and X.B. Hou, *Star-shaped POSS–methacrylate copolymers with phenyl–triazole as terminal groups, synthesis, and the pyrolysis analysis.* Journal of Applied Polymer Science, 2014. **131**(16).

45. Zhou, J., Y. Zhao, K. Yu, X. Zhou, and X. Xie, *Synthesis, thermal stability and photoresponsive behaviors of azobenzene-tethered polyhedral oligomeric silsesquioxanes.* New Journal of Chemistry, 2011. **35**(12): p. 2781-2792.

46. Mishra, K., K.P. Bastola, R.P. Singh, and R. Vaidyanathan, *Effect of graphene oxide on the interlaminar fracture toughness of carbon fiber/epoxy composites.* Polymer Engineering & Science, 2019. **59**(6): p. 1199-1208.

CHAPTER III

EFFECTS OF HYBRID POLYMER MODIFIER IN EPOXY COMPOSITES

Abstract:

In this work, a hybrid polymer modifier – MEGO is dispersed in an epoxy matrix has been used to improve the viscoelastic, thermal, and mechanical properties of the resulting nanocomposites. Dynamical mechanical analysis (DMA), differential scanning calorimetry (DSC), thermogravimetric analysis (TGA), flexural test, and fractography using scanning electron microscopy (SEM) were performed on neat, 0.05, 0.1, 0.25 and 0.5 wt.% MEGO filled epoxy to identify the effect of loading on the properties mentioned above. DMA result showed an increase of glass transition temperature (T_g) and storage modulus by ~ 4 °C and ~ 10%, respectively, at 0.1 wt.% MEGO loading. DSC analysis also confirmed the increase of T_g by ~ 7 °C at 0.1 wt.% MEGO loading, supporting the trend of DMA results. TGA results showed that incorporating a larger amount of additives had made the composites thermally more stable. Flexural strength and modulus of MEGO/Epoxy composite were enhanced at low wt.% loading (Maximum increase at 0.1 wt.% MEGO loading). However, at loading higher than 0.1 wt.%, T_g, flexural strength, flexural modulus was decreased, suggesting the 0.1wt.% as an upper limit for MEGO

loading. SEM fractography confirmed rougher and lesser uniform fracture surface, dendritic river-surface pattern inferring the bifurcation crack deflection mechanism for 0.05 and 0.1 wt.% MEGO loading, compared with that of the neat sample. SEM micrograph of 0.25, and 0.5 wt.% loadings revealed the aggregation of MEGO, justifying the decrease in viscoelastic and mechanical properties of MEGO/Epoxy composite.

Additionally, four-point flexural test and DCB test were performed to study the effects of MEGO on CFRP composites. Results from the tests confirmed that the interlaminar fracture toughness of CFRP can be enhanced up to ~ 70% without compromising the flexural properties. SEM images confirmed the improved fiber-matrix adhesion with addition of MEGO in matrix, justifying the improvement in fracture toughness with hybrid polymer modifier -MEGO loading.

3.1 Introduction:

Polymers are an integrated part of modern society. Synthetic polymers are some of the most extensively used materials in day-to-day life due to their unparalleled combination of lightweight, low cost, and relative ease of processing. They also gained great acceptance in the technical application because of the wide range of physical and chemical properties achievable with simple processing. Polymers properties are mainly determined by the monomer units and polymerization process[1]. Despite their wide range of properties, it is challenging to have a synthetic polymer with both superior strength, toughness, and modulus. To overcome this challenge, researchers came up with the concept of adding a secondary phase to reinforce the polymers[2, 3]. Such reinforced synthetic polymers are known as polymer composites. Specific to epoxies, carbon-based

nanofillers such as carbon nanotubes [4, 5], graphene [6, 7], and graphene oxide (GO) [8-10] are found to be effective in enhancing mechanical properties by reducing its brittleness.

Polymer nanocomposites achieve improved mechanical properties at a much lower loading level of nanoparticles than traditional composites, owing to a drastically increased interfacial area. Similarly, adding inorganic fillers into the polymer matrix can improve the electrical and thermal conductivity [11, 12], mechanical and rheological properties like modulus, impact strength, and elongation at break [13-15] of the polymer matrix. Though adding nanoparticles as a secondary phase can enhance the polymer's mechanical, thermal, and electrical properties, nanoparticle agglomeration is a serious problem faced in polymer nanocomposites [11], leading to poor dispersion. Poorly dispersed nanomaterials can have adverse effects on the strength of the composite because the nanomaterials can function as structural defects [12-14]. In carbon nanofillers, this drawback is directly connected with the van der Waal interaction and π-π stacking between the graphene sheets [15-17] and their high aspect ratios. While single-layer graphene can be produced using highly advanced techniques, it isn't easy to retain a single layer state once it is dispersed in the polymer matrix.

Achieving an excellent dispersion in polymer matrices is a challenging job. Specifically, two factors, the high surface energy of nanomaterial and the inability of polymer matrices to stabilize nanomaterial, are responsible for this challenging issue. The high surface energy of nanomaterials always triggers aggregation. At the same time, unlike protic solvents, polymer matrices are unable to stabilize the nanoparticles via repulsive force

between particles [2, 18-20]. When these two factors are active at the same time, the agglomeration problem becomes more serious.

A wide range of research, including covalent and non-covalent surface modification, has been reported to overcome the agglomeration issue. Specific to carbon-based nanoparticles, solvent casting, melt mixing, and in-situ polymerization are widely reported[21-24]. However, solvent casting and melt mixing are not suitable for thermoset polymer because they either leave residual solvent or cause irreversible curing of the polymer matrix. So, in-situ polymerization is the only viable option for producing high-quality thermoset polymer composites. This method requires dispersing graphene or its derivatives into polymer resin before mixing them with hardeners.

The easiest method, shear mixing, is not enough to provide shear stress to break down the GO agglomerates in viscous polymer resins. Better dispersion of carbon-based nanofillers in epoxy is possible by sonication [3] or three-roll milling [25], or a combination of both. Previous research indicates that the graphene oxide derivatives or their modified form can toughen thermosets at low loading levels [26-32]. For example, 0.5 wt.% triblock copolymers grafted graphene oxide enhanced the fracture toughness of epoxy resin by 400% [26].

In this work, we synthesized a hybrid polymer modifier MEGO (Synthesis and characterization of MEGO are covered in chapter 2) and dispersed it in Epon 862 to prepare polymer composites. With the different concentrations of MEGO in Epon 862, we analyzed the thermal stability, glass transition temperature, flexural strength, and modulus of polymer (Epon 862 + EPIKURE 3370) composites. In addition, we also

investigated the effect of MEGO on carbon fiber-reinforced composites too. Two mechanical tests for CFRP were successfully performed: Duel cantilever beam (DCB) test and 4- point flexural test. Scanning electron microscopy (SEM) was performed to analyze the fracture surface of the fractured area.

3.2 Materials and Methodology:

3.2.1 Materials:

A 2.5% graphene oxide dispersion in water was purchased from Graphenea Inc. (Cambridge, MA). Nitric acid, acetonitrile, and cerium ammonium nitrate (CAN) were purchased from Alpha Aesar (Haverhill, MA). Methacryl POSS (MAPOSS) cage mixture was purchased from Hybridplastics (Hattiesburg, MS). Epoxy resin EPON 862 and EPIKURE 3370 were purchased from Hexion LLC (Columbus, OH). 6K, 2 × 2 Twill Wave Carbon Fabric Fiber was purchased from FIBERGLAST DEVELOPMENT CORP (Brookville, OH). Acetone was purchased from BDH VWR analytical (Radnor, PA). All the reagents and chemicals were used without further purifications.

3.2.2 Preparation of Polymer Composites:

MAPOSS hybridized GO, i.e., MEGO, was obtained in a cake form. Cake MEGO was dried under a vacuum oven at room temperature such that the MEGO: Acetone equals 1:3 (afterward wet MEGO). A 3% MEGO master batch was prepared by mixing 300 g of Epon 862 resin with 36 g of wet MEGO (equivalent to 9 g Dry MEGO), and then the hand-mixed MEGO with resin was poured into the feed roller and collected at the apron of three-roll mill. All the 3% MEGO 3-roll mill (3R) masterbatch dispersion was

prepared throughout this research work by feeding the roller seven times for the shake of consistency. That 3% masterbatch dispersion was used in a required amount to make Neat, 0.05, 0.1, 0.25 and 0.5 wt.% polymer composite samples. In addition, to see the effects of sonication, 3% MEGO masterbatch was sonicated for 30 minutes with amplitude 40, run time 30 s, and off-time 10 s. For avoiding the overheating of resin, ultrasonication was carried out in an ice bath. Similar wt.% (Neat, 0.05, 0.1, 0.25 and 0.5 wt.%) samples were prepared for the three-roll mill followed by ultrasonication (3R+S) dispersion. The sample preparation process is summarized in Fig. 3.1.

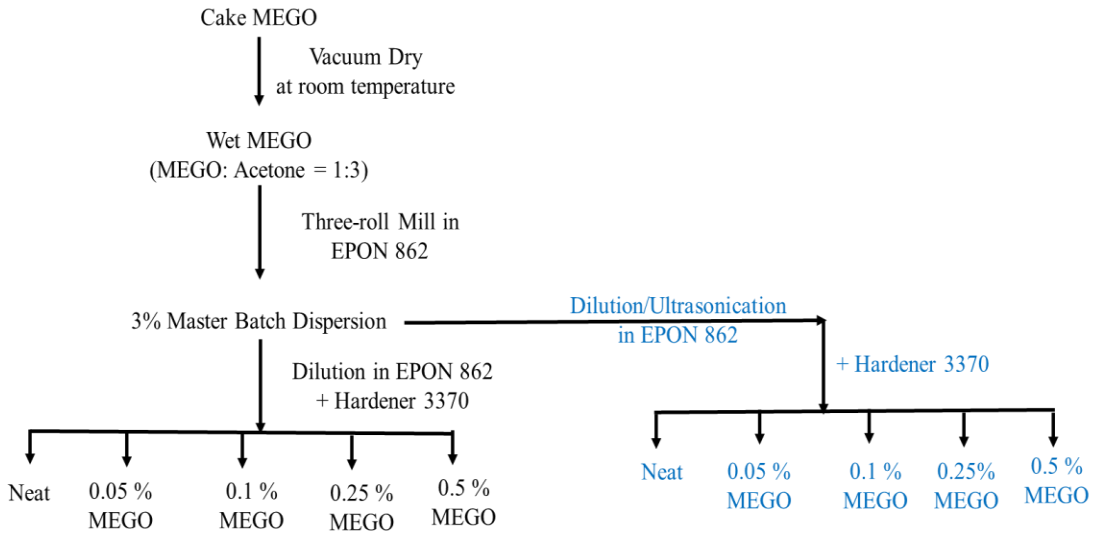

Fig. 3.1: Flow chart for polymer composite sample preparation

3.2.3 Preparation of Carbon Fiber Reinforced Polymer (CFRP) Composites:

The effect of MEGO in fiber-reinforced polymer composites is another important topic of this research. Two mechanical tests: Flexural and double cantilever beam (DCB) tests, were planned, and the samples were prepared according to their ASTM standards (ASTM 6272 and ASTM 5528). For the flexural test, four sheets of carbon fiber (CF) sheets (8"

by 8") were used, whereas 12 CF sheets (8" by 8") were used for DCB samples. Additionally, in DCB samples, a thin Teflon sheet (9µm thick, 63mm width) was inserted in the middle layer, which serves as a crack initiation during the test. Dispersion with different loading wt.% (Neat, 0.05, 0.1, 0.5) of wet MEGO in Epon 862 plus Epikure 3370 was prepared as described above in section "**Preparation of Polymer Composites**." Since no significant results were observed in polymer composite for 0.1GO and 0.25MEGO dispersion, those composition were not included in CFRP composite test analysis. Prepared dispersion was hand lay-up on the CF layers and kept under vacuum overnight. After 24 h room temperature cure process, composites were post cured at 100 °C for 2 h. For all composite samples, the ratio of Epon 862 to Epikure 3372 was taken 100: 44, as provided by the supplier. In the case of CFRP, the weight ratio of CF to Epoxy was maintained at 1: 1.1throughout the work. Figure 3.2 shows the digital image of the process and CFRP block samples.

Fig 3.2: CFRP samples and preparation process

3.3 Characterization:

3.3.1 Dynamic Mechanical Analysis (DMA):

Dynamic mechanical analysis (DMA) was carried out to analyze the viscoelastic properties of polymer composites on DMA Q800 (TA Instruments, USA). A double cantilever clamp was used at custom mode for a rectangular specimen of 55×12×3 mm^3. All tests were conducted between temperatures 30 °C and 100 °C with a temperature ramp of 5 $^{°C}$/min at frequencies of 1 Hz under custom mode.

3.3.2 Differential Scanning Calorimetry (DSC)

DSC, an effective way to determine the glass transition temperature of the polymers. DSC analysis was done using Q2000 (TA Instruments). A sample weight of around 4 mg was taken for each study. Three measurements were made for each composition, and the average and standard deviation was calculated. Aluminum Pans and Lids were obtained from DSC Consumables, Inc. The samples were loaded into the Aluminum pans and crimped with a lid. Each sample was subject to three thermal cycles. The first heating cycle was 0 to 100 °C at a rate of 5 °C/min, the second cooling cycle was 100 to 0 °C at 5 °C/min, and the final step was again heating the sample from 0 to 100 °C at 5 °C/min. The first two cycles were performed to erase of sample thermal history.

3.3.3 Thermogravimetric analysis (TGA)

Thermogravimetric analysis of polymer composites was performed using a high-resolution Thermogravimetric analyzer (TA Q-50, TA instruments, New Castle, DE). The

samples were heated at a 20 °C/min rate from room temperature to 950 °C under an air atmosphere. During the test, 40 ml/min of continuous airflow was maintained.

3.3.4 Scanning Electron Microscopy (SEM)

The polymer composite and CFRP fracture surface morphology were investigated using the Hitachi S-4800 field emission scanning electron microscope (FE-SEM). All polymer and CFRP samples were metal (Iridium) sputter coated for 90 s using Leica EM ACE600. The scanning was carried out with 10 or 15 KV for magnification 400X, 1,000X, 2,000X, and 4,000X.

3.3.5 Three-point bend test:

The flexural strength and modulus of polymer composite samples were determined by a three-point bend test on Instron 5582 according to ASTM D790[33]. The testing set up are displayed in Figure 3.3. Samples were tested at a standard crosshead motion (R) which is calculated using the formula

$$R = \frac{ZL^2}{6d}$$

Where L is the length of the support span, d is the thickness of the specimen, and Z is the rate of straining of outer fiber (taken as 0.01)

The flexural strength (σ_f) and flexural strain (ε_f) were then determined using the formula,

$$\sigma_f = \frac{3PL}{2bd^2}$$

$$\varepsilon_f = \frac{6Dd}{L^2}$$

Where P is the load, D is the maximum deflection of the center of the beam, L is the length of the support span, b is the width of the specimen, d is the thickness of the specimen.

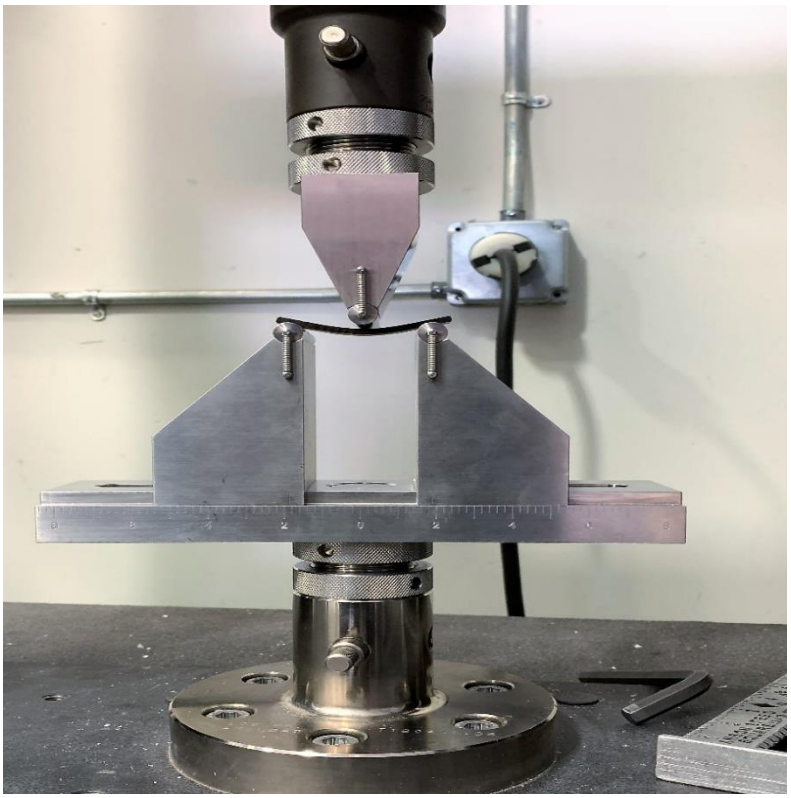

Fig.3.3: Three-point bend setup for determination of flexural properties.

Modulus of elasticity (E_b) was determined using the formula,

$$E_b = \frac{L^3 m}{4bd^3}$$

Where, m is the slope of the tangent obtained from the straight-line portion of the stress-strain curve.

3.3.6 Four-point bend test:

The flexural strength or stress in the outer fiber throughout the load span of carbon fiber polymer (CFRP) composite samples was determined by a four-point bend test on Instron 5582 according to ASTM D6272 [34]. The significant difference between four-point and three-point bending modes is the location of the maximum bending moment and maximum axial fiber stress. In four-point bending, the maximum axial fiber stress is uniformly distributed between the loading noses. In three-point bending, the maximum axial fiber stress is located immediately under the loading nose.

All carbon fiber reinforced samples were tested with a set load span equal to one-half of the support span. For one half of the support span set up (Figure 3.4), the crosshead motion is calculated using the following equation

$$R = \frac{0.167ZL^2}{d}$$

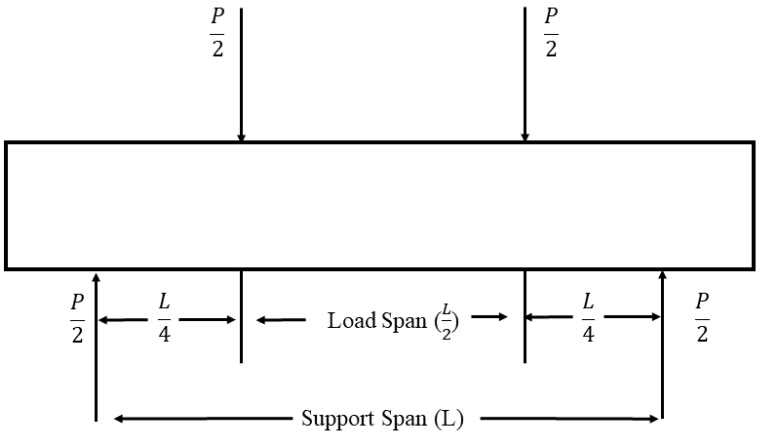

Fig.3.4: Schematic representation of four-point bend test set up

Where R is rate of crosshead motion (mm/min), L is Support span (mm), d = thickness of specimen (mm), and Z is rate of straining of the outer fibers (mm/mm. min)

The maximum stress in the outer fibers at the moment of break is equal to the flexural strength. Also, the tangent modulus of elasticity is the ratio, within the elastic limit, of stress to corresponding strain. For the load span of half of the support span, flexural strength and flexural modulus are calculated by using the following equation

$$S = \frac{3PL}{4bd^2}$$

$$E_b = \frac{0.17L^3m}{bd^3}$$

Where, S is Flexural strength or stress in the outer fiber throughout the load span (MPa), E_b is Flexural modulus (MPa), P is load at a given point on the load-deflection curve (N), L is Support span (mm), b is width of the specimen (mm), and d is thickness of specimen (mm).

3.3.7 Double Cantilever Beam Test:

The mode I interlaminar fracture toughness (G_{IC}) of continuous fiber-reinforced composite material can be determined by the test method described under ASTM 5528 [35]. A bock of CFRP with 12 piles of laminates having a non-adhesive Teflon film insert in the middle layer was cut into one inch (25.4 mm) width sample. Each sample (1" width and 8" length) were attached with the piano hinges, painted with white ink (correction ink), and marked with scale, as shown in Figure 3.5.

Fig. 3.5: Ready to test DCB samples.

One of the most reliable data analysis methods for G_{IC} calculation is Modified Beam Theory (MBT). The mathematical relation for strain energy release rate of a perfectly built-in double cantilever beam is given as

$$G_I = \frac{3P\delta}{2ba}$$

Where P is load (N), δ is crack mouth opening displacement (mm), b is specimen width (mm), a is delamination length (mm).

Since the condition of a perfect built-in sample is ideal, a correction was made on the above relation to calculate mode I interlaminar fracture toughness.

$$G_I = \frac{3P\delta}{2b(a+\Delta)}$$

A correction factor Δ is determined experimentally by generating a least-squares plot of the cube root of compliance, $C^{1/3}$, as a function of delamination length, as shown in Figure 3.6.

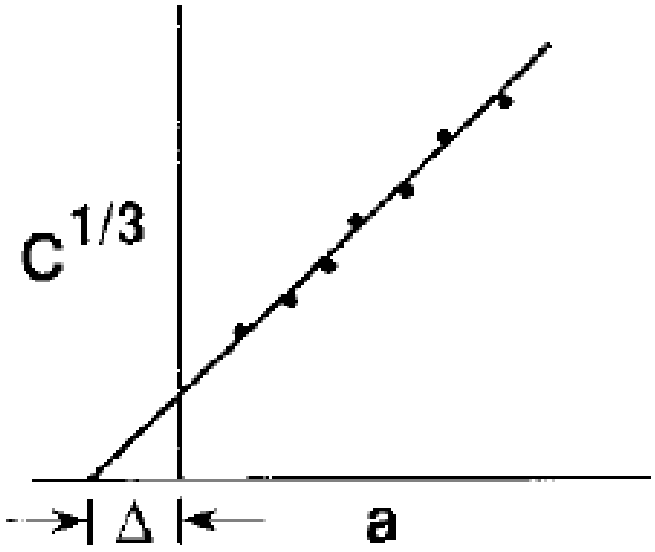

Fig. 3.6: Modified Beam Theory for determination of correction factor Δ [35]

3.4 Results and Discussion:

3.4.1 Dynamic Mechanical Analysis (DMA):

The effect of hybrid nano-filler MEGO on the viscoelastic properties of epoxy (Epon 862+Epikure 3370) matrices were studied using dynamic mechanical analysis (DMA). For each set of composition, at least five samples were tested. The tan δ and storage modulus curves as a function of temperature for neat epon 862, 0.1GO, 0.05, 0.1, 0.25, and 0.5 wt.% MEGO + Epon 862 polymer composite (three-roll mill dispersion (3R) and three-roll mill dispersion followed by ultra-sonication (3R+S) dispersion) are shown in Figure 3.7 – 3.12 and results are summarized in Table 3.1 and 3.2 respectively. Both dispersions showed a trend of increase in glass transition temperature and storage modulus up to 0.1% MEGO addition in the EPON 862. But the notable point is that the 3R+S data sets are more scattered, leading to higher standard deviation, making them less reliable to make a conclusion based on them.

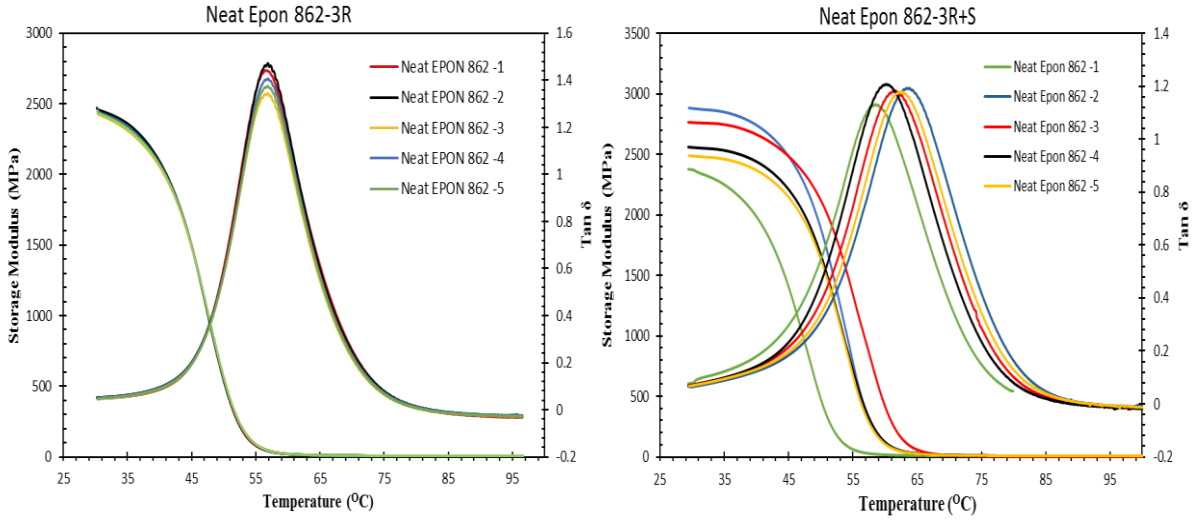

Fig. 3.7: Storage modulus and Tan δ curves for Neat Epon 862 (a) 3R and (b) 3R+S dispersion samples.

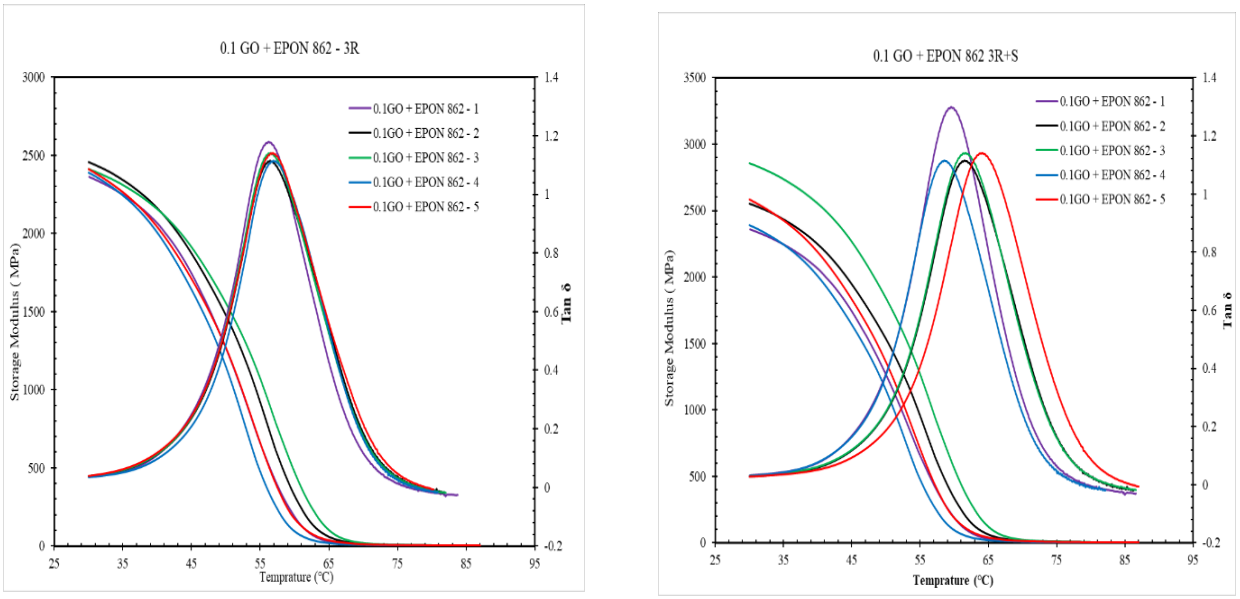

Fig. 3.8: Storage modulus and Tan δ curves for 0.1 GO + Epon 862 (a) 3R and (b) 3R+S dispersion samples.

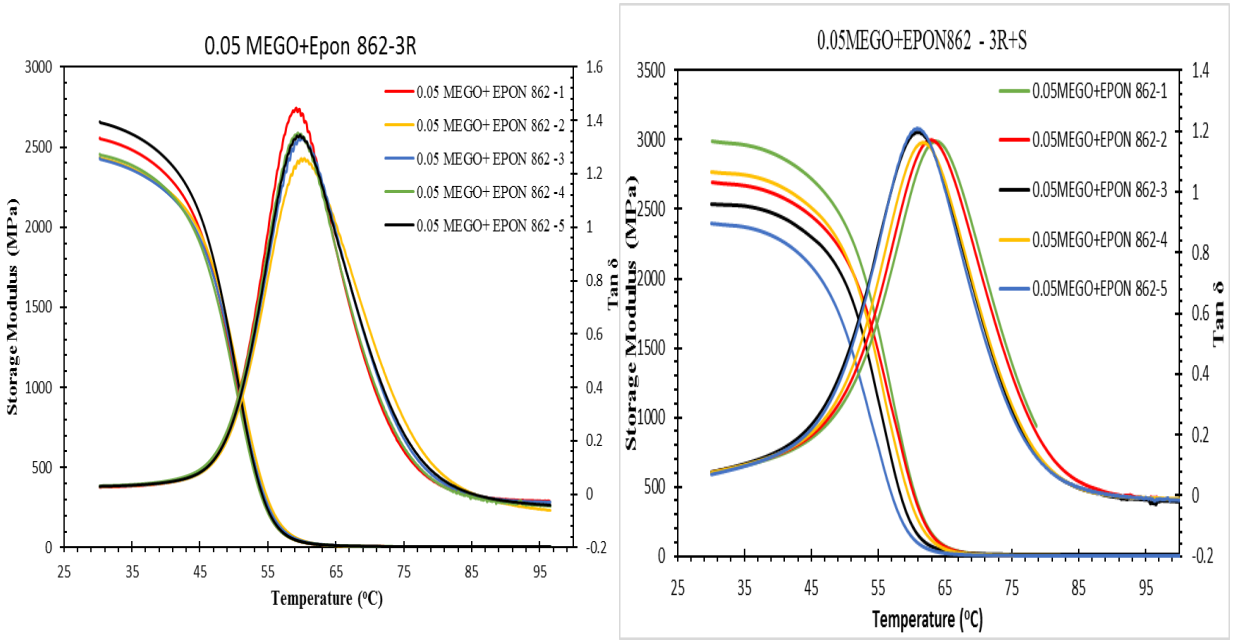

Fig. 3.9: Storage modulus and Tan δ curves for 0.05MEGO+Epon 862 (a) 3R and (b) 3R+S dispersion samples.

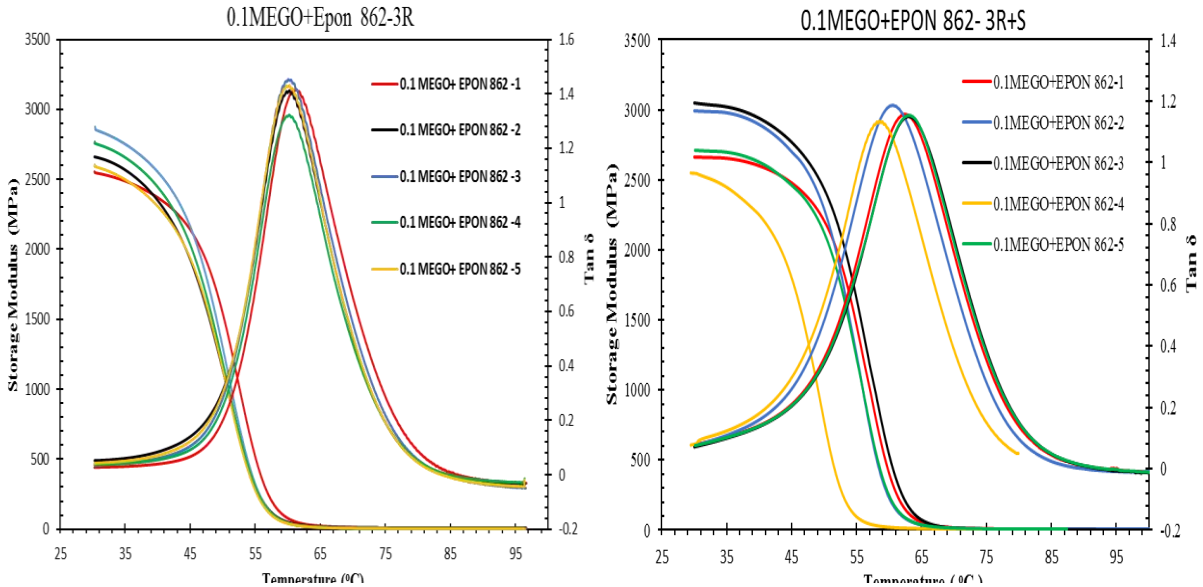

Fig. 3.10: Storage modulus and Tan δ curves for 0.1MEGO+Epon 862 (a) 3R and (b) 3R+S dispersion.

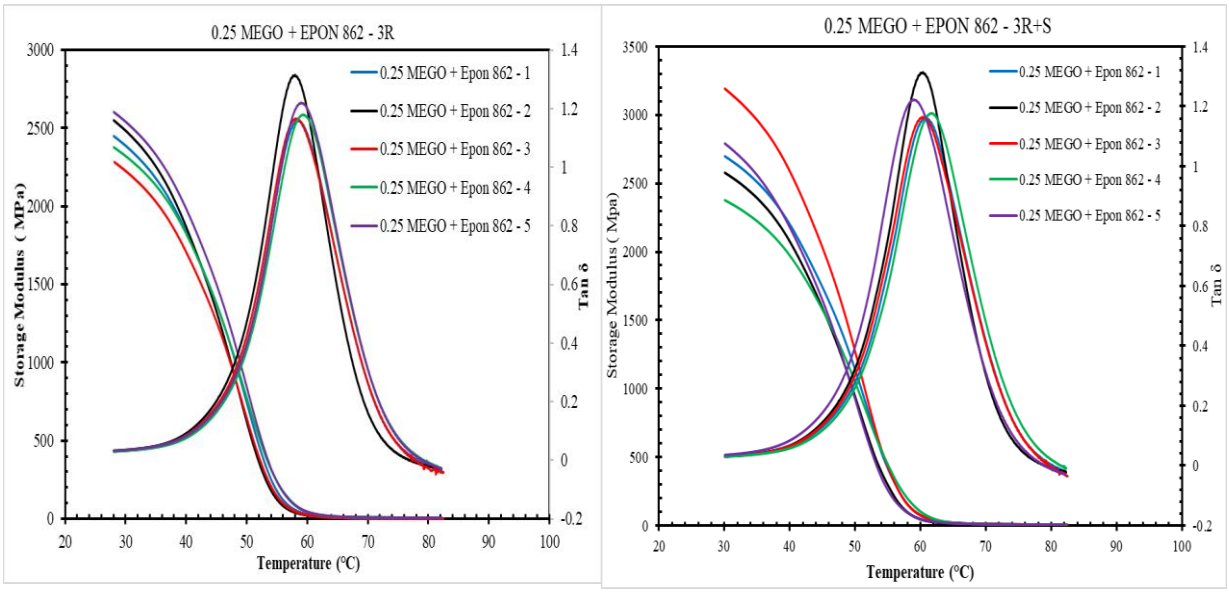

Fig. 3.11: Storage modulus and Tan δ curves for 0.25MEGO+Epon 862 (a) 3R and (b) 3R+S dispersion.

The glass transition temperature (T_g) of polymer nanocomposites was determined from the mechanical data. The ratio of the loss modulus to storage modulus in a viscoelastic material is defined as Tan δ. The peak position of Tan δ is accepted as glass transition temperature (T_g). It is observed that the T_g of the 3R dispersion sample at 0.1 wt.%

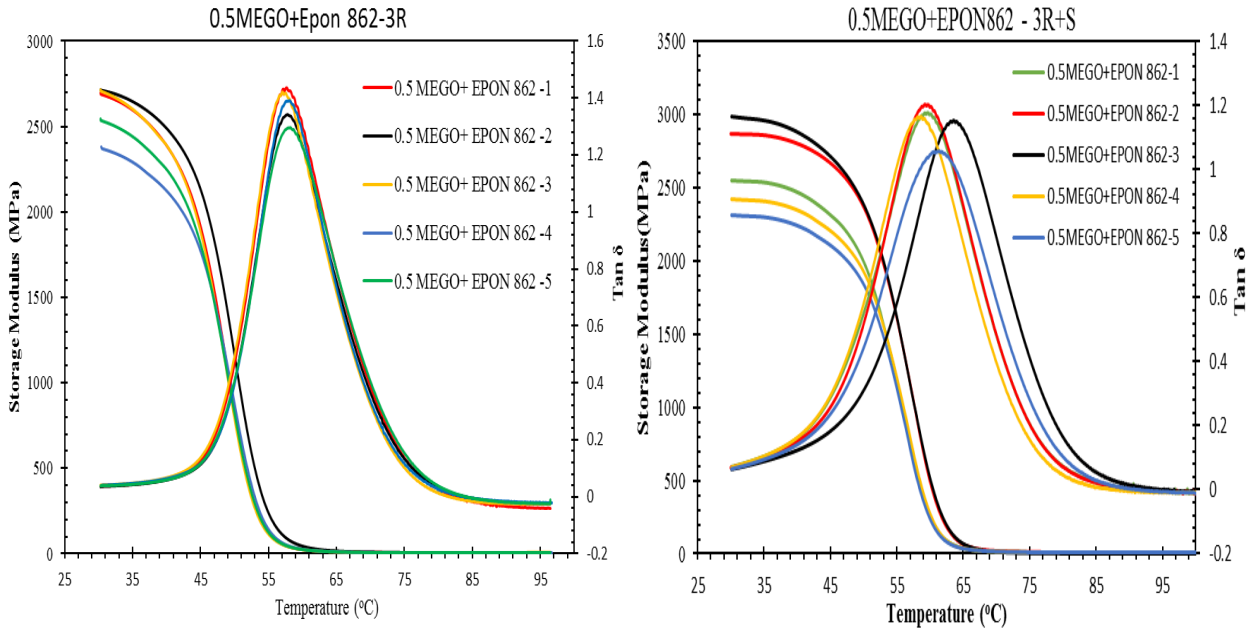

Fig. 3.12: Storage modulus and Tan δ curves for 0.5MEGO+Epon 862 (a) 3R and (b) 3R+S dispersion.

MEGO loading was increased by ~ 4 °C compared to neat resin. Similarly, for the 3R+S dispersion sample, the improvement in T_g is recorded by ~ 1 °C. Also, dispersion of GO in Epon showed a decrease in glass transition temperatures. Which could be due to the reduced cross- linking of polymer because of radical trapping. Similar results were reported by other researchers too [36].

The polymer composite samples for 3R and 3R+S dispersion samples were run at 1Hz frequency to determine the storage modulus. The storage modulus represents the energy stored in the elastic structure of the samples, and the loss modulus represents the amount

Table 3.1: Storage modulus and Tan δ data summary for 3R dispersion samples.

Sample (3R)	Tg (^{o}C)	Storage Mod. (Mpa)	Avg.T_g (^{o}C)	Avg. Storage Mod.(Mpa)
Neat Epon 862-1	56.6	2449	56.82±0.14	2456± 8
Neat Epon 862-2	56.95	2469		
Neat Epon 862-3	56.77	2449		
Neat Epon 862-4	56.86	2459		
Neat Epon 862-5	56.9	2454		
0.1% GO + EPON 862 -1	56.25	2361	56.55±0.27	2406± 34
0.1% GO + EPON 862 -2	56.36	2455		
0.1% GO + EPON 862 -3	56.49	2413		
0.1% GO + EPON 862 -4	56.87	2391		
0.1% GO + EPON 862 -5	56.79	2409		
0.05% WET MEGO+ EPON 862-1	59.19	2558	59.6 ± 0.3	2508.6±99
0.05% WET MEGO+ EPON 862-2	59.93	2439		
0.05% WET MEGO+ EPON 862-3	59.58	2430		
0.05% WET MEGO+ EPON 862-4	59.53	2455		
0.05% WET MEGO+ EPON 862-5	59.92	2661		
0.1% WET MEGO+ EPON 862-1	61.25	2554	60.42±0.48	2691±129
0.1% WET MEGO+ EPON 862-2	60.3	2657		
0.1% WET MEGO+ EPON 862-3	60.07	2875		
0.1% WET MEGO+ EPON 862-4	60.15	2766		
0.1% WET MEGO+ EPON 862-5	60.32	2603		
0.25% WET MEGO+ EPON 862-1	58.38	2649	58.54±0.61	2652±140
0.25% WET MEGO+ EPON 862-2	58.01	2758		
0.25% WET MEGO+ EPON 862-3	58.01	2467		
0.25% WET MEGO+ EPON 862-4	59.41	2571		
0.25% WET MEGO+ EPON 862-5	58.9	2814		
0.5% WET MEGO+ EPON 862 -1	57.72	2697	57.78±0.43	2610±146
0.5% WET MEGO+ EPON 862 -2	57.85	2714		
0.5% WET MEGO+ EPON 862 -3	57.08	2713		
0.5% WET MEGO+ EPON 862 -4	57.99	2380		
0.5% WET MEGO+ EPON 862 -5	58.24	2546		

Table 3.2: Storage modulus and Tan δ data summary for 3R+S dispersion samples

Sample (3R+S)	Tg (^oC)	Storage Mod. (Mpa)	Avg.T_g (^oC)	Avg. Storage Mod. (Mpa)
Neat Epon 862-1	58.57	2880	61.16 ± 1.95	2615±204
Neat Epon 862-2	63.39	2380		
Neat Epon 862-3	61.3	2766		
Neat Epon 862-4	59.94	2557		
Neat Epon 862-5	62.6	2493		
0.1% GO + EPON 862 -1	59.58	2361	61.04±2.13	2550± 198
0.1% GO + EPON 862 -2	61.44	2553		
0.1% GO + EPON 862 -3	61.6	2858		
0.1% GO + EPON 862 -4	58.52	2391		
0.1% GO + EPON 862 -5	64.04	2585		
0.05% WET MEGO+ EPON 862-1	63.66	2990	61.79 ± 1.54	2678±224
0.05% WET MEGO+ EPON 862-2	62.98	2695		
0.05% WET MEGO+ EPON 862-3	60.78	2539		
0.05% WET MEGO+ EPON 862-4	61.61	2765		
0.05% WET MEGO+ EPON 862-5	59.9	2401		
0.1% WET MEGO+ EPON 862-1	62.44	2661	61.12 ± 1.73	2791±217
0.1% WET MEGO+ EPON 862-2	60.65	2990		
0.1% WET MEGO+ EPON 862-3	63.02	3048		
0.1% WET MEGO+ EPON 862-4	58.6	2547		
0.1% WET MEGO+ EPON 862-5	60.9	2709		
0.25% WET MEGO+ EPON 862-1	60.7	2698	60.39 ± 1.02	2727 ± 333
0.25% WET MEGO+ EPON 862-2	60.4	2576		
0.25% WET MEGO+ EPON 862-3	60.2	3193		
0.25% WET MEGO+ EPON 862-4	61.7	2377		
0.25% WET MEGO+ EPON 862-5	58.9	2789		
0.5% WET MEGO+ EPON 862 -1	59.74	2547	60.46 ± 2.13	2626.6±291
0.5% WET MEGO+ EPON 862 -2	59.31	2865		
0.5% WET MEGO+ EPON 862 -3	63.61	2991		
0.5% WET MEGO+ EPON 862 -4	58.17	2421		
0.5% WET MEGO+ EPON 862 -5	61.49	2309		

of dissipated energy, i.e., viscous part. The average storage modulus of all composites was improved in comparison to that of neat resins. Specifically, the storage modulus was

improved by ~10% and ~ 7% for 0.1% loading of MEGO for 3R and 3R+S dispersion samples, respectively.

The increase in T_g and storage modulus of MEGO loaded polymer nanocomposite are expected due to better filler/matrix adhesion and a greater degree of stress transfer at the interface. The incorporation of filler in the resin's matrix has increased the stiffness of the matrix with the reinforcing effect. The comparison of average T_g and storage modulus for 3R and 3R+S dispersion are presented in Figures 3.13 and 3.14.

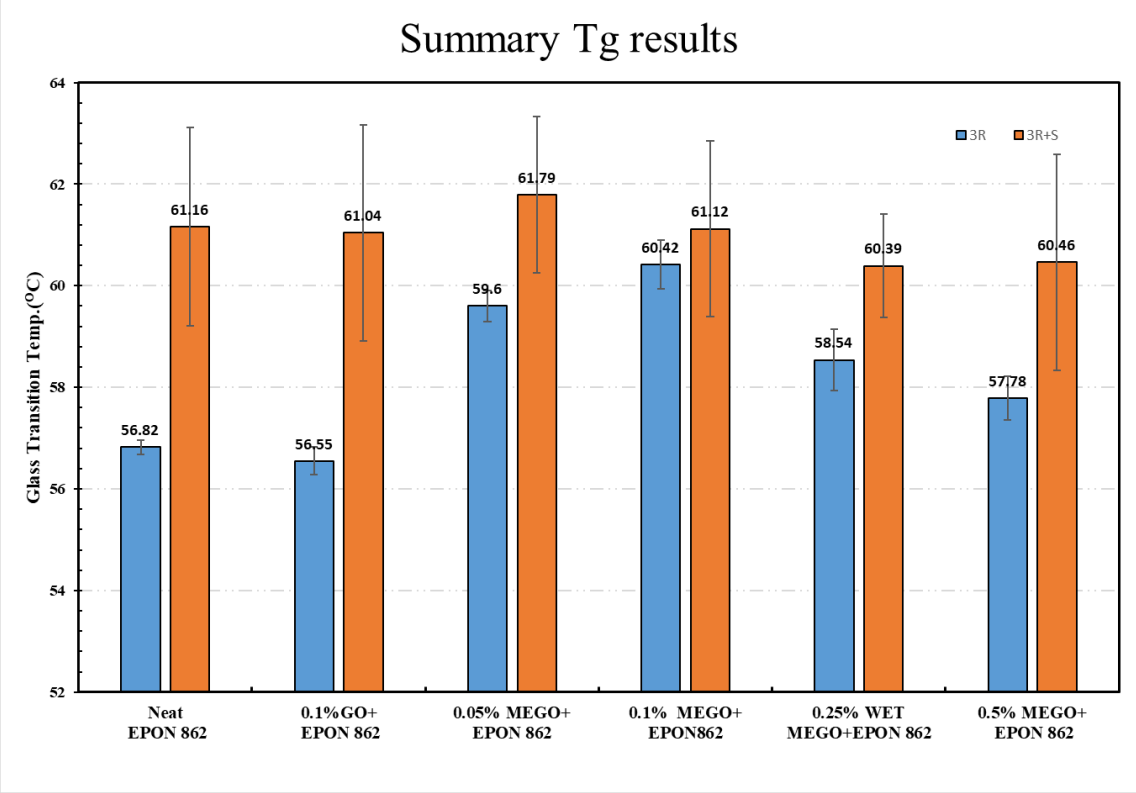

Fig. 3.13: Summary of glass transition temperature results for 3R and 3R+S dispersion samples

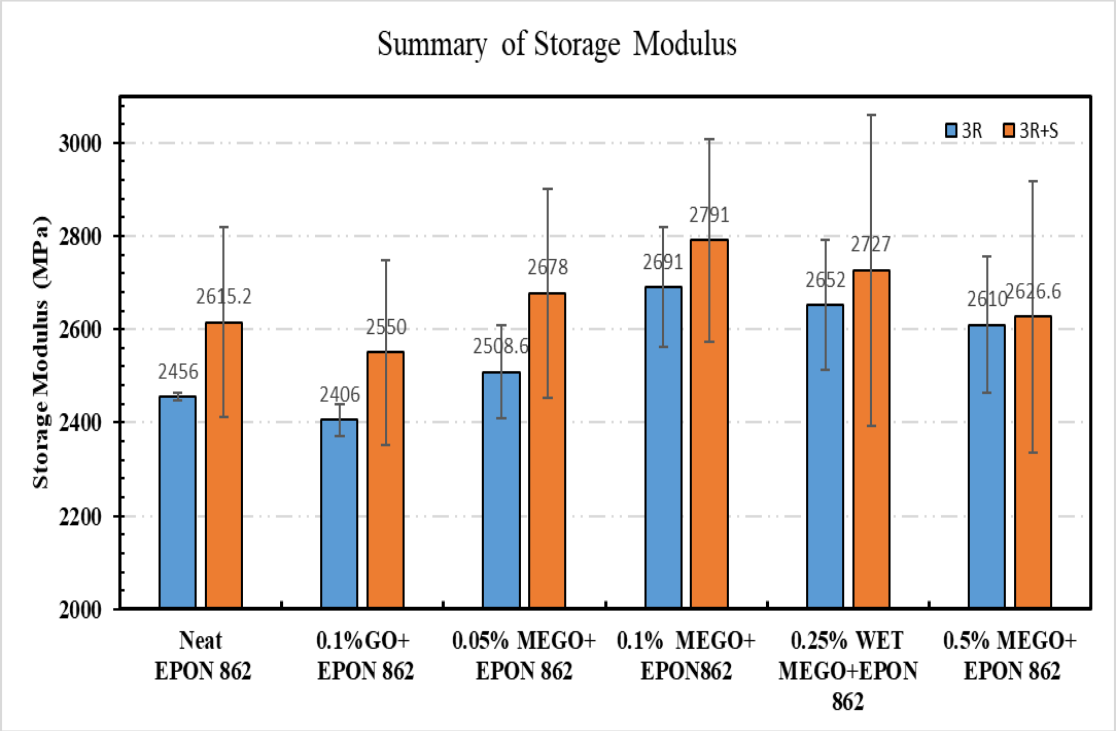

Fig. 3.14: Summary of storage modulus results for 3R and 3R+S dispersion samples

Majzoobi and his group studied the effect of sonication time on the mechanical properties of epoxy nanocomposites. They reported that each weight percentage of GO in epoxy has an optimum sonication time for better mechanical results. They also claimed that the extra sonication time is causing local damage to the polymer chain and nanofiller, leading to more destructive mechanical properties [36]. Though 3R+S dispersion showed better dispersion under optical microscopy analysis, the DMA results are more scattered. The more scattered result for 3R+S dispersion samples is believed to be because of the improper sonication process for dispersion. So, it warns to investigate proper sonication process (time, amplitude, temperature) for MEGO dispersion in Epon 862 before proceeding to further mechanical testing. Relying on the more consistent data for 3R

dispersion, further work will be procced only for 3-roll (3R) dispersion by keeping 3R+S dispersion as a part of future work of this research.

3.4.2 Differential Scanning Calorimetry (DSC):

Differential scanning calorimetry (DSC) experiments of neat epoxy and its composites samples were performed to observe the thermal transitions. For the DSC experiment, approximately 4 mg of samples were used. Samples were heated in standard mode from 0 to 100 °C at a heating rate of 5 °C/minutes under N_2 gas atmosphere. Three cycles of heating, cooling, and heating were performed for each sample, and the third cycle of heating was chosen for thermal analysis. For each composition, three samples were tested, which are shown in Figures 3.15 to 3.20. Figure 3.21 displays a comparison of DSC curves of MEGO- Epon polymer composite (0.05, 0.1, 0.25 and 0.5 wt.% loading of MEGO) with neat Epon 862 and GO/Epoxy composite, and the results are summarized in Table 3.3. An illustrative representation of the average glass transition temperature of all compositions is presented in Figure 3.22. All composite with MEGO loading shows an increase in glass transition temperature. The highest improvement in Tg was recorded for 0.1MEGO+Epon 862 polymer composite by ~ 7 ºC. This improvement in Tg with the addition of a hybrid modifier confirms the excellent compatibility of MEGO and the tendency to form crosslinks with polymer matrix. The presence of crosslinks and bulky

groups in the matrix restricts the segmental motion of molecules, thus attributing to the increase of Tg for MEGO/Epoxy composite.

Table 3.3: DSC glass Transition temperature data summary for 3R dispersion.

Sample (3R)	Tg (^{0}C)	Avg.T_g (^{0}C)
Neat Epon 862-1	59.41	59.65±0.22
Neat Epon 862-2	59.84	
Neat Epon 862-3	59.7	
0.1% GO+ EPON 862-1	58.48	58.51±0.11
0.1% GO+ EPON 862-2	58.63	
0.1% GO+ EPON 862-3	58.41	
0.05% MEGO+ EPON 862-1	64.4	64.38 ± 0.18
0.05% MEGO+ EPON 862-2	64.19	
0.05% MEGO+ EPON 862-3	64.54	
0.1% MEGO+ EPON 862-1	66.43	66.35±0.08
0.1% MEGO+ EPON 862-2	66.35	
0.1% MEGO+ EPON 862-3	66.28	
0.25% MEGO+ EPON 862 -1	64.87	64.82±0.05
0.25% MEGO+ EPON 862 -2	64.82	
0.25% MEGO+ EPON 862 -3	64.77	
0.5% MEGO+ EPON 862 -1	63.47	63.66±0.18
0.5% MEGO+ EPON 862 -2	63.68	
0.5% MEGO+ EPON 862 -3	63.83	

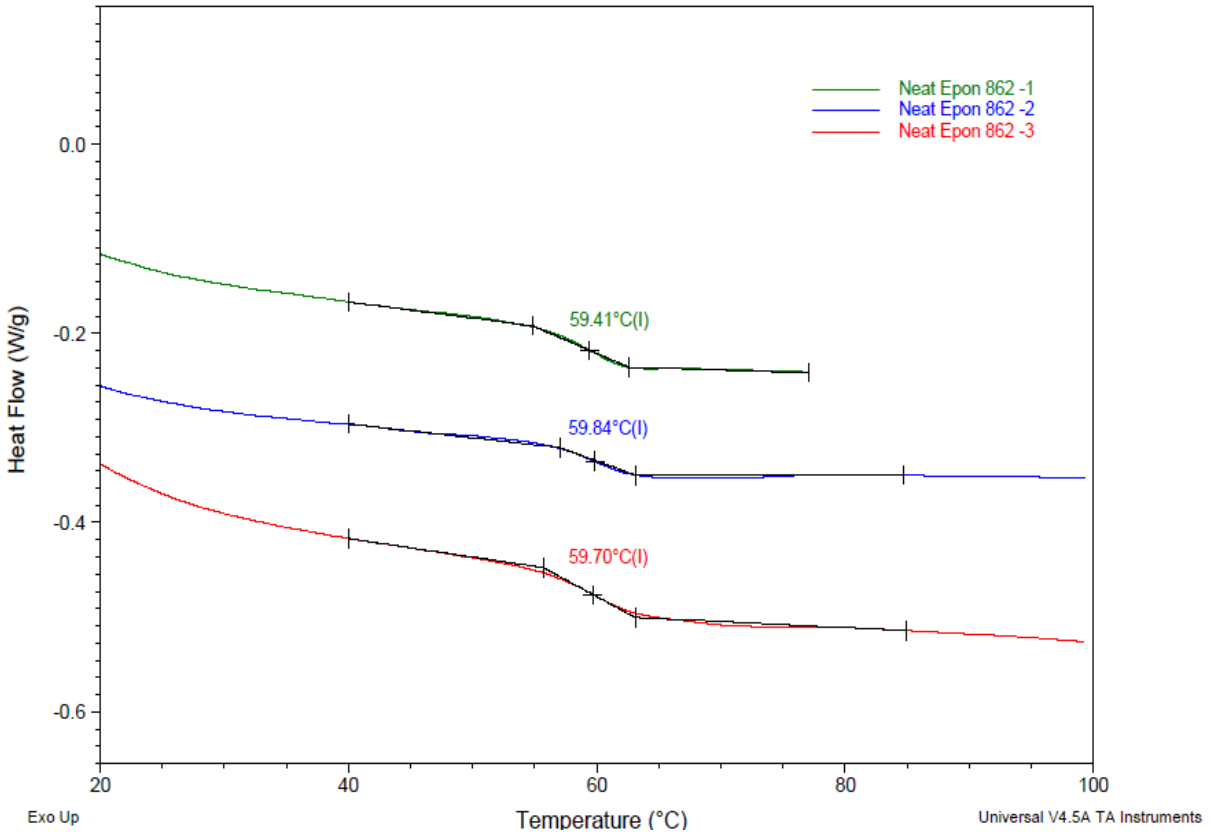

Fig. 3.15: DSC plots of Neat Epon 862.

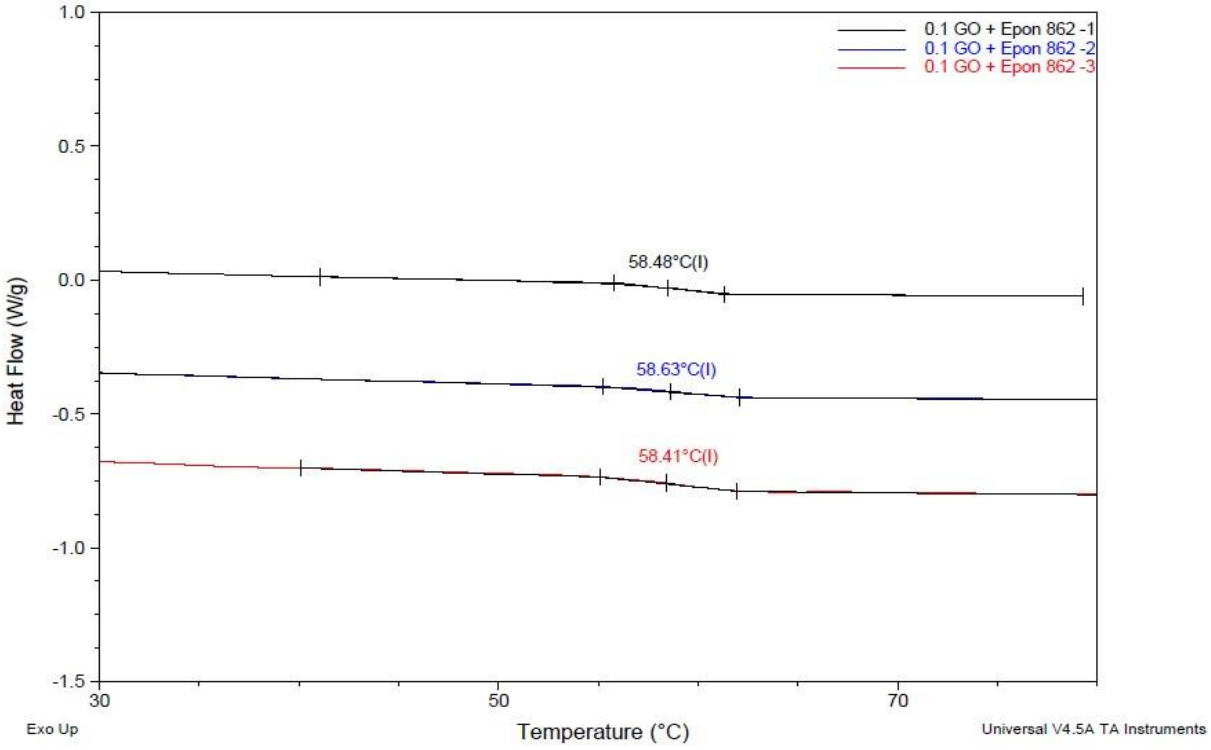

Fig. 3.16: DSC plots of 0.1GO+Epon 862.

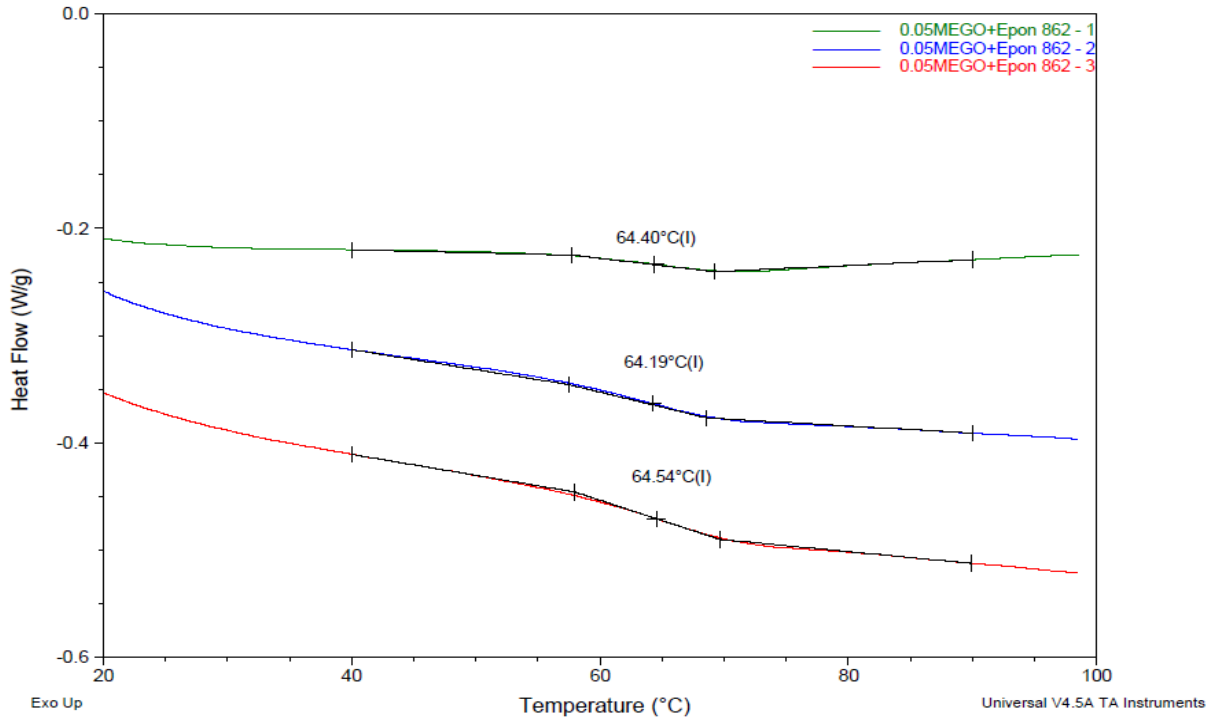

Fig. 3.17: DSC plots of 0.05MEGO+Epon 862.

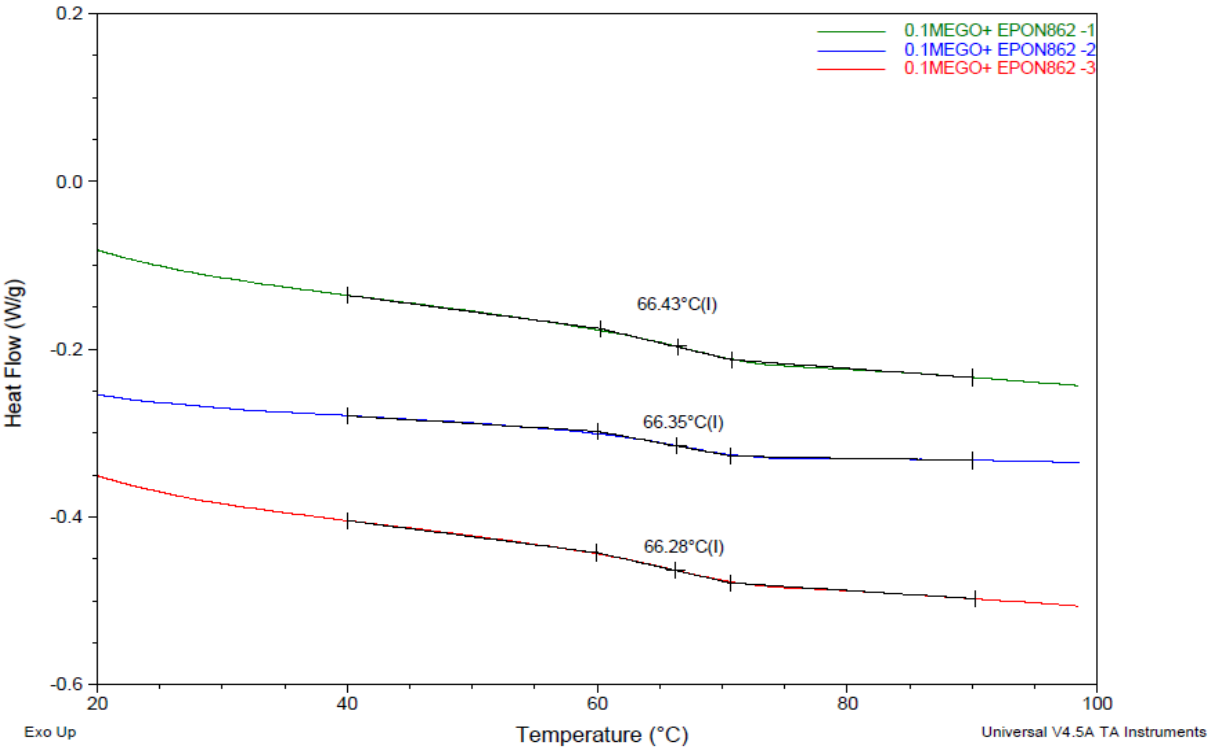

Fig. 3.18: DSC plots of 0.1MEGO+Epon 862.

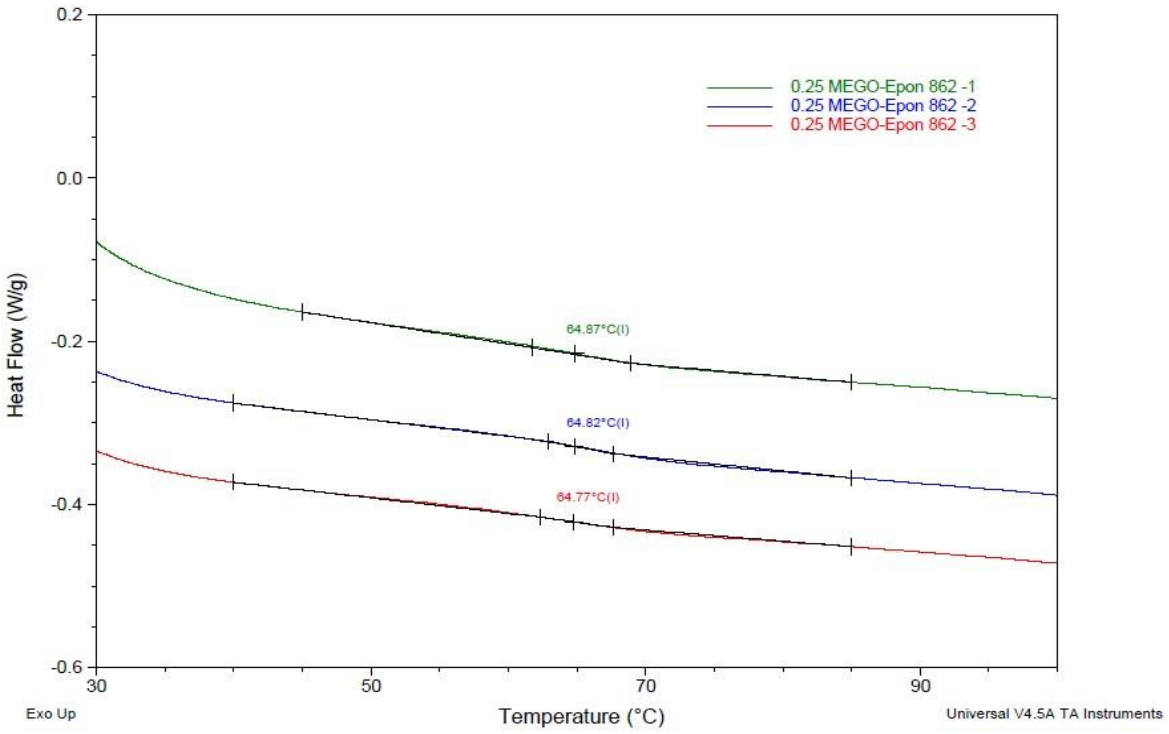

Fig. 3.19: DSC plots of 0.25MEGO+Epon 862.

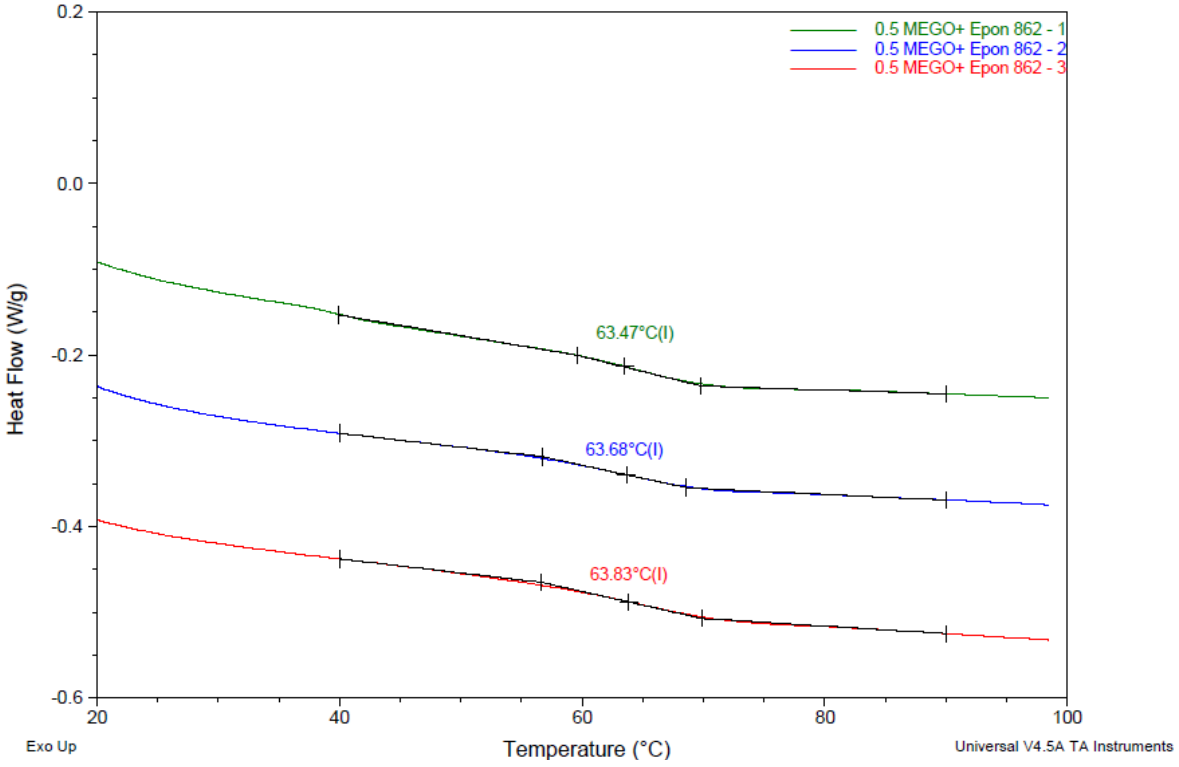

Fig. 3.20: DSC plots of 0.5MEGO+Epon 862.

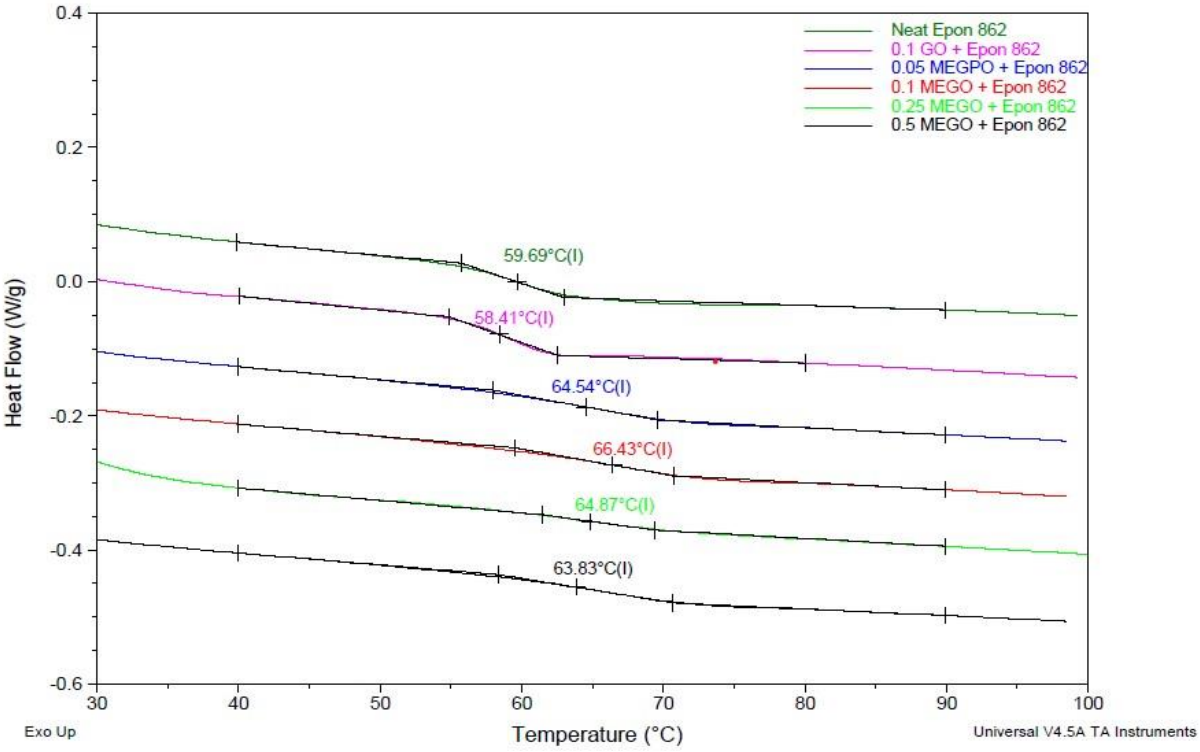

Fig. 3.21: DSC plots of neat, 0.1 GO, 0.05, 0.1, 0.25, 0.5 MEGO + Epon 862.

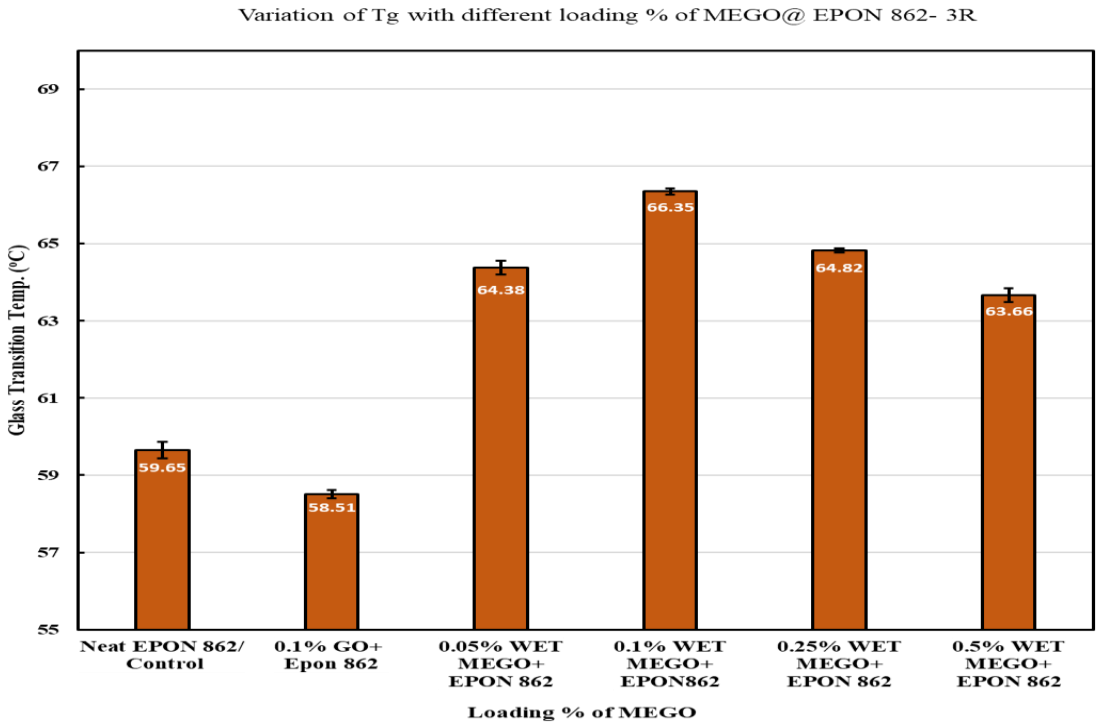

Fig. 3.22: Variation of Tg with different wt.% loading of MEGO in Epon 862.

3.4.3 TGA of Polymer Composite:

Thermal analysis of polymer matrix composite is another major interest in this study. The polymeric material can have a variation in its thermal stability depending upon the process parameter and its loading states[37] [38]. Therefore, TGA analysis was carried out to understand the epoxy's thermal stability variation with MEGO and GO loading. TGA of epoxy gives the variation in weight change as a function of temperature and time. Such weight change data as a function of temperature can unearth the information about decomposition, oxidation reaction, vaporization, and sublimation process in polymer composites [39]. Figure 3.23 elucidates the degradation under air atmosphere for the neat

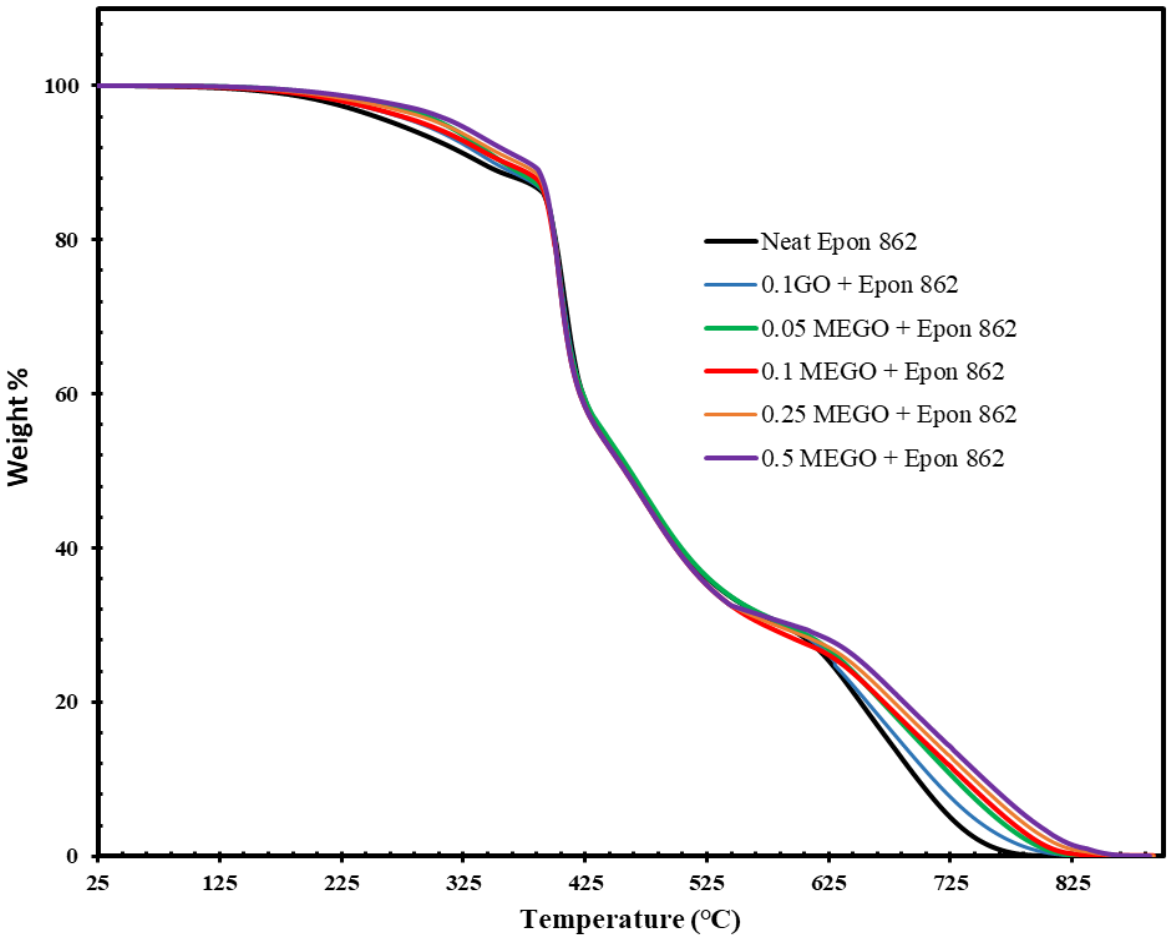

Fig. 3.23: Thermogravimetric analysis of neat epoxy and its composite

Epon 862 and its nanocomposites. TGA curves of all samples show a three-step weight loss process within the temperature range of 25 to 900 ºC. The first step of weight degradation is observed due to the vaporization of residue and loosely bonded small molecules. The second step corresponds to the degradation of the long polymer chain, and the third or last weight loss step belongs to the oxidation of char contain[40, 41]. The thermal plots in Figure 3.23 showed that the addition of hybrid nano-additives – MEGO increased the thermal degradation temperature of composites. Results showed that the incorporation of a larger amount of additives had made the composites thermally more stable. The increase in thermal stability of polymer composites was due to the formation of a siloxane layer in degraded samples after heating the composites at higher temperatures.

3.4.4 Flexural Strength and Flexural Modulus:

The flexural properties of Epoxy composite were determined using an Instron 5582 universal tester under a 3-point bend test in accordance with ASTM D790[33]. The flexural tests were performed with a span of ~ 45 mm by maintaining a span-to-thickness ratio of 16:1 and a speed of ~ 0.1mm/min. At least five specimens were tested, and the polymer composite's flexural strength and flexural modulus were reported. The stress-

strain graphs were plotted for one best representative sample of each composite composition and are presented in Figure 3.24.

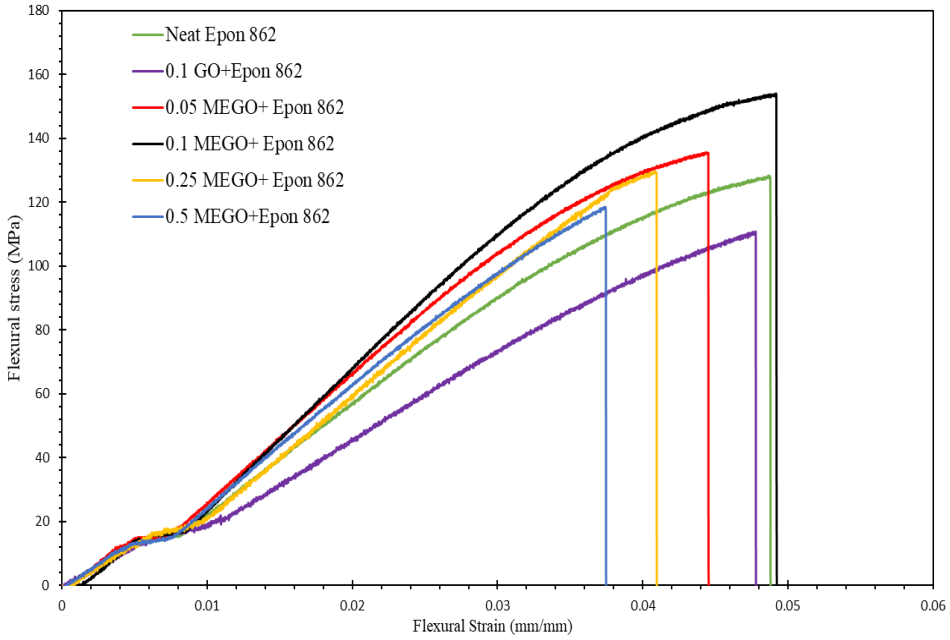

Fig. 3.24: Flexural stress-strain plot of neat Epon 862 and it's composite.

Table 3.4: Flexural test data summary of neat epon 862 and its composite

Sample	Flexural StrengthMPa)	Flexural Modulus (Mpa)
Neat EPON 862	134 ± 7	2888 ± 199
GO + EPON 862	111 ± 5	2756 ± 271
0.05 MEGO + EPON 862	140 ± 8	3270 ± 215
0.1 MEGO + EPON 862	149 ± 5	3679 ± 468
0.25 MEGO + EPON 862	126 ± 7	3407 ± 207
0.5 MEGO + EPON 862	118 ± 2	3355 ± 251

The average flexural modulus and flexural strength of the MEGO/Epon 862 nanocomposites at different loading wt.% are summarized in Table 3.4 and visually presented in Figure 3.25.

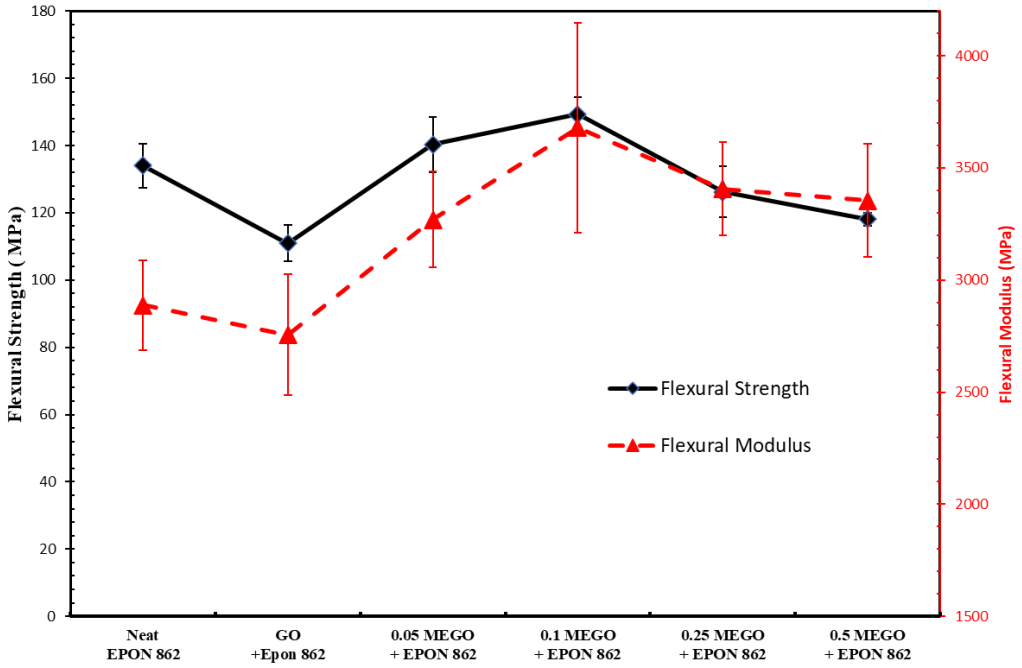

Fig. 3.25: Variation of flexural strength and modulus with different wt.% loading of MEGO in Epon 862

The experimental data showed that the maximum improvement in flexural strength and modulus was achieved at 0.1% MEGO loading by 11.5% and 27.4%, respectively. Beyond 0.1% MEGO loading (i.e., at 0.25 and 0.5wt.%), a decrease in flexural strength and modulus was observed. The increase in flexural strength and modulus up to 0.1wt.% MEGO content could be due to the crosslinking of functional groups of nanofillers with matrix leading to better compatibility. However, a decrease in strength and modulus at 0.5wt.% MEGO loading is observed, which could be due to the aggregation of nanofiller leading to poor bonding with matrix and creation of multiple stress concentration points in the matrix.

For the comparison purposes, 0.1wt.% GO dispersed epoxy composite were prepared. The mechanical and viscoelastic properties of GO/Epoxy composite were reduced. It can be inferred that such lowering of flexural strength, modulus and viscoelastic properties can result from retarding of the epoxy polymerization and serious agglomeration [36]. Graphitic nanomaterial can serve as radical trap during polymerization process causing retardation in polymerization. Also, chances of agglomeration of GO becomes high because of $\pi - \pi$ interaction, and Van der Walls interactions [42]. To further understand these results, fracture surfaces were analyzed using SEM.

3.4.5 MEGO/Epon composite fracture surface analysis:

The fracture surfaces of flexural test samples of neat epon and its composites were examined under scanning electron microscopy (SEM). Fig. 3.26 to 3.31 displays the micrograph of fracture surface for all composite compositions considered for the flexural test. SEM analysis confirms a significant variation in fracture surface of MEGO reinforced composite from that of control neat and GO reinforced sample. As seen in Fig. 3.26, neat Epon shows a featureless smooth fracture surface confirming fast proliferation of cracks, brittle failure, and low toughness of fracture [43-45]. GO reinforced composite shows a serious agglomeration. MEGO/Epon composite micrographs exhibit irregular and rougher fracture surfaces than neat Epon. Fig. 3.28 and 3.29 show a river-surface form of the fracture micrograph for 0.05 and 0.1 wt.% loading of MEGO. The river-surface form is more dominant in 0.1 wt.% MEGO loading compared with the 0.05 wt.%

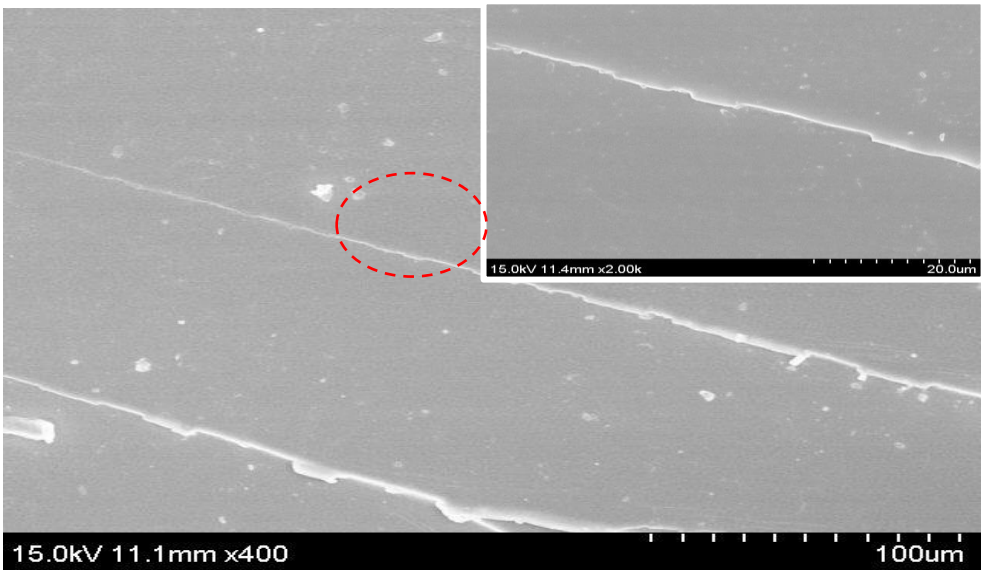

Fig. 3.26: Fracture surface SEM image of Neat Epon 862.

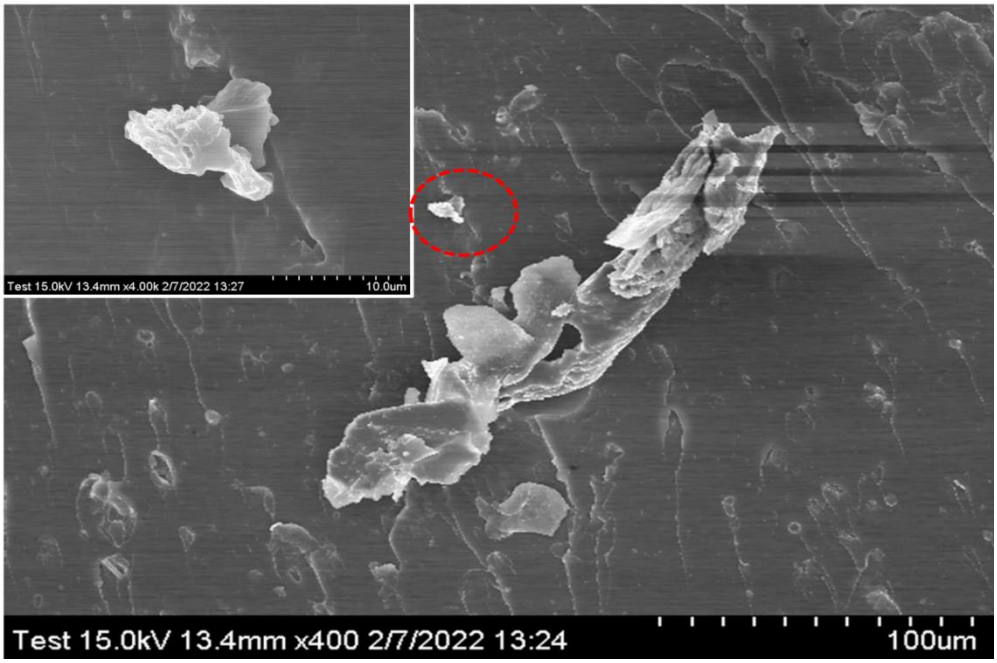

Fig. 3.27: Fracture surface SEM image of GO + Epon 862.

loading inferring MEGO is more compatible at 0.1wt.% loading. MEGO in epoxy acts as mechanical obstructions for cracks, slowing down the crack propagation for improved mechanical properties. The formation of dendritic river-surface pattern with no phase separation in 0.05 and 0.1 MEGO/Epon composite sample is due to improved

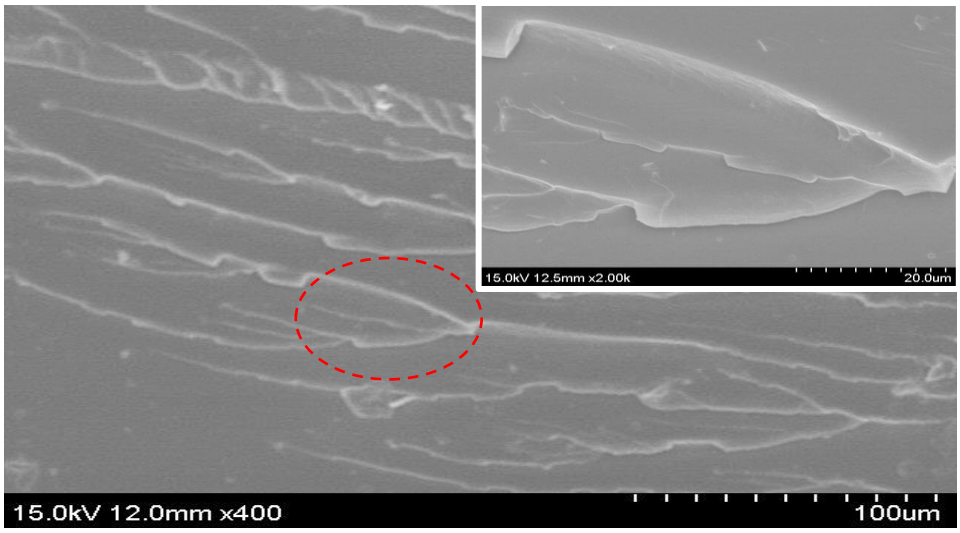

Fig. 3.28: Fracture surface SEM image of 0.05wt.% MEGO loading on Epon 862.

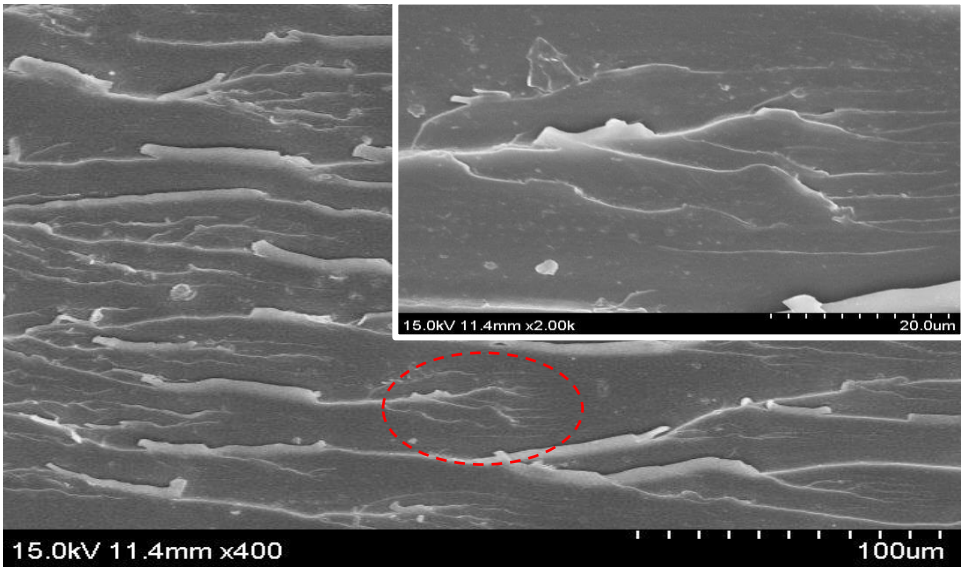

Fig. 3.29: Fracture surface SEM image of 0.1wt.% MEGO loading on Epon 862.

compatibility and crosslinking between MEGO and Epon 862. MEGO knit the polymer chain leading to robust barriers to slow down the crack propagation by crack deflection (Bifurcation) mechanism [43, 44, 46, 47], which justifies the improvement in flexural strength and modulus of MEGO/Epoxy composite at 0.05 and 0.1 wt.% loading [48]. Fig.

3.30 and 3.31 displays the fracture surface of 0.25 wt.% and 0.5wt.% MEGO/Epon composite, which are considerably different from the fracture micrograph of 0.05 and 0.1 wt.% MEGO loading. SEM micrograph of 0.25 and 0.5 MEGO/Epoxy composite shows less crack deflection mechanism and reinforcing nano additive MEGO agglomeration.

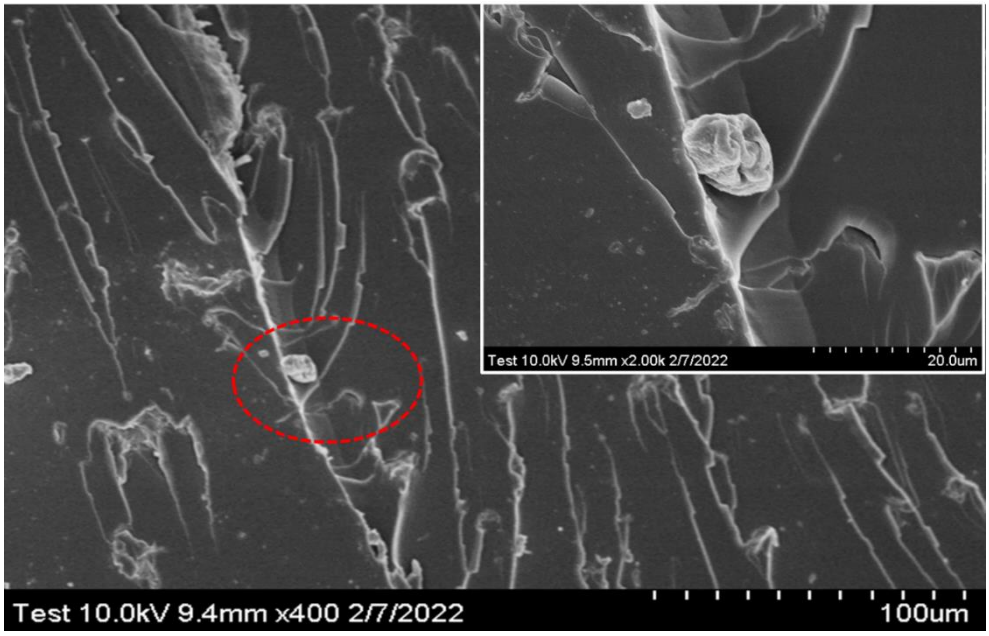

Fig. 3.30: Fracture surface SEM image of 0.25wt.% MEGO loading on Epon 862.

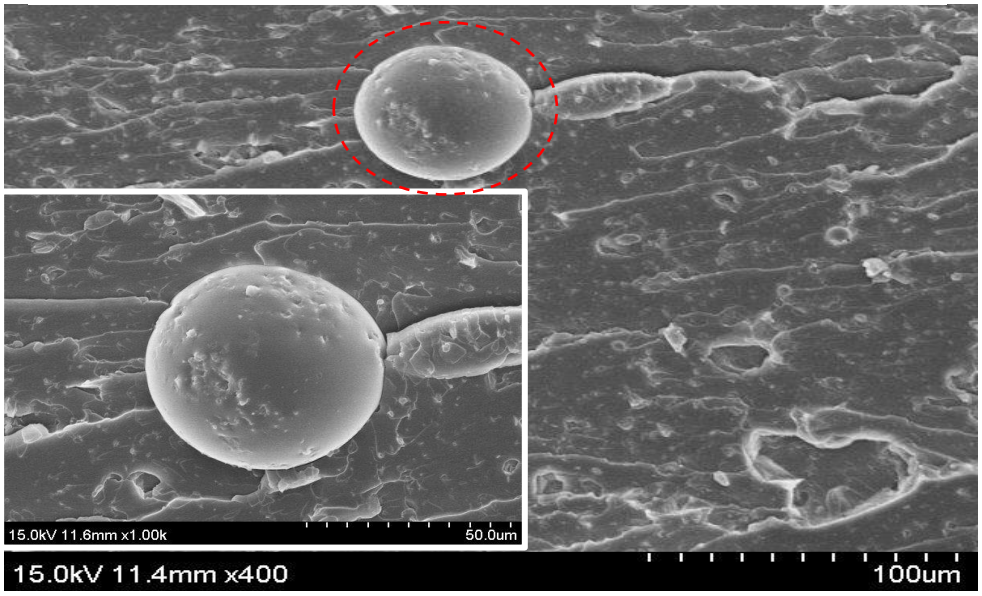

Fig. 3.31: Fracture surface SEM image of 0.5wt.% MEGO loading on Epon 862.

Irregular 'Patch' like patterns are more dominant, inferring the rapid movement of crack [49]. At 0.25 and 0.5 wt.% loading, MEGO aggregation signifies less compatibility with polymer matrix, justifying the decrease in viscoelastic and mechanical properties.

3.4.6 MEGO toughening of carbon fiber reinforced composite

3.4.6.1 Flexural properties

Figure 3.32 displays the representative flexural stress vs flexural strain behavior of MEGO toughened CFRP and Table 3.5 summarizes the flexural strength and modulus of all composite samples. For each composition, five samples were tested (Figure 3.33 displays stress vs strain curve for all 5 samples of 0.5wt.% MEGO toughened CFRP), and average value are presented in Figure 3.34. The flexural properties of CFRP with toughening agent MEGO are very close to the neat CFRP, showing not much change in the flexural strength and modulus. The flexural properties of CFRPs remains almost

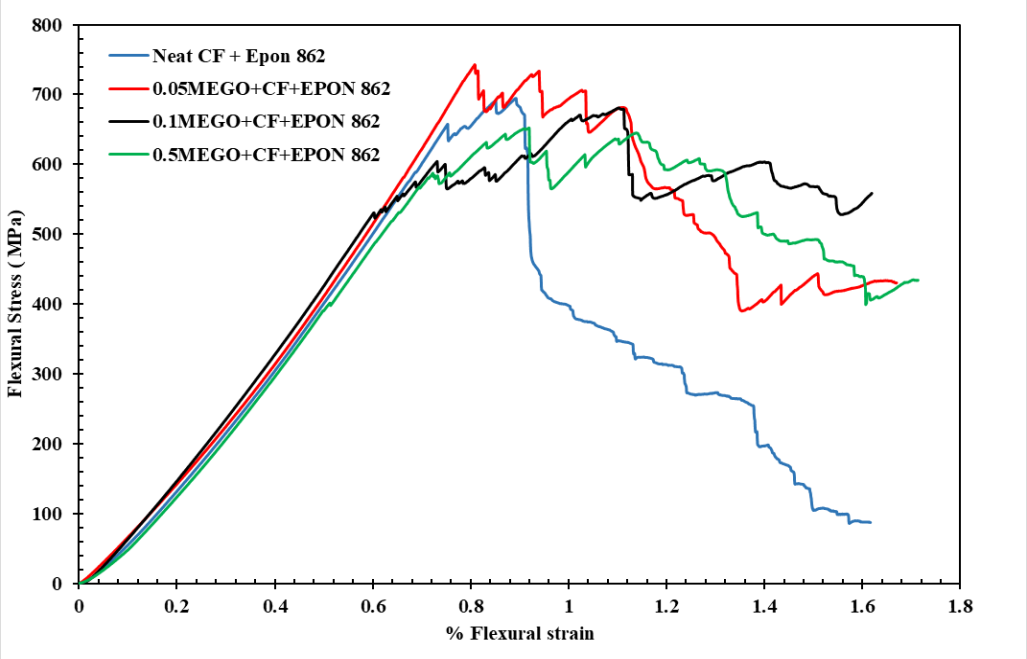

Fig. 3.32: Flexural Stress vs flexural strain of MEGO toughened CFRP

unaffected because these properties of CFRP are generally dominated by the carbon fibers[50].

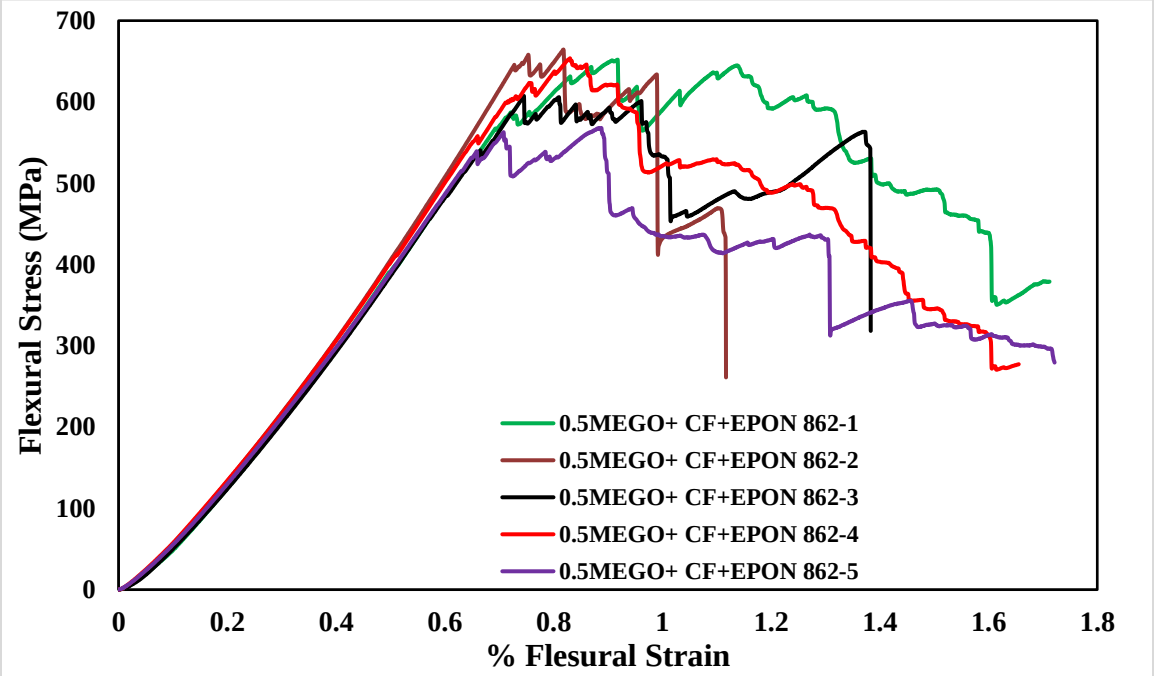

Fig. 3.33: Flexural Stress vs flexural strain of 0.5wt.% MEGO toughened CFRP

Table. 3.5: Flexural properties of MEGO toughened CFRP

Sample	Flexural Modulus (GPa)	Flexural Strength (MPa)
Neat CF+Epon 862	105.8 ± 2.6	704.5 ± 7.28
0.05 MEGO+CF+ Epon 862	100.6 ± 11.6	697.24 ± 35.44
0.1 MEGO+CF+ Epon 862	95.3 ± 7.3	663.1 ± 27.05
0.5 MEGO+CF+ Epon 862	98.7 ± 6.4	654.4 ± 27.7

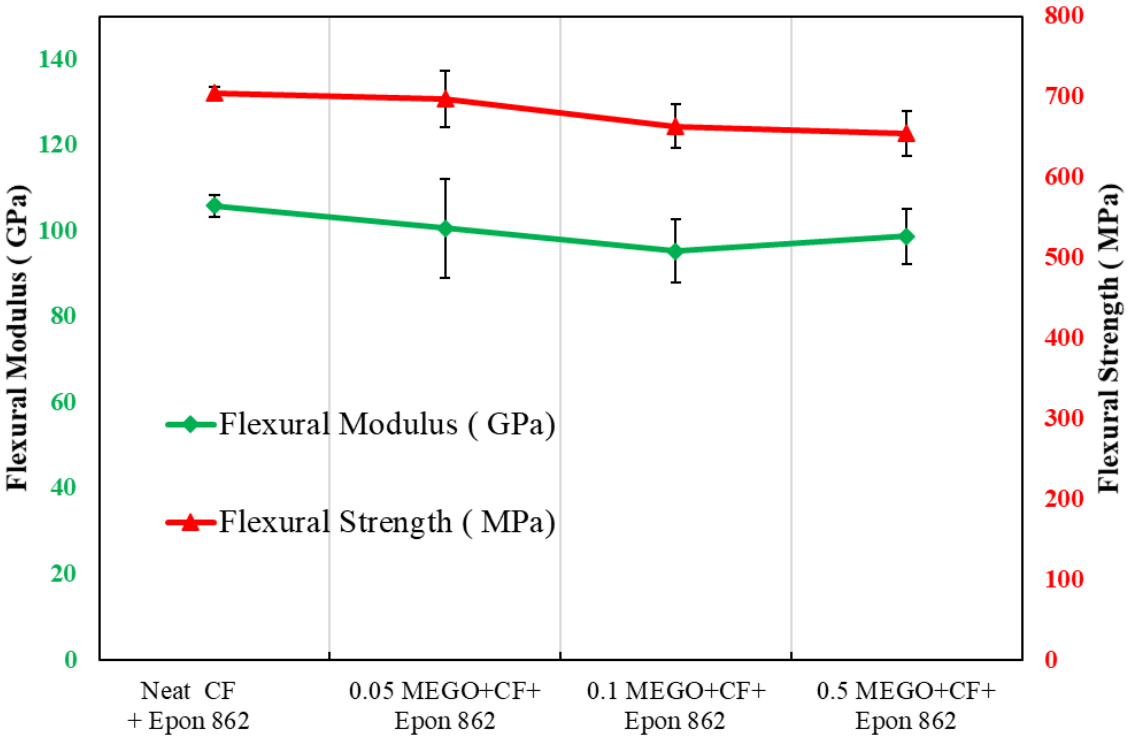

Fig. 3.34: Summarized flexural properties of toughened CFRP as a function of MEGO loading

3.4.6.2 Interlaminar fracture toughness of CFRP as a function of MEGO loading

Mode -I fracture toughness provides an insight of the energy absorption capability of multi-layer fiber reinforced polymer composites. Double cantilever beam test (ASTM 5528) was carried out to MEGO toughened CFRP. For each composition, five samples were tested, and average data were analyzed. Figure 3.35 represents the load vs crack mouth opening displacement (CMOD) graph of MEGO reinforced CFRP. Figure 3.36 (a to d) represents the compliance factor versus crack length for representative samples tested, from where the correction factor Δ were calculated.

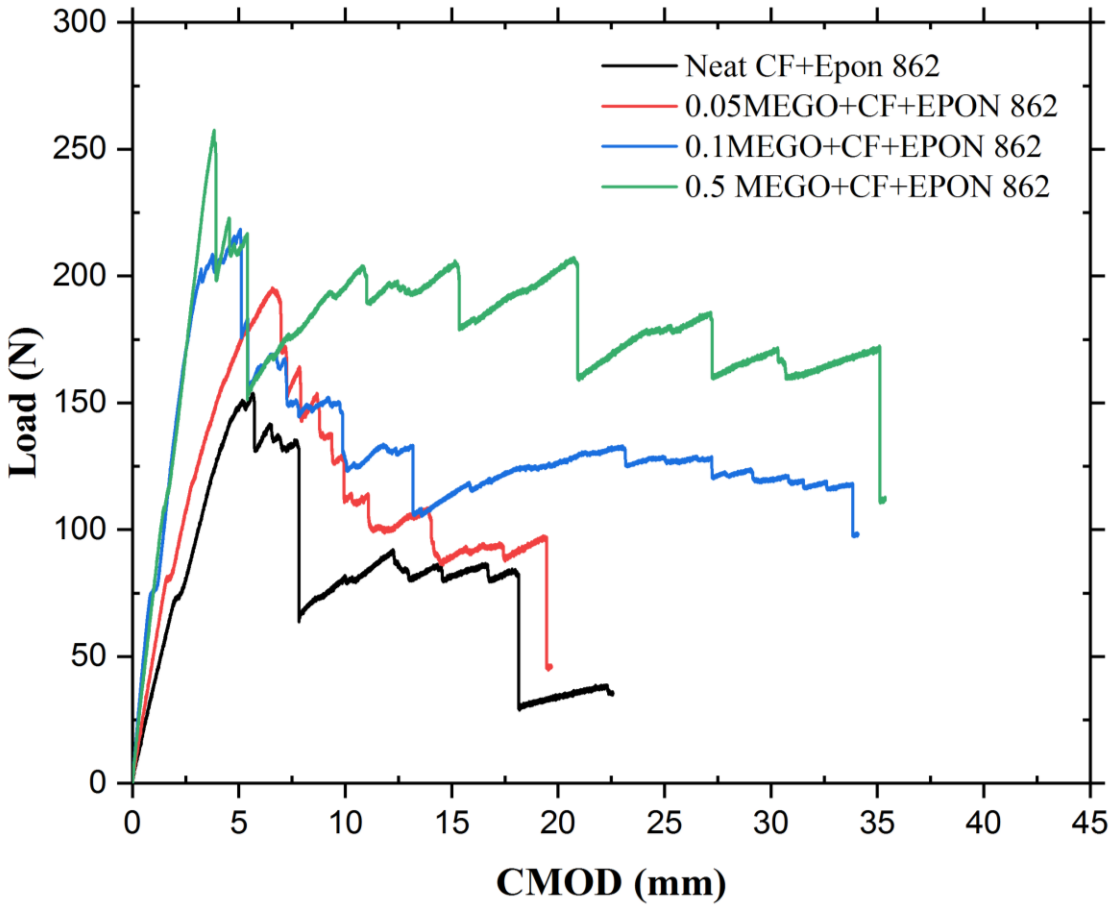

Fig. 3.35: Representative Mode I interlaminar fracture test for MEGO toughened CFRP composites.

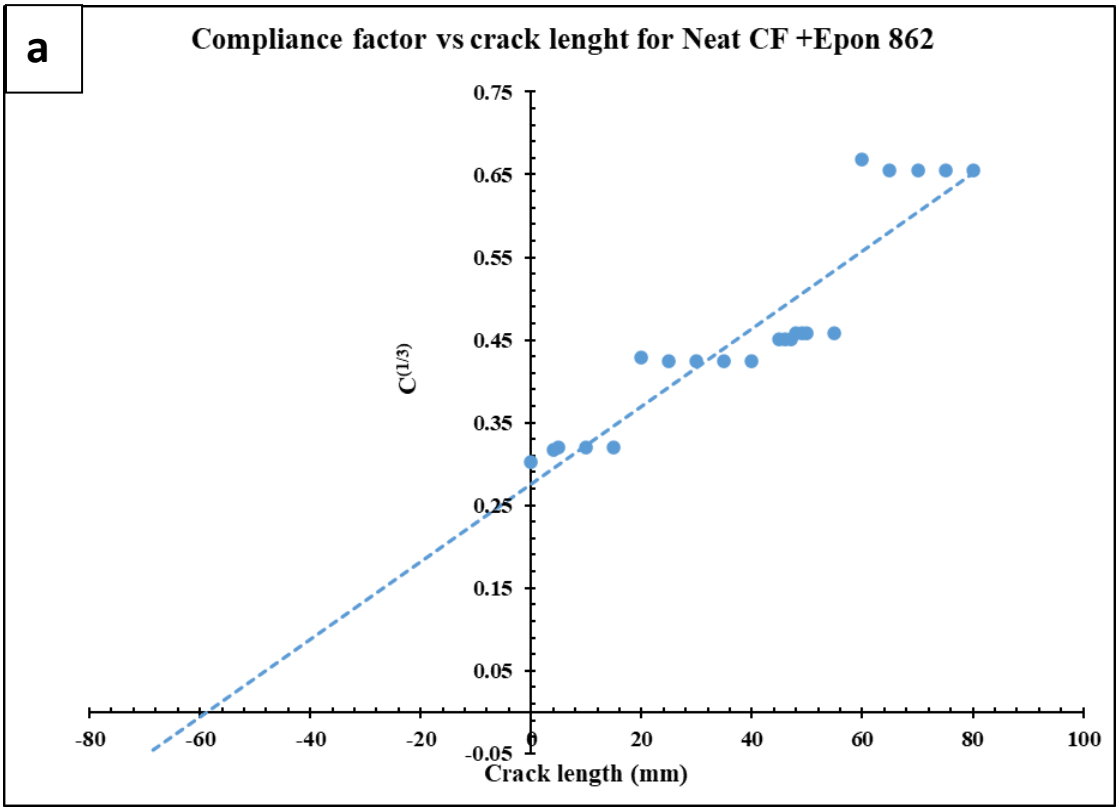
a
Compliance factor vs crack lenght for Neat CF +Epon 862
C(1/3)
Crack length (mm)
0.75
0.65
0.55
0.45
0.35
0.25
0.15
0.05
-0.05
-80
-60
-40
-20
0
20
40
60
80
100

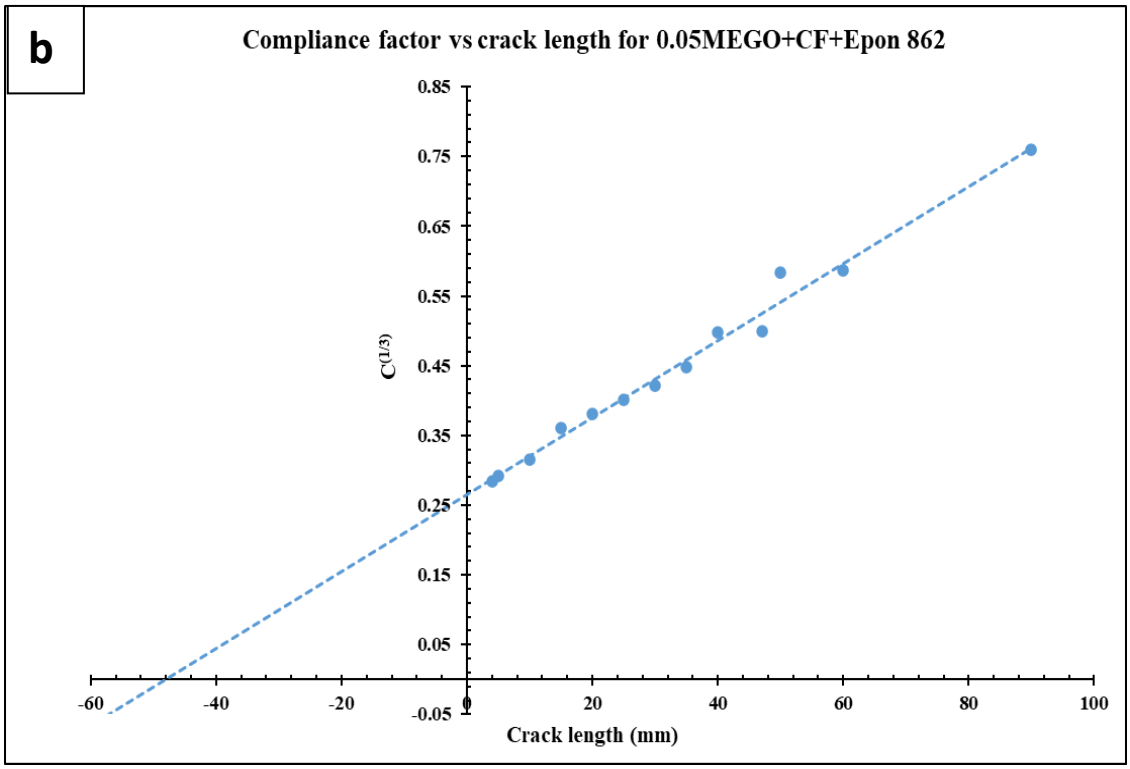
b
Compliance factor vs crack length for 0.05MEGO+CF+Epon 862
C(1/3)
Crack length (mm)
0.85
0.75
0.65
0.55
0.45
0.35
0.25
0.15
0.05
-0.05
-60
-40
-20
0
20
40
60
80
100

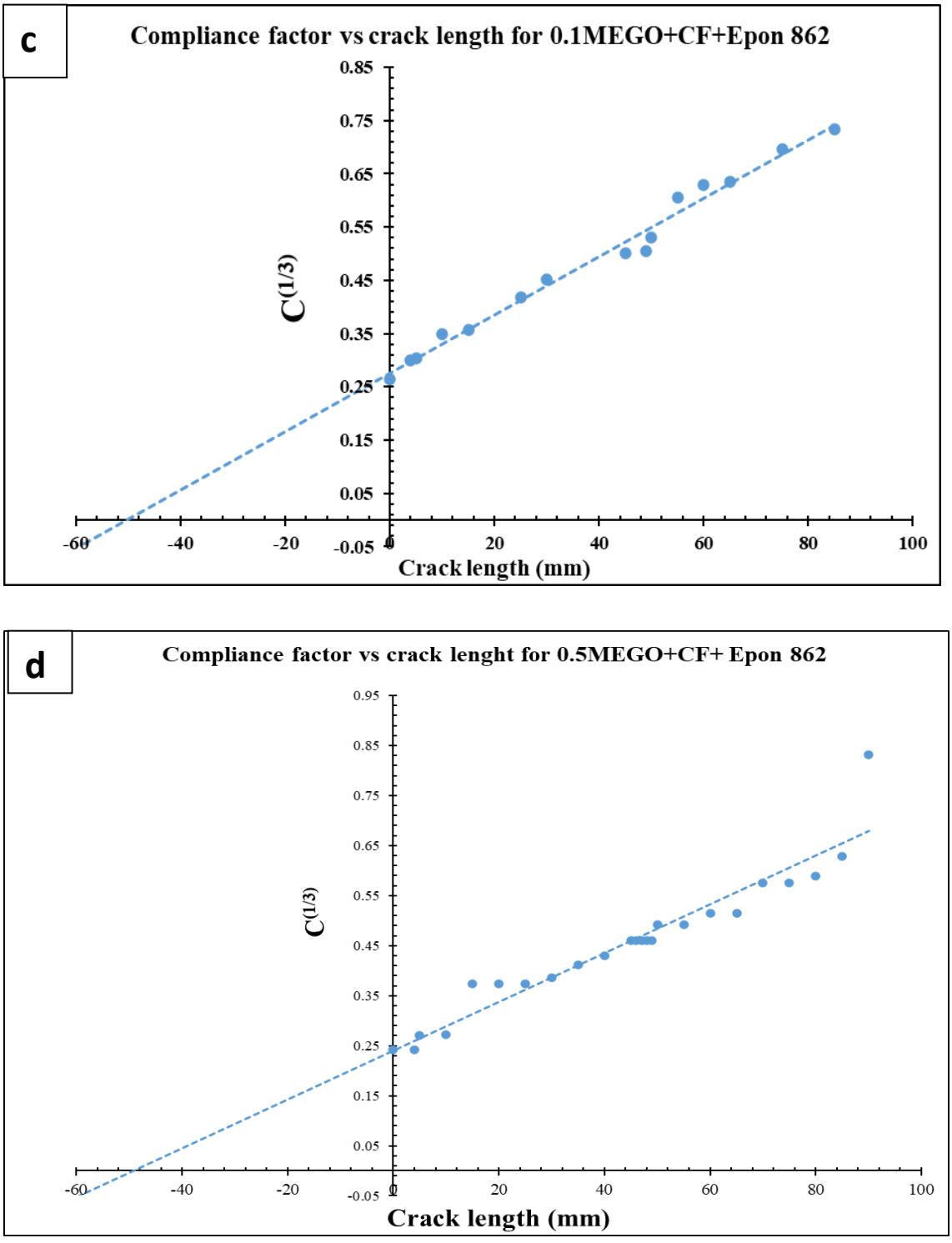

Fig. 3.36: Compliance factor versus crack length for (a) Neat (b) 0.05 MEGO (c) 0.1 MEGO and (d) 0.5 MEGO loading on CFRP composite.

Figure 3.37 and Table 3.6 summarizes the mode I interlaminar fracture toughness values obtained from the double cantilever beam tests. The results showed that the mode I interlaminar fracture toughness increases by ~ 27%, ~ 48%, and ~ 70% for 0.05, 0.1 and 0.5 wt.% loading of MEGO respectively.

Table. 3.6: Mode I interlaminar fracture toughness of MEGO toughened CFRP

Samples	**G_{IC}(KJ/m^2)**
Neat CF+Epon 862	0.62 ± 0.03
0.05 MEGO +CF +Epon 862	0.79 ± 0.028
0.1 MEGO + CF + Epon 862	0.92 ± 0.09
0.5 MEGO + CF + Epon 862	1.05 ± 0.02

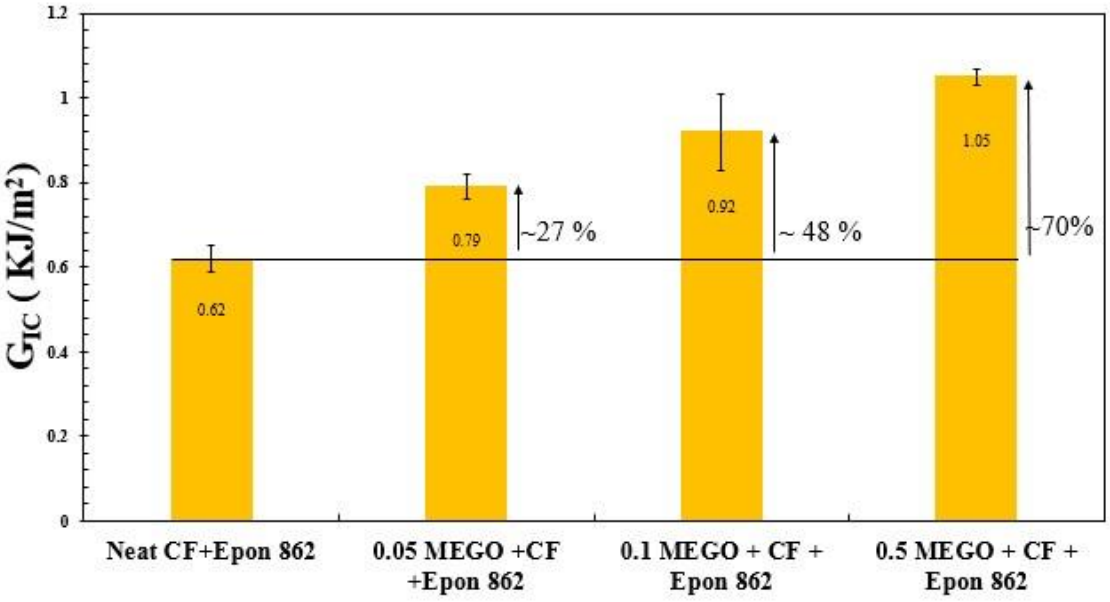

Fig. 3.37: Mode I interlaminar fracture toughness of MEGO toughened CFRP.

The load has increased linearly in the linear elastic region in each sample until the crack initiation point. Then, the load decreased gradually once the crack propagated

further in the composite. The load versus extension curves displays a saw tooth pattern inferring the crack growth is not continuous but it is a sequence of growth and arrest. Compared to the neat sample, saw tooth patterns are more dominant in the samples with MEGO loading. The result indicates that higher MEGO loading provides better resistance to crack propagation. Mishra et al. reported similar phenomenon in fracture growth when GO dispersion in PVP was introduced in interlaminar region of CFRP [42]. It has been reported that the residual oxygen functional groups on carbon fiber surface will enhance the interfacial bonding between fiber, GO, and matrix through hydrogen bonding, $\pi - \pi$ interaction, and van der Walls interactions [42]. Based on the improvement on fracture toughness of MEGO added CFRP, we believe that MEGO has enhanced the mechanical and chemical interactions between fiber and matrix leading to better mechanical performance. For the further understanding of toughening mechanisms, SEM analysis of the fracture surface of DCB test samples was carried out.

3.4.6.3 SEM fractography

To have a better understanding of toughening mechanisms in CFRP, the fractured surfaces after the DCB experiment were characterized using scanning electron microscope (SEM). Figure 3.38 - 3.41 displays the SEM fractographs of the DCB samples. Figure 3.38 show SEM images of fracture surface of the neat/ control sample, where carbon fibers are deboned cleanly from the epoxy matrix showing poor adhesion[51]. This also infers that the crack progression took place across the fiber-matrix adhesion[42]. Brittle fracture of epoxy between adjacent carbon fiber bundles is also displayed inferring the low resistance to crack propagation[52, 53]. Clearly, these observations explain the low toughness of neat samples. Figure 3.39, 3.40, and 3.41

presents the SEM fractography of 0.05, 0.1, and 0.5 wt.% MEGO loading respectively. As MEGO loading is increasing, more rougher fracture surface is observed. The addition of MEGO leads to the better adhesion between fiber and matrix. SEM images shows more and more adhesion between fiber and matrix as MEGO loading increases, providing the better resistance to crack propagation, and hence the toughness value increases. Similar features were observed by Zhang et al. when they incorporated carbon nanotubes/ polysulfone nanoparticles on the laminate carbon fiber / epoxy composites[51]. Overall, MEGO loading increased the interaction (could be chemical or mechanical) between fiber and matrix, leading to the better toughening mechanism.

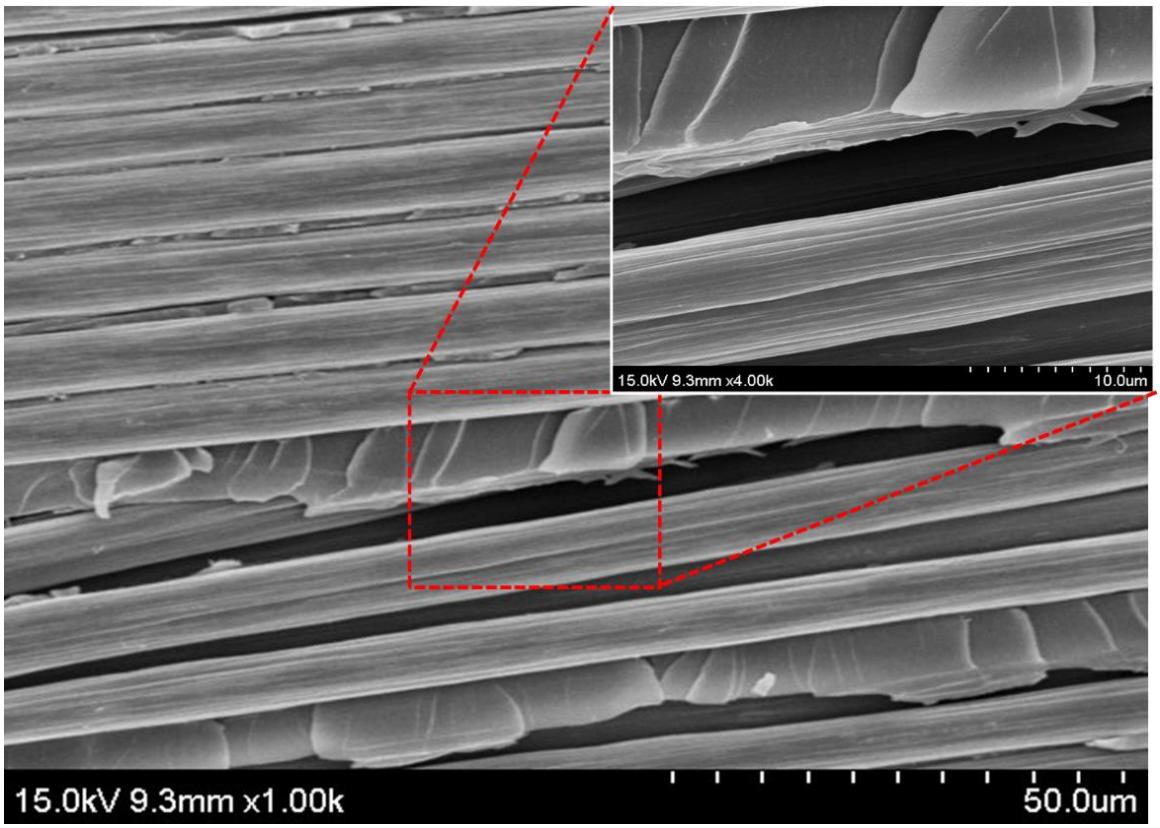

Fig. 3.38: SEM image of Neat CF+Epon 862 fracture surface.

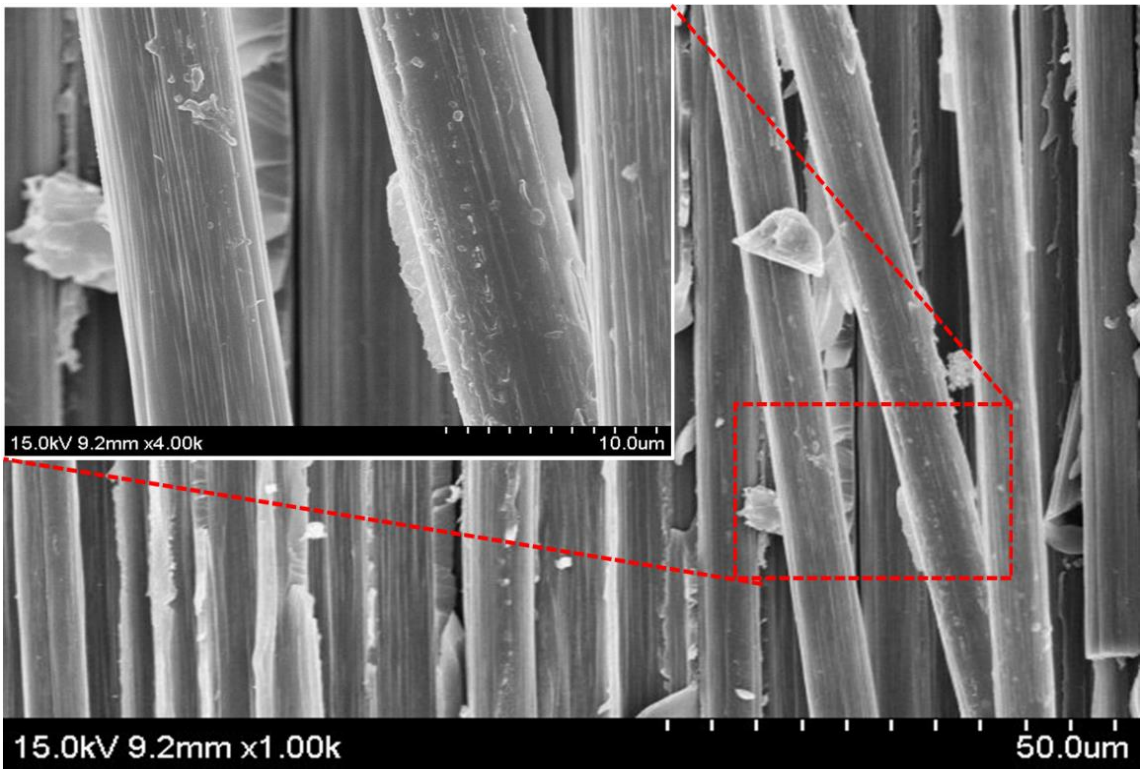

Fig. 3.39: SEM image of 0.05MEGO+ CF + Epon 862 fracture surface.

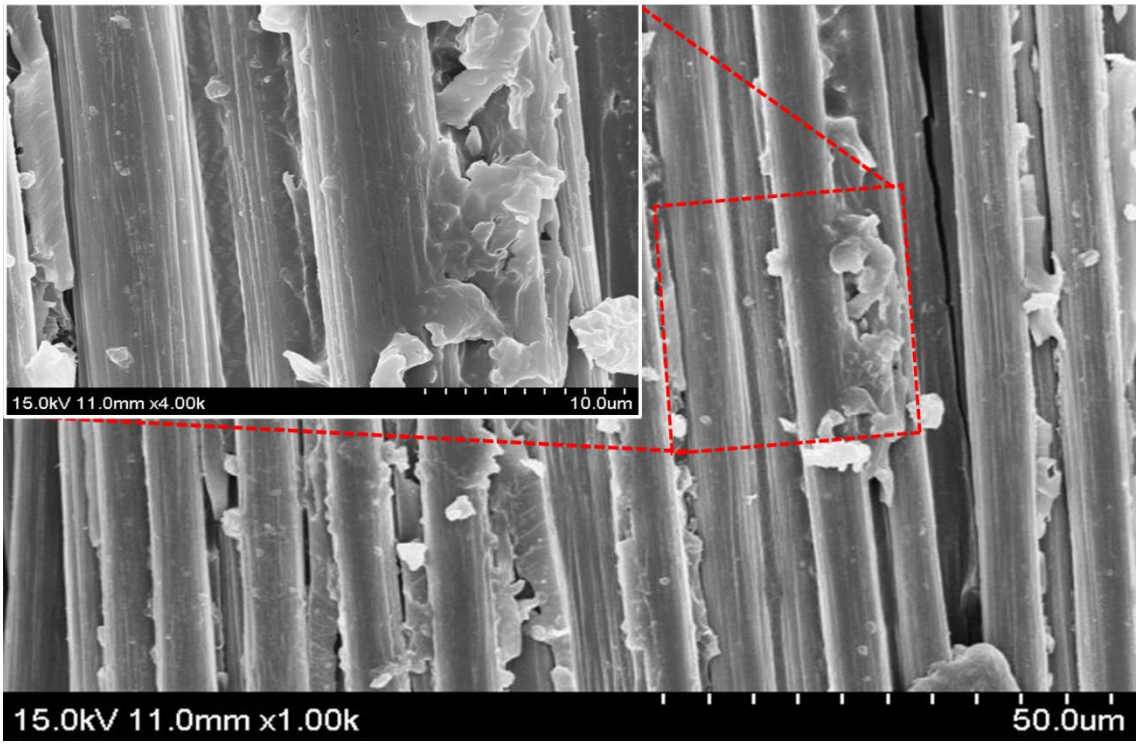

Fig. 3.40: SEM image of 0.1MEGO+CF + Epon 862 fracture surface.

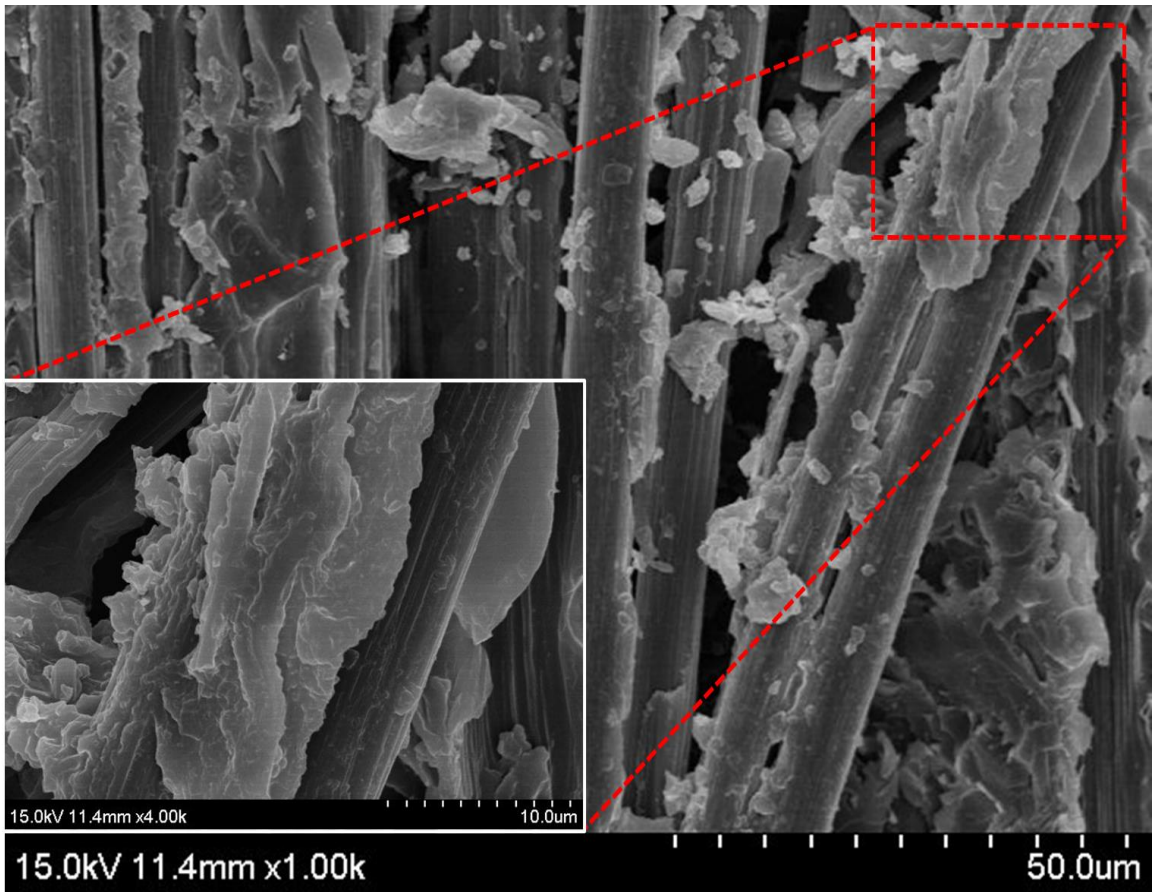

Fig. 3.41: SEM image of 0.5MEGO + Epon 862 fracture surface.

3.5 Conclusion:

This work aims to study the effect of nanohybrid material "MEGO" (MAPOSS hybridizeded GO) in the Epoxy and CFRP composites. Our research demonstrates that the dispersion of MEGO at very low wt.% in epoxy matrix is a promising way to improve epoxy and CFRP composites' thermal and mechanical properties. Although visible light microscopy analysis showed 3R+S dispersion superior over 3R dispersion, DMA results for 3R+S were more scattered, making them less reliable to draw a conclusion. Because of that, 3R dispersion was considered throughout the work with a solid recommendation to study the appropriate sonication process in the future. The DMA result showed that at 0.1wt.% loading of MEGO in Epon 862 improves T_g by ~ 4ºC and storage modulus by

~10%. The DSC result also confirmed the increase in T_g by ~ 7 ºC at 0.1 wt.% loadings. Both DMA and DSC results agreed that the optimum improvement could be achieved at 0.1 wt.% loadings. The TGA result showed that incorporating a larger amount of MEGO makes the composites thermally more stable due to the formation of the siloxane layer in degraded samples. The flexural test showed that the maximum improvement in flexural strength and modulus was achieved at 0.1wt.% MEGO loading by 11% and 27%, respectively. The optimal loading level is 0.1 wt.%, and reduction of T_g, flexural strength, the flexural modulus was observed by increasing the loading beyond the optimum. This phenomenon was justified from the SEM analysis of the fracture surface of Epon 862 and its composite.

The effect of MEGO on CFRP composite were studied under flexural and DCB test. From these mechanical tests, it was verified that the interlaminar fracture toughness of CFRP can be enhanced up to ~ 70% (at 0.5 wt.% MEGO loading) without compromising the flexural properties. The SEM images showed the improved fiber – matrix adhesion with addition of MEGO loading, which justifies the improvement in toughness with addition of hybrid polymer modifier.

REFERENCE:

1. Lendlein, A., *Polymers in biomedicine*. 2010, Wiley Online Library.
2. Liff, S.M., N. Kumar, and G.H. McKinley, *High-performance elastomeric nanocomposites via solvent-exchange processing.* Nature materials, 2007. **6**(1): p. 76-83.
3. Qian, Y., C.I. Lindsay, C. Macosko, and A. Stein, *Synthesis and properties of vermiculite-reinforced polyurethane nanocomposites.* ACS applied materials & interfaces, 2011. **3**(9): p. 3709-3717.
4. Nadler, M., J. Werner, T. Mahrholz, U. Riedel, and W. Hufenbach, *Effect of CNT surface functionalisation on the mechanical properties of multi-walled carbon nanotube/epoxy-composites.* Composites Part A: Applied Science and Manufacturing, 2009. **40**(6-7): p. 932-937.
5. Hernández-Pérez, A., F. Avilés, A. May-Pat, A. Valadez-González, P. Herrera-Franco, and P. Bartolo-Pérez, *Effective properties of multiwalled carbon nanotube/epoxy composites using two different tubes.* Composites Science and Technology, 2008. **68**(6): p. 1422-1431.
6. Fang, M., K. Wang, H. Lu, Y. Yang, and S. Nutt, *Covalent polymer functionalization of graphene nanosheets and mechanical properties of composites.* Journal of Materials Chemistry, 2009. **19**(38): p. 7098-7105.
7. Wang, X., W. Xing, P. Zhang, L. Song, H. Yang, and Y. Hu, *Covalent functionalization of graphene with organosilane and its use as a reinforcement in epoxy composites.* Composites science and technology, 2012. **72**(6): p. 737-743.

8. Li, Z., R. Wang, R.J. Young, L. Deng, F. Yang, L. Hao, W. Jiao, and W. Liu, *Control of the functionality of graphene oxide for its application in epoxy nanocomposites.* Polymer, 2013. **54**(23): p. 6437-6446.

9. Ji, X., L. Cui, Y. Xu, and J. Liu, *Non-covalent interactions for synthesis of new graphene based composites.* Composites Science And Technology, 2015. **106**: p. 25-31.

10. Pour, Z.S. and M. Ghaemy, *Polymer grafted graphene oxide: for improved dispersion in epoxy resin and enhancement of mechanical properties of nanocomposite.* Composites Science and Technology, 2016. **136**: p. 145-157.

11. Gudarzi, M.M. and F. Sharif, *Enhancement of dispersion and bonding of graphene-polymer through wet transfer of functionalized graphene oxide.* Express Polymer Letters, 2012. **6**(12).

12. Song, Y.S. and J.R. Youn, *Influence of dispersion states of carbon nanotubes on physical properties of epoxy nanocomposites.* Carbon, 2005. **43**(7): p. 1378-1385.

13. Suetsugu, Y., *State of dispersion–mechanical properties correlation in small particle filled polymer composites.* International Polymer Processing, 1990. **5**(3): p. 184-190.

14. Hussain, M., Y. Oku, A. Nakahira, and K. Niihara, *Effects of wet ball-milling on particle dispersion and mechanical properties of particulate epoxy composites.* Materials Letters, 1996. **26**(3): p. 177-184.

15. Huang, X., Z. Yin, S. Wu, X. Qi, Q. He, Q. Zhang, Q. Yan, F. Boey, and H. Zhang, *Graphene-based materials: synthesis, characterization, properties, and applications.* small, 2011. **7**(14): p. 1876-1902.

16. Norhayati, H., M. Zuhailimuna, H. Mohd Zobir, M.I. Illyas, M. Azmi, K. Azlan, A.B. Suriani, M. Mazidah, and J. AdilaMohamad, *A Brief Review On Recent Graphene Oxide-Based Material Nanoco Mposites: Synthesis And Applications.* 2016.

17. Noh, Y.J., H.-I. Joh, J. Yu, S.H. Hwang, S. Lee, C.H. Lee, S.Y. Kim, and J.R. Youn, *Ultra-high dispersion of graphene in polymer composite via solvent freefabrication and functionalization.* Scientific reports, 2015. **5**(1): p. 1-7.

18. Khare, H. and D. Burris, *A quantitative method for measuring nanocomposite dispersion.* Polymer, 2010. **51**(3): p. 719-729.

19. He, S., Y. Qian, K. Liu, C.W. Macosko, and A. Stein, *Modified-graphene-oxide-containing styrene masterbatches for thermosets.* Industrial & Engineering Chemistry Research, 2017. **56**(40): p. 11443-11450.

20. Si, Y. and E.T. Samulski, *Synthesis of water soluble graphene.* Nano letters, 2008. **8**(6): p. 1679-1682.

21. Pokharel, P., *High performance polyurethane nanocomposite films prepared from a masterbatch of graphene oxide in polyether polyol.* Chemical Engineering Journal, 2014. **253**: p. 356-365.

22. Bao, C., L. Song, W. Xing, B. Yuan, C.A. Wilkie, J. Huang, Y. Guo, and Y. Hu, *Preparation of graphene by pressurized oxidation and multiplex reduction and its polymer nanocomposites by masterbatch-based melt blending.* Journal of Materials Chemistry, 2012. **22**(13): p. 6088-6096.

23. Bai, L., S. He, J.W. Fruehwirth, A. Stein, C.W. Macosko, and X. Cheng, *Localizing graphene at the interface of cocontinuous polymer blends:*

Morphology, rheology, and conductivity of cocontinuous conductive polymer composites. Journal of Rheology, 2017. **61**(4): p. 575-587.

24. Park, S., S. He, J. Wang, A. Stein, and C.W. Macosko, *Graphene-polyethylene nanocomposites: Effect of graphene functionalization.* Polymer, 2016. **104**: p. 1-9.

25. Prolongo, S., R. Moriche, A. Jiménez-Suárez, M. Sánchez, and A. Ureña, *Advantages and disadvantages of the addition of graphene nanoplatelets to epoxy resins.* European Polymer Journal, 2014. **61**: p. 206-214.

26. Jayan, J.S., A. Saritha, B. Deeraj, and K. Joseph, *Triblock copolymer grafted Graphene oxide as nanofiller for toughening of epoxy resin.* Materials Chemistry and Physics, 2020. **248**: p. 122930.

27. He, S., N.D. Petkovich, K. Liu, Y. Qian, C.W. Macosko, and A. Stein, *Unsaturated polyester resin toughening with very low loadings of GO derivatives.* Polymer, 2017. **110**: p. 149-157.

28. Li, T., S. He, A. Stein, L.F. Francis, and F.S. Bates, *Synergistic toughening of epoxy modified by graphene and block copolymer micelles.* Macromolecules, 2016. **49**(24): p. 9507-9520.

29. Rafiee, M.A., J. Rafiee, Z. Wang, H. Song, Z.-Z. Yu, and N. Koratkar, *Enhanced mechanical properties of nanocomposites at low graphene content.* ACS nano, 2009. **3**(12): p. 3884-3890.

30. Rafiee, M.A., J. Rafiee, I. Srivastava, Z. Wang, H. Song, Z.Z. Yu, and N. Koratkar, *Fracture and fatigue in graphene nanocomposites.* small, 2010. **6**(2): p. 179-183.

31. Zhang, M., H. Yan, X. Yang, and C. Liu, *Effect of functionalized graphene oxide with a hyperbranched cyclotriphosphazene polymer on mechanical and thermal properties of cyanate ester composites.* Rsc Advances, 2014. **4**(86): p. 45930-45938.

32. Ren, F., G. Zhu, P. Ren, Y. Wang, and X. Cui, *In situ polymerization of graphene oxide and cyanate ester–epoxy with enhanced mechanical and thermal properties.* Applied Surface Science, 2014. **316**: p. 549-557.

33. ASTM, I., *Standard test methods for flexural properties of unreinforced and reinforced plastics and electrical insulating materials.* ASTM D790-07, 2007.

34. ASTM, I., *Standared Test Method for Flexural Properties of Unreinforced and Reinforced Plastics and Electrical Insulating Materialas by Four-Point Bending, ASTM D6272-17*. March 2017.

35. ASTM, I., *Standard Test Method for Mode I Interlaminar Fracture Toughness of Unidirectional Fiber-Reinforced Polymer Matrix Composites. ASTM D 5528-01*. July 2008.

36. Zhu, J., A. Imam, R. Crane, K. Lozano, V.N. Khabashesku, and E.V. Barrera, *Processing a glass fiber reinforced vinyl ester composite with nanotube enhancement of interlaminar shear strength.* Composites Science and Technology, 2007. **67**(7-8): p. 1509-1517.

37. Pal, R., S.L. Goyal, and I. Rawal, *Lightweight graphene encapsulated with polyaniline for excellent electromagnetic shielding performance in X-band (8.2–12.4 GHz).* Materials Science and Engineering: B, 2021. **270**: p. 115227.

38. Upadhyay, J. and A. Kumar, *Structural, thermal and dielectric studies of polypyrrole nanotubes synthesized by reactive self degrade template method.* Materials Science and Engineering: B, 2013. **178**(15): p. 982-989.

39. Ng, H., N.M. Saidi, F.S. Omar, K. Ramesh, S. Ramesh, and S. Bashir, *Thermogravimetric analysis of polymers.* Encyclopedia of polymer science and technology, 2002: p. 1-29.

40. Wang, X., L. Song, H. Yang, W. Xing, B. Kandola, and Y. Hu, *Simultaneous reduction and surface functionalization of graphene oxide with POSS for reducing fire hazards in epoxy composites.* Journal of Materials Chemistry, 2012. **22**(41): p. 22037-22043.

41. Cao, Y., J. Feng, and P. Wu, *Preparation of organically dispersible graphene nanosheet powders through a lyophilization method and their poly (lactic acid) composites.* Carbon, 2010. **48**(13): p. 3834-3839.

42. Mishra, K., K.P. Bastola, R.P. Singh, and R. Vaidyanathan, *Effect of graphene oxide on the interlaminar fracture toughness of carbon fiber/epoxy composites.* Polymer Engineering & Science, 2019. **59**(6): p. 1199-1208.

43. Chan, M.-l., K.-t. Lau, T.-t. Wong, M.-p. Ho, and D. Hui, *Mechanism of reinforcement in a nanoclay/polymer composite.* Composites Part B: Engineering, 2011. **42**(6): p. 1708-1712.

44. Shettar, M., C.S. Kowshik, M. Manjunath, and P. Hiremath, *Experimental investigation on mechanical and wear properties of Nanoclay–epoxy composites.* Journal of Materials Research and Technology, 2020. **9**(4): p. 9108-9116.

45. Mishra, K., G. Pandey, and R.P. Singh, *Enhancing the mechanical properties of an epoxy resin using polyhedral oligomeric silsesquioxane (POSS) as nano-reinforcement.* Polymer Testing, 2017. **62**: p. 210-218.

46. Domun, N., H. Hadavinia, T. Zhang, T. Sainsbury, G. Liaghat, and S. Vahid, *Improving the fracture toughness and the strength of epoxy using nanomaterials–a review of the current status.* Nanoscale, 2015. **7**(23): p. 10294-10329.

47. Mishra, K., L.K. Babu, D. Dhakal, P. Lamichhane, and R.K. Vaidyanathan, *The effect of solvent on the mechanical properties of polyhedral oligomeric silsesquioxane (POSS)–epoxy nanocomposites.* SN Applied Sciences, 2019. **1**(8): p. 1-7.

48. Bilyeu, B., W. Brostow, and K.P. Menard, *Epoxy thermosets and their applications II. Thermal analysis.* Journal of Materials Education, 2000. **22**(4/6): p. 107-130.

49. Zhao, R. and W. Luo, *Fracture surface analysis on nano-SiO2/epoxy composite.* Materials Science and Engineering: A, 2008. **483**: p. 313-315.

50. Liu, K., S. He, Y. Qian, Q. An, A. Stein, and C.W. Macosko, *Nanoparticles in glass fiber-reinforced polyester composites: comparing toughening effects of modified graphene oxide and core-shell rubber.* Polymer Composites, 2019. **40**(S2): p. E1512-E1524.

51. Zheng, N., Y. Huang, H.-Y. Liu, J. Gao, and Y.-W. Mai, *Improvement of interlaminar fracture toughness in carbon fiber/epoxy composites with carbon nanotubes/polysulfone interleaves.* Composites Science and Technology, 2017. **140**: p. 8-15.

52. Wicks, S.S., R.G. de Villoria, and B.L. Wardle, *Interlaminar and intralaminar reinforcement of composite laminates with aligned carbon nanotubes.* Composites Science and Technology, 2010. **70**(1): p. 20-28.

53. Arai, M., Y. Noro, K.-i. Sugimoto, and M. Endo, *Mode I and mode II interlaminar fracture toughness of CFRP laminates toughened by carbon nanofiber interlayer.* Composites Science and Technology, 2008. **68**(2): p. 516-525.

CHAPTER IV

SUMMARY AND FUTURE PERSPECTIVES

4.1 Summary

In this work, two major research projects have been executed successfully. The research works are classified into main three categories. The first category included the synthesis technique of hybrid polymer modifier (HPM) via redox reaction mechanism for scaled- up production. The second part contained the characterization of HPM to confirm the hybridization of MAPOSS to GO, and the final category included the study of thermal and mechanical behavior of HPM reinforced epoxy composites, and carbon fiber reinforced polymer (CFRP) composites.

Firstly, chapter I, covers the general background of composite, followed by the recent brief market analysis. A detailed literature review in the field of redox reaction mechanisms focusing on grafting of polymer to the carbon-based graphitic nanomaterial has been covered. Based on the detail study on background and past research work, a set of hypotheses was purposed, and chapter I was wrapped up with a list of purposed work to chase the goals set up by hypotheses.

In chapter II, a simple and scalable redox reaction mechanism has been employed for the modification of GO with MAPOSS. Analysis of FTIR signatures and XRD spectra confirmed the reaction between MAPOSS and GO. The XRD peak was downshifted by 0.95°, inferring that the modification of GO with MAPOSS increased the interplanner distance by 0.8 Å. The decrease in intensity of the peak in the XRD spectrum confirms the increase in random orientation of the hybrid material. XRF result showed that 10.2 mass % of silicon was added to GO because of MAPOSS grafting. The increased ratio of I_D/I_G ($(I_D/I_G)_{GO} = 1.30$, $(I_D/I_G)_{MEGO} = 1.43$) in Raman spectroscopy is totally in agreement with the FTIR, XRD and XRF results. In addition, TEM images also support the hybridization of GO with MAPOSS. TGA curves showed a significant improvement in thermal stability and char yield (2% increased to 22%) after the hybridization. The particle size distribution studies indicated that the wet hybrid material showed better dispersion than dry MEGO. The use of the three-roll mill showed promising dispersion technique of MEGO in EPON 862 resin. This dispersion method could be a potential method to enhance the mechanical and thermal properties of polymer nanocomposites. As a continued part of this work, two methods of dispersion - three-roll mill and three-roll mill followed by ultra-sonication for wet MEGO were considered for composite fabrication.

In chapter III, study on the effect of nanohybrid material "MEGO" (MAPOSS grafted GO) in the Epoxy matrix has been presented. Our research demonstrates that the dispersion of MEGO at very low wt.% in Epoxy matrix is a promising way to improve epoxy composites' thermal and mechanical properties. Although visible light microscopy

analysis showed 3R+S dispersion superior over 3R dispersion, DMA results for 3R+S were more scattered, making them less reliable to draw a conclusion. Because of that, 3R dispersion was considered throughout the work with a solid recommendation to study the appropriate sonication process in the future. The DMA result showed that at 0.1wt.% loading of MEGO in Epon 862 improves T_g by ~ 4ºC and storage modulus by ~10%. The DSC result also confirmed the increase in T_g by ~ 7 ºC at 0.1 wt.% loadings. Both DMA and DSC results agreed that the optimum improvement could be achieved at 0.1 wt.% loadings. The TGA result showed that incorporating a larger amount of MEGO makes the composites thermally more stable due to the formation of the siloxane layer in degraded samples. The flexural test showed that the maximum improvement in flexural strength and modulus was achieved at 0.1wt.% MEGO loading by 11% and 27%, respectively. The optimal loading level is 0.1 wt.%, and reduction of T_g, flexural strength, and flexural modulus with the MEGO loading beyond the optimum. This phenomenon was justified from the SEM analysis of the fracture surface of Epon 862 and its composite.

The effect of MEGO on CFRP composite were studied under flexural and DCB test. From these mechanical tests, it was verified that the interlaminar fracture toughness of CFRP can be enhanced up to ~ 70% (at 0.5 wt.% MEGO loading) without compromising the flexural properties. The SEM images showed the improved fiber – matrix adhesion with addition of MEGO loading, which justifies the improvement in toughness with addition of hybrid polymer modifier.

4.2 Future perspectives

This work mainly focuses on hybridization of GO with MAPOSS to study its effects on epoxy and CFRP composites. However, there are still possibilities to enhance the compatibility of hybrid polymer modifier by replacing MAPOSS with more reactive and compatible POSS. Generally nano additives are desired in dry powder form to eliminate the effects solvents. MAPOSS hybridized GO i.e., MEGO, occurs in millimeter sized chunk and exhibit poor dispersion in dry state. So, it is highly recommended to work on modification of synthesis process to achieve final product in dry fine powder form. The presence of solvent in wet MEGO might have adverse effects on mechanical properties of composite which can be completely addressed by dry MEGO. The previous study in similar area showed that the dispersion of GO in PVP is a promising technique to incorporate in epoxy and fiber reinforced polymer composite for enhancement in mechanical properties. Adopting this idea in future to disperse MEGO in PVP could take to the enhancement in mechanical properties of epoxy and CFRP composite into new level.

The dispersion technique 3R + S showed promising results under optical microscope image analysis but higher standard deviation in DMA result warns to investigate proper sonication process (time, amplitude, temperature) in future for MEGO dispersion with this method. In addition to that the characterization of inter-particle force of attraction or repulsion would give more insight into the chances of nanoparticle agglomeration in polymer matrix too.

The effect of MEGO in CFRP was characterized by flexural and DCB test. More additional mechanical tests like fiber pull out, and fragmentation test is recommended in future for further in-depth understanding. SEM fractography showed the improvement in fiber-matrix interactions with addition of MEGO. In future nuclear magnetic resonance (NMR) spectroscopy would be an interesting characterization for insight understanding of fiber-matrix interactions.

REFERENCES

REFERENCES FOR CHAPTER I

1. Air Force SBIR\STTR. *New Composite Materials Will Promote Bigger Fuel Savings And Better Fatigue Resistance In Aircraft*. 2016, April 1st [cited August, 2021; Available from: https://www.afsbirsttr.af.mil/News-Media/Success-Stories/Article/1480873/new-composite-materials-will-promote-bigger-fuel-savings-and-better-fatigue-res/.
2. CompositesWorld. *Aviation Outlook: Fuel pricing ignites demand for composites in commercial transports*. 2006, June 30th [cited August 2021; Available from: https://www.compositesworld.com/articles/aviation-outlook-fuel-pricing-ignites-demand-for-composites-in-commercial-transports.
3. Chad Schell, G.J.L., Blake Marshall,. *Composites*. 2020, June [cited August, 2021; Available from: Advanced Manufacturing Office (AMO) Peer Review presented at Washington DC https://manufacturing.energy.gov.
4. Chawla, K.K., *Composite materials: science and engineering,Third Edition*, Springer Science & Business Media, New york 2012, ISBN 978-0-387-74364-6 ISBN 978-0-387-7436503(eBook), DOI 10.1007/978-0-787-74365-3.
5. Park, S.-J. and M.-K. Seo, *Interface science and composites*. Vol. 18. 2011: Academic Press.

6. MARKETSANDMARKETS. *Composites Market by Fiber Type (Glass Fiber Composites, Carbon Fiber Composites, Natural Fiber Composites), Resin Type (Thermoset Composites, Thermoplastic Composites), Manufacturing Process, End-use Industry and Region - Global Forecast to 2025*. 2020 [cited 2020 November, 2020]; Available from: https://www.marketsandmarkets.com/Market-Reports/composite-market-200051282.html?gclid=EAIaIQobChMIpc7Xjonx7AIVEPfjBx24yAalEAAYASAAEgI-wPD_BwE.

7. GrabdViewResearch. *Composites Market Size Worth $160.54 Billion By 2027 | CAGR: 7.6%*. 2020 [cited 2020 November, 2020]; Available from: https://www.grandviewresearch.com/press-release/global-composites-market.

8. MARKETSANDMARKETS. *Nanocomposites Market by Type (Carbon Nanotubes, Nanoclay Metal Oxide, Nanofiber, Graphene), Resin Type, Application (Packaging, Automotive, Electrical & Semiconductors, Coatings, Aerospace & Defense, Energy), Region - Global Forecast to 2024*. 2021 [cited 2021 02/26/2021]; Available from: https://www.marketsandmarkets.com/Market-Reports/nanocomposites-market-141476334.html#utm_source=Mailgun-260221&utm_medium=NA.

9. MARKETSANDMARKETS. *"COMPOSITES MARKET - GLOBAL FORECAST TO 2022*. 2017 [cited 2020 November, 202].

10. Gudarzi, M.M. and F. Sharif, *Enhancement of dispersion and bonding of graphene-polymer through wet transfer of functionalized graphene oxide.* Express Polymer Letters, 2012. **6**(12).

11. Rajak, D.K., D.D. Pagar, P.L. Menezes, and E. Linul, *Fiber-reinforced polymer composites: Manufacturing, properties, and applications.* Polymers, 2019. **11**(10): p. 1667.

12. Lichtenhan, J.D., T.S. Haddad, J.J. Schwab, M.J. Carr, K.P. Chaffee, and P.T. Mather, *The next generation of silicon-based plastics: Polyhedral oligomeric silsesquioxane (POSS) nanocomposites.* American Chemical Society, Polymer Preprints, Division of Polymer Chemistry, 1998. **39**(1): p. 489-490.

13. Król-Morkisz, K. and K. Pielichowska, *Thermal decomposition of polymer nanocomposites with functionalized nanoparticles*, in *Polymer Composites with Functionalized Nanoparticles*. 2019, Elsevier. p. 405-435.

14. Kuo, S.-W. and F.-C. Chang, *POSS related polymer nanocomposites.* Progress in polymer science, 2011. **36**(12): p. 1649-1696.

15. Pielichowski, K., J. Njuguna, B. Janowski, and J. Pielichowski, *Polyhedral oligomeric silsesquioxanes (POSS)-containing nanohybrid polymers*, in *Supramolecular Polymers Polymeric Betains Oligomers*. 2006, Springer. p. 225-296.

16. Raftopoulos, K.N. and K. Pielichowski, *Segmental dynamics in hybrid polymer/POSS nanomaterials.* Progress in Polymer Science, 2016. **52**: p. 136-187.

17. Zhao, J., Y. Fu, and S. Liu, *Polyhedral oligomeric silsesquioxane (POSS)-modified thermoplastic and thermosetting nanocomposites: a review.* Polymers and Polymer Composites, 2008. **16**(8): p. 483-500.

18. Gnanasekaran, D., K. Madhavan, and B. Reddy, *Developments of polyhedral oligomeric silsesquioxanes (POSS), possnanocomposites and their applications: A review.* 2009.

19. Ayandele, E., B. Sarkar, and P. Alexandridis, *Polyhedral oligomeric silsesquioxane (POSS)-containing polymer nanocomposites.* Nanomaterials, 2012. **2**(4): p. 445-475.

20. Huang, X., Z. Yin, S. Wu, X. Qi, Q. He, Q. Zhang, Q. Yan, F. Boey, and H. Zhang, *Graphene-based materials: synthesis, characterization, properties, and applications.* small, 2011. **7**(14): p. 1876-1902.

21. Norhayati, H., M. Zuhailimuna, H. Mohd Zobir, M.I. Illyas, M. Azmi, K. Azlan, A.B. Suriani, M. Mazidah, and J. AdilaMohamad, *A Brief Review On Recent Graphene Oxide-Based Material Nanoco Mposites: Synthesis And Applications.* 2016.

22. Mathur, R.B., B.P. Singh, and S. Pande, *Carbon nanomaterials: synthesis, structure, properties and applications*. 2016: CRC Press.

23. Tang, J., H. Zhou, Y. Liang, X. Shi, X. Yang, and J. Zhang, *Properties of graphene oxide/epoxy resin composites.* Journal of Nanomaterials, 2014. **2014**.

24. Pei, S. and H.-M. Cheng, *The reduction of graphene oxide.* Carbon, 2012. **50**(9): p. 3210-3228.

25. Braun, D., *Origins and development of initiation of free radical polymerization processes.* International Journal of Polymer Science, 2009.

26. Garra, P., C. Dietlin, F. Morlet-Savary, F. Dumur, D. Gigmes, J.-P. Fouassier, and J. Lalevée, *Redox two-component initiated free radical and cationic*

polymerizations: Concepts, reactions and applications. Progress in Polymer Science, 2019. **94**: p. 33-56.

27. Ma, L., X. Yang, L. Gao, M. Lu, C. Guo, Y. Li, Y. Tu, and X. Zhu, *Synthesis and characterization of polymer grafted graphene oxide sheets using a Ce (IV)/HNO3 redox system in an aqueous solution.* carbon, 2013. **53**: p. 269-276.
28. Liu, J., G. Liu, and W. Liu, *Preparation of water-soluble β-cyclodextrin/poly (acrylic acid)/graphene oxide nanocomposites as new adsorbents to remove cationic dyes from aqueous solutions.* Chemical Engineering Journal, 2014. **257**: p. 299-308.
29. Chauke, V.P., A. Maity, and A. Chetty, *High-performance towards removal of toxic hexavalent chromium from aqueous solution using graphene oxide-alpha cyclodextrin-polypyrrole nanocomposites.* Journal of Molecular Liquids, 2015. **211**: p. 71-77.
30. Mkhoyan, K.A., A.W. Contryman, J. Silcox, D.A. Stewart, G. Eda, C. Mattevi, S. Miller, and M. Chhowalla, *Atomic and electronic structure of graphene-oxide.* Nano letters, 2009. **9**(3): p. 1058-1063.
31. Lin, Z., Y. Liu, Z. Li, and C.-p. Wong,Lin, Z., Y. Liu, Z. Li, and C.-p. Wong, *Novel preparation of functionalized graphene oxide for large scale, low cost, and self-cleaning coatings of electronic devices*. in *2011 IEEE 61st Electronic Components and Technology Conference (ECTC)*. 2011. IEEE.
32. Potts, J.R., D.R. Dreyer, C.W. Bielawski, and R.S. Ruoff, *Graphene-based polymer nanocomposites.* Polymer, 2011. **52**(1): p. 5-25.

33. Sengupta, R., M. Bhattacharya, S. Bandyopadhyay, and A.K. Bhowmick, *A review on the mechanical and electrical properties of graphite and modified graphite reinforced polymer composites.* Progress in polymer science, 2011. **36**(5): p. 638-670.

34. Rafiee, M.A., J. Rafiee, Z. Wang, H. Song, Z.-Z. Yu, and N. Koratkar, *Enhanced mechanical properties of nanocomposites at low graphene content.* ACS nano, 2009. **3**(12): p. 3884-3890.

35. Rafiee, M.A., W. Lu, A.V. Thomas, A. Zandiatashbar, J. Rafiee, J.M. Tour, and N.A. Koratkar, *Graphene nanoribbon composites.* ACS nano, 2010. **4**(12): p. 7415-7420.

36. Wang, Y., Z. Shi, J. Fang, H. Xu, and J. Yin, *Graphene oxide/polybenzimidazole composites fabricated by a solvent-exchange method.* Carbon, 2011. **49**(4): p. 1199-1207.

37. Gui, D., C. Liu, F. Chen, and J. Liu, *Preparation of polyaniline/graphene oxide nanocomposite for the application of supercapacitor.* Applied surface science, 2014. **307**: p. 172-177.

38. Wang, H., Q. Hao, X. Yang, L. Lu, and X. Wang, *A nanostructured graphene/polyaniline hybrid material for supercapacitors.* Nanoscale, 2010. **2**(10): p. 2164-2170.

39. Xu, X., J. Shen, N. Li, and M. Ye, *Facile synthesis of reduced graphene oxide/CoWO4 nanocomposites with enhanced electrochemical performances for supercapacitors.* Electrochimica Acta, 2014. **150**: p. 23-34.

40. Zhao, X., J. Zhang, J. Zhang, C. Gong, X. Gu, Z. Ma, J. Zhou, L. Yu, and Z. Zhang, *Construction of spongy antimony-doped tin oxide/graphene nanocomposites using commercially available products and its excellent electrochemical performance.* Journal of Power Sources, 2015. **294**: p. 223-231.

41. Li, Y., D. Wang, W. Li, and Y. He, *Photoelectric conversion properties of electrochemically codeposited graphene oxide–ZnO nanocomposite films.* Journal of Alloys and Compounds, 2015. **648**: p. 942-950.

42. Xu, G., F. Jiang, Z.-a. Ren, and L.-w. Yang, *Polyhedral MnO nanocrystals anchored on reduced graphene oxide as an anode material with superior lithium storage capability.* Ceramics International, 2015. **41**(9): p. 10680-10688.

43. She, X., X. Zhang, J. Liu, L. Li, X. Yu, Z. Huang, and S. Shang, *Microwave-assisted synthesis of Mn3O4 nanoparticles@ reduced graphene oxide nanocomposites for high performance supercapacitors.* Materials research bulletin, 2015. **70**: p. 945-950.

44. Mehrali, M., S.T. Latibari, M. Mehrali, H.S.C. Metselaar, and M. Silakhori, *Shape-stabilized phase change materials with high thermal conductivity based on paraffin/graphene oxide composite.* Energy conversion and management, 2013. **67**: p. 275-282.

45. He, H.-Y., *Photoinduced superhydrophilicity and high photocatalytic activity of ZnO–reduced graphene oxide nanocomposite films for self-cleaning applications.* Materials Science in Semiconductor Processing, 2015. **31**: p. 200-208.

46. Luo, L., Y. Yang, A. Zhang, M. Wang, Y. Liu, L. Bian, F. Jiang, and X. Pan, *Hydrothermal synthesis of fluorinated anatase TiO2/reduced graphene oxide*

nanocomposites and their photocatalytic degradation of bisphenol A. Applied Surface Science, 2015. **353**: p. 469-479.

47. Song, Y., K. Qu, C. Zhao, J. Ren, and X. Qu, *Graphene oxide: intrinsic peroxidase catalytic activity and its application to glucose detection.* Advanced Materials, 2010. **22**(19): p. 2206-2210.

48. Yan, X., X. Zhang, H. Liu, Y. Liu, J. Ding, Y. Liu, Q. Cai, and J. Zhang, *Fabrication of SDBS intercalated-reduced graphene oxide/polypyrrole nanocomposites for supercapacitors.* Synthetic metals, 2014. **196**: p. 1-7.

49. Gong, L., I.A. Kinloch, R.J. Young, I. Riaz, R. Jalil, and K.S. Novoselov, *Interfacial stress transfer in a graphene monolayer nanocomposite.* Advanced Materials, 2010. **22**(24): p. 2694-2697.

50. Stankovich, S., R.D. Piner, X. Chen, N. Wu, S.T. Nguyen, and R.S. Ruoff, *Stable aqueous dispersions of graphitic nanoplatelets via the reduction of exfoliated graphite oxide in the presence of poly (sodium 4-styrenesulfonate).* Journal of Materials Chemistry, 2006. **16**(2): p. 155-158.

51. Wang, X., J. Jin, and M. Song, *Cyanate ester resin/graphene nanocomposite: curing dynamics and network formation.* European polymer journal, 2012. **48**(6): p. 1034-1041.

52. Yu, A., P. Ramesh, M.E. Itkis, E. Bekyarova, and R.C. Haddon, *Graphite nanoplatelet− epoxy composite thermal interface materials.* The Journal of Physical Chemistry C, 2007. **111**(21): p. 7565-7569.

53. Mishra, K., G. Pandey, and R.P. Singh, *Enhancing the mechanical properties of an epoxy resin using polyhedral oligomeric silsesquioxane (POSS) as nano-reinforcement.* Polymer Testing, 2017. **62**: p. 210-218.

54. Ahmadi-Moghadam, B. and F. Taheri, *Influence of graphene nanoplatelets on modes I, II and III interlaminar fracture toughness of fiber-reinforced polymer composites.* Engineering Fracture Mechanics, 2015. **143**: p. 97-107.

55. Zhu, J., A. Imam, R. Crane, K. Lozano, V.N. Khabashesku, and E.V. Barrera, *Processing a glass fiber reinforced vinyl ester composite with nanotube enhancement of interlaminar shear strength.* Composites Science and Technology, 2007. **67**(7-8): p. 1509-1517.

56. Degirmenci, M., S. Hicri, and H. Yilmaz, *Synthesis and characterization of a novel water-soluble mid-chain macrophotoinitiator of polyacrylamide by Ce (IV)/HNO3 redox system.* European polymer journal, 2008. **44**(11): p. 3776-3781.

57. Wang, B., D. Yang, J.Z. Zhang, C. Xi, and J. Hu, *Stimuli-responsive polymer covalent functionalization of graphene oxide by Ce (IV)-induced redox polymerization.* The Journal of Physical Chemistry C, 2011. **115**(50): p. 24636-24641.

58. Xue, Y., Y. Liu, F. Lu, J. Qu, H. Chen, and L. Dai, *Functionalization of graphene oxide with polyhedral oligomeric silsesquioxane (POSS) for multifunctional applications.* The journal of physical chemistry letters, 2012. **3**(12): p. 1607-1612.

59. Wang, X., Y. Hu, L. Song, H. Yang, B. Yu, B. Kandola, and D. Deli, *Comparative study on the synergistic effect of POSS and graphene with melamine*

phosphate on the flame retardance of poly (butylene succinate). Thermochimica acta, 2012. **543**: p. 156-164.

60. Valentini, L., S.B. Bon, O. Monticelli, and J.M. Kenny, *Deposition of amino-functionalized polyhedral oligomeric silsesquioxanes on graphene oxide sheets immobilized onto an amino-silane modified silicon surface.* Journal of Materials Chemistry, 2012. **22**(13): p. 6213-6217.
61. Valentini, L., S.B. Bon, M. Cardinali, O. Monticelli, and J.M. Kenny, *POSS vapor grafting on graphene oxide film.* Chemical Physics Letters, 2012. **537**: p. 84-87.
62. Valentini, L., M. Cardinali, J.M. Kenny, M. Prato, and O. Monticelli, *A photoresponsive hybrid nanomaterial based on graphene and polyhedral oligomeric silsesquioxanes.* European Journal of Inorganic Chemistry, 2012. **2012**(32): p. 5282-5287.
63. Antoniou, K.S., M. Karakassides, D. Gournis, and P. Rudolf, *Carbon nanostructures containing polyhedral oligomeric silsesquioxanes (POSS).* Chemistry, 2016. **20**(6): p. 662-673.
64. Yu, W., J. Fu, X. Dong, L. Chen, and L. Shi, *A graphene hybrid material functionalized with POSS: Synthesis and applications in low-dielectric epoxy composites.* Composites science and technology, 2014. **92**: p. 112-119.
65. Qu, L., Y. Sui, C. Zhang, P. Li, X. Dai, B. Xu, and D. Fang, *POSS-functionalized graphene oxide hybrids with improved dispersive and smoke-suppressive properties for epoxy flame-retardant application.* European Polymer Journal, 2020. **122**: p. 109383.

66. Maleque, M.A. and M.S. Salit, *Mechanical failure of materials*, in *Materials Selection and Design*. 2013, Springer. p. 17-38.

67. Liu, D., *Impact-induced delamination—a view of bending stiffness mismatching.* Journal of composite materials, 1988. **22**(7): p. 674-692.

68. Kumar, C.S., M. Fotouhi, M. Saeedifar, and V. Arumugam, *Acoustic emission based investigation on the effect of temperature and hybridization on drop weight impact and post-impact residual strength of hemp and basalt fibres reinforced polymer composite laminates.* Composites Part B: Engineering, 2019. **173**: p. 106962.

REFERENCES FOR CHAPTER II

1. Pascault, J., H. Sautereau, J. Verdu, and R. Williams, *Are cured thermosets inhomogeneous?* Thermosetting Polymers. New York: Marcel Dekker, 2002.
2. He, S., N.D. Petkovich, K. Liu, Y. Qian, C.W. Macosko, and A. Stein, *Unsaturated polyester resin toughening with very low loadings of GO derivatives.* Polymer, 2017. **110**: p. 149-157.
3. Nadler, M., J. Werner, T. Mahrholz, U. Riedel, and W. Hufenbach, *Effect of CNT surface functionalisation on the mechanical properties of multi-walled carbon nanotube/epoxy-composites.* Composites Part A: Applied Science and Manufacturing, 2009. **40**(6-7): p. 932-937.
4. Hernández-Pérez, A., F. Avilés, A. May-Pat, A. Valadez-González, P. Herrera-Franco, and P. Bartolo-Pérez, *Effective properties of multiwalled carbon nanotube/epoxy composites using two different tubes.* Composites Science and Technology, 2008. **68**(6): p. 1422-1431.
5. Fang, M., K. Wang, H. Lu, Y. Yang, and S. Nutt, *Covalent polymer functionalization of graphene nanosheets and mechanical properties of composites.* Journal of Materials Chemistry, 2009. **19**(38): p. 7098-7105.
6. Wang, X., W. Xing, P. Zhang, L. Song, H. Yang, and Y. Hu, *Covalent functionalization of graphene with organosilane and its use as a reinforcement in epoxy composites.* Composites science and technology, 2012. **72**(6): p. 737-743.
7. Li, Z., R. Wang, R.J. Young, L. Deng, F. Yang, L. Hao, W. Jiao, and W. Liu, *Control of the functionality of graphene oxide for its application in epoxy nanocomposites.* Polymer, 2013. **54**(23): p. 6437-6446.

8. Ji, X., L. Cui, Y. Xu, and J. Liu, *Non-covalent interactions for synthesis of new graphene based composites.* Composites Science And Technology, 2015. **106**: p. 25-31.

9. Pour, Z.S. and M. Ghaemy, *Polymer grafted graphene oxide: for improved dispersion in epoxy resin and enhancement of mechanical properties of nanocomposite.* Composites Science and Technology, 2016. **136**: p. 145-157.

10. Rezić, I., T. Haramina, and T. Rezić, *Metal nanoparticles and carbon nanotubes—perfect antimicrobial nano-fillers in polymer-based food packaging materials*, in *food packaging*. 2017, Elsevier. p. 497-532.

11. Wong, C. and R.S. Bollampally, *Thermal conductivity, elastic modulus, and coefficient of thermal expansion of polymer composites filled with ceramic particles for electronic packaging.* Journal of applied polymer science, 1999. **74**(14): p. 3396-3403.

12. Bauhofer, W. and J.Z. Kovacs, *A review and analysis of electrical percolation in carbon nanotube polymer composites.* Composites science and technology, 2009. **69**(10): p. 1486-1498.

13. Shen, C., Y. Zhou, R. Dou, W. Wang, B. Yin, and M.-b. Yang, *Effect of the core-forming polymer on phase morphology and mechanical properties of PA6/EPDM-g-MA/HDPE ternary blends.* Polymer, 2015. **56**: p. 395-405.

14. Ferri, J.M., O. Fenollar, A. Jorda-Vilaplana, D. García-Sanoguera, and R. Balart, *Effect of miscibility on mechanical and thermal properties of poly (lactic acid)/polycaprolactone blends.* Polymer International, 2016. **65**(4): p. 453-463.

15. Huang, A., X. Peng, and L.-S. Turng, *In-situ fibrillated polytetrafluoroethylene (PTFE) in thermoplastic polyurethane (TPU) via melt blending: Effect on rheological behavior, mechanical properties, and microcellular foamability.* Polymer, 2018. **134**: p. 263-274.

16. Gudarzi, M.M. and F. Sharif, *Enhancement of dispersion and bonding of graphene-polymer through wet transfer of functionalized graphene oxide.* Express Polymer Letters, 2012. **6**(12).

17. Huang, X., Z. Yin, S. Wu, X. Qi, Q. He, Q. Zhang, Q. Yan, F. Boey, and H. Zhang, *Graphene-based materials: synthesis, characterization, properties, and applications.* small, 2011. **7**(14): p. 1876-1902.

18. Norhayati, H., M. Zuhailimuna, H. Mohd Zobir, M.I. Illyas, M. Azmi, K. Azlan, A.B. Suriani, M. Mazidah, and J. AdilaMohamad, *A Brief Review On Recent Graphene Oxide-Based Material Nanoco Mposites: Synthesis And Applications.* 2016.

19. Noh, Y.J., H.-I. Joh, J. Yu, S.H. Hwang, S. Lee, C.H. Lee, S.Y. Kim, and J.R. Youn, *Ultra-high dispersion of graphene in polymer composite via solvent freefabrication and functionalization.* Scientific reports, 2015. **5**(1): p. 1-7.

20. Liu, J., G. Liu, and W. Liu, *Preparation of water-soluble β-cyclodextrin/poly (acrylic acid)/graphene oxide nanocomposites as new adsorbents to remove cationic dyes from aqueous solutions.* Chemical Engineering Journal, 2014. **257**: p. 299-308.

21. Chauke, V.P., A. Maity, and A. Chetty, *High-performance towards removal of toxic hexavalent chromium from aqueous solution using graphene oxide-alpha*

cyclodextrin-polypyrrole nanocomposites. Journal of Molecular Liquids, 2015. **211**: p. 71-77.

22. Mkhoyan, K.A., A.W. Contryman, J. Silcox, D.A. Stewart, G. Eda, C. Mattevi, S. Miller, and M. Chhowalla, *Atomic and electronic structure of graphene-oxide.* Nano letters, 2009. **9**(3): p. 1058-1063.
23. Lin, Z., Y. Liu, Z. Li, and C.-p. Wong,Lin, Z., Y. Liu, Z. Li, and C.-p. Wong, *Novel preparation of functionalized graphene oxide for large scale, low cost, and self-cleaning coatings of electronic devices*. in *2011 IEEE 61st Electronic Components and Technology Conference (ECTC)*. 2011. IEEE.
24. Antoniou, K.S., M. Karakassides, D. Gournis, and P. Rudolf, *Carbon nanostructures containing polyhedral oligomeric silsesquioxanes (POSS).* Chemistry, 2016. **20**(6): p. 662-673.
25. Król-Morkisz, K. and K. Pielichowska, *Thermal decomposition of polymer nanocomposites with functionalized nanoparticles*, in *Polymer Composites with Functionalized Nanoparticles*. 2019, Elsevier. p. 405-435.
26. Kuo, S.-W. and F.-C. Chang, *POSS related polymer nanocomposites.* Progress in polymer science, 2011. **36**(12): p. 1649-1696.
27. Pielichowski, K., J. Njuguna, B. Janowski, and J. Pielichowski, *Polyhedral oligomeric silsesquioxanes (POSS)-containing nanohybrid polymers*, in *Supramolecular Polymers Polymeric Betains Oligomers*. 2006, Springer. p. 225-296.

28. Zhao, J., Y. Fu, and S. Liu, *Polyhedral oligomeric silsesquioxane (POSS)-modified thermoplastic and thermosetting nanocomposites: a review.* Polymers and Polymer Composites, 2008. **16**(8): p. 483-500.

29. Gnanasekaran, D., K. Madhavan, and B. Reddy, *Developments of polyhedral oligomeric silsesquioxanes (POSS), possnanocomposites and their applications: A review.* 2009.

30. Ayandele, E., B. Sarkar, and P. Alexandridis, *Polyhedral oligomeric silsesquioxane (POSS)-containing polymer nanocomposites.* Nanomaterials, 2012. **2**(4): p. 445-475.

31. Xue, Y., Y. Liu, F. Lu, J. Qu, H. Chen, and L. Dai, *Functionalization of graphene oxide with polyhedral oligomeric silsesquioxane (POSS) for multifunctional applications.* The journal of physical chemistry letters, 2012. **3**(12): p. 1607-1612.

32. Yu, W., J. Fu, X. Dong, L. Chen, and L. Shi, *A graphene hybrid material functionalized with POSS: Synthesis and applications in low-dielectric epoxy composites.* Composites science and technology, 2014. **92**: p. 112-119.

33. Wang, X., L. Song, H. Yang, W. Xing, B. Kandola, and Y. Hu, *Simultaneous reduction and surface functionalization of graphene oxide with POSS for reducing fire hazards in epoxy composites.* Journal of Materials Chemistry, 2012. **22**(41): p. 22037-22043.

34. Valentini, L., S.B. Bon, O. Monticelli, and J.M. Kenny, *Deposition of amino-functionalized polyhedral oligomeric silsesquioxanes on graphene oxide sheets immobilized onto an amino-silane modified silicon surface.* Journal of Materials Chemistry, 2012. **22**(13): p. 6213-6217.

35. Qu, L., Y. Sui, C. Zhang, P. Li, X. Dai, B. Xu, and D. Fang, *POSS-functionalized graphene oxide hybrids with improved dispersive and smoke-suppressive properties for epoxy flame-retardant application.* European Polymer Journal, 2020. **122**: p. 109383.

36. Valentini, L., M. Cardinali, J.M. Kenny, M. Prato, and O. Monticelli, *A photoresponsive hybrid nanomaterial based on graphene and polyhedral oligomeric silsesquioxanes.* European Journal of Inorganic Chemistry, 2012. **2012**(32): p. 5282-5287.

37. Galande, C., A.D. Mohite, A.V. Naumov, W. Gao, L. Ci, A. Ajayan, H. Gao, A. Srivastava, R.B. Weisman, et al., *Quasi-molecular fluorescence from graphene oxide.* Scientific reports, 2011. **1**(1): p. 1-5.

38. Yu, B., K. Wang, Y. Hu, F. Nan, J. Pu, H. Zhao, and P. Ju, *Tribological properties of synthetic base oil containing polyhedral oligomeric silsesquioxane grafted graphene oxide.* RSC advances, 2018. **8**(42): p. 23606-23614.

39. Guo, D., J. Chen, L. Wen, P. Wang, S. Xu, J. Cheng, X. Wen, S. Wang, C. Huang, et al., *A superhydrophobic polyacrylate film with good durability fabricated via spray coating.* Journal of Materials Science, 2018. **53**(22): p. 15390-15400.

40. De Silva, K.K.H., H.-H. Huang, and M. Yoshimura, *Progress of reduction of graphene oxide by ascorbic acid.* Applied Surface Science, 2018. **447**: p. 338-346.

41. Ye, Y., D. Zhang, J. Li, T. Liu, J. Pu, H. Zhao, and L. Wang, *One-step synthesis of superhydrophobic polyhedral oligomeric silsesquioxane-graphene oxide and*

its application in anti-corrosion and anti-wear fields. Corrosion Science, 2019. **147**: p. 9-21.

42. Zhang, C., T. Li, H. Song, Y. Han, Y. Dong, Y. Wang, and Q. Wang, *Improving the thermal conductivity and mechanical property of epoxy composites by introducing polyhedral oligomeric silsesquioxane-grafted graphene oxide.* Polymer Composites, 2018. **39**(S3): p. E1890-E1899.
43. Farivar, F., P.L. Yap, K. Hassan, T.T. Tung, D.N. Tran, A.J. Pollard, and D. Losic, *Unlocking thermogravimetric analysis (TGA) in the fight against "Fake graphene" materials.* Carbon, 2021. **179**: p. 505-513.
44. Qiang, X., F. Chen, X.Y. Ma, and X.B. Hou, *Star-shaped POSS–methacrylate copolymers with phenyl–triazole as terminal groups, synthesis, and the pyrolysis analysis.* Journal of Applied Polymer Science, 2014. **131**(16).
45. Zhou, J., Y. Zhao, K. Yu, X. Zhou, and X. Xie, *Synthesis, thermal stability and photoresponsive behaviors of azobenzene-tethered polyhedral oligomeric silsesquioxanes.* New Journal of Chemistry, 2011. **35**(12): p. 2781-2792.
46. Mishra, K., K.P. Bastola, R.P. Singh, and R. Vaidyanathan, *Effect of graphene oxide on the interlaminar fracture toughness of carbon fiber/epoxy composites.* Polymer Engineering & Science, 2019. **59**(6): p. 1199-1208.

REFERENCES FOR CHAPTER III

1. Lendlein, A., *Polymers in biomedicine*. 2010, Wiley Online Library.
2. Liff, S.M., N. Kumar, and G.H. McKinley, *High-performance elastomeric nanocomposites via solvent-exchange processing.* Nature materials, 2007. **6**(1): p. 76-83.
3. Qian, Y., C.I. Lindsay, C. Macosko, and A. Stein, *Synthesis and properties of vermiculite-reinforced polyurethane nanocomposites.* ACS applied materials & interfaces, 2011. **3**(9): p. 3709-3717.
4. Nadler, M., J. Werner, T. Mahrholz, U. Riedel, and W. Hufenbach, *Effect of CNT surface functionalisation on the mechanical properties of multi-walled carbon nanotube/epoxy-composites.* Composites Part A: Applied Science and Manufacturing, 2009. **40**(6-7): p. 932-937.
5. Hernández-Pérez, A., F. Avilés, A. May-Pat, A. Valadez-González, P. Herrera-Franco, and P. Bartolo-Pérez, *Effective properties of multiwalled carbon nanotube/epoxy composites using two different tubes.* Composites Science and Technology, 2008. **68**(6): p. 1422-1431.
6. Fang, M., K. Wang, H. Lu, Y. Yang, and S. Nutt, *Covalent polymer functionalization of graphene nanosheets and mechanical properties of composites.* Journal of Materials Chemistry, 2009. **19**(38): p. 7098-7105.
7. Wang, X., W. Xing, P. Zhang, L. Song, H. Yang, and Y. Hu, *Covalent functionalization of graphene with organosilane and its use as a reinforcement in epoxy composites.* Composites science and technology, 2012. **72**(6): p. 737-743.

8. Li, Z., R. Wang, R.J. Young, L. Deng, F. Yang, L. Hao, W. Jiao, and W. Liu, *Control of the functionality of graphene oxide for its application in epoxy nanocomposites.* Polymer, 2013. **54**(23): p. 6437-6446.

9. Ji, X., L. Cui, Y. Xu, and J. Liu, *Non-covalent interactions for synthesis of new graphene based composites.* Composites Science And Technology, 2015. **106**: p. 25-31.

10. Pour, Z.S. and M. Ghaemy, *Polymer grafted graphene oxide: for improved dispersion in epoxy resin and enhancement of mechanical properties of nanocomposite.* Composites Science and Technology, 2016. **136**: p. 145-157.

11. Gudarzi, M.M. and F. Sharif, *Enhancement of dispersion and bonding of graphene-polymer through wet transfer of functionalized graphene oxide.* Express Polymer Letters, 2012. **6**(12).

12. Song, Y.S. and J.R. Youn, *Influence of dispersion states of carbon nanotubes on physical properties of epoxy nanocomposites.* Carbon, 2005. **43**(7): p. 1378-1385.

13. Suetsugu, Y., *State of dispersion–mechanical properties correlation in small particle filled polymer composites.* International Polymer Processing, 1990. **5**(3): p. 184-190.

14. Hussain, M., Y. Oku, A. Nakahira, and K. Niihara, *Effects of wet ball-milling on particle dispersion and mechanical properties of particulate epoxy composites.* Materials Letters, 1996. **26**(3): p. 177-184.

15. Huang, X., Z. Yin, S. Wu, X. Qi, Q. He, Q. Zhang, Q. Yan, F. Boey, and H. Zhang, *Graphene-based materials: synthesis, characterization, properties, and applications.* small, 2011. **7**(14): p. 1876-1902.

16. Norhayati, H., M. Zuhailimuna, H. Mohd Zobir, M.I. Illyas, M. Azmi, K. Azlan, A.B. Suriani, M. Mazidah, and J. AdilaMohamad, *A Brief Review On Recent Graphene Oxide-Based Material Nanoco Mposites: Synthesis And Applications.* 2016.

17. Noh, Y.J., H.-I. Joh, J. Yu, S.H. Hwang, S. Lee, C.H. Lee, S.Y. Kim, and J.R. Youn, *Ultra-high dispersion of graphene in polymer composite via solvent freefabrication and functionalization.* Scientific reports, 2015. **5**(1): p. 1-7.

18. Khare, H. and D. Burris, *A quantitative method for measuring nanocomposite dispersion.* Polymer, 2010. **51**(3): p. 719-729.

19. He, S., Y. Qian, K. Liu, C.W. Macosko, and A. Stein, *Modified-graphene-oxide-containing styrene masterbatches for thermosets.* Industrial & Engineering Chemistry Research, 2017. **56**(40): p. 11443-11450.

20. Si, Y. and E.T. Samulski, *Synthesis of water soluble graphene.* Nano letters, 2008. **8**(6): p. 1679-1682.

21. Pokharel, P., *High performance polyurethane nanocomposite films prepared from a masterbatch of graphene oxide in polyether polyol.* Chemical Engineering Journal, 2014. **253**: p. 356-365.

22. Bao, C., L. Song, W. Xing, B. Yuan, C.A. Wilkie, J. Huang, Y. Guo, and Y. Hu, *Preparation of graphene by pressurized oxidation and multiplex reduction and its polymer nanocomposites by masterbatch-based melt blending.* Journal of Materials Chemistry, 2012. **22**(13): p. 6088-6096.

23. Bai, L., S. He, J.W. Fruehwirth, A. Stein, C.W. Macosko, and X. Cheng, *Localizing graphene at the interface of cocontinuous polymer blends:*

Morphology, rheology, and conductivity of cocontinuous conductive polymer composites. Journal of Rheology, 2017. **61**(4): p. 575-587.

24. Park, S., S. He, J. Wang, A. Stein, and C.W. Macosko, *Graphene-polyethylene nanocomposites: Effect of graphene functionalization.* Polymer, 2016. **104**: p. 1-9.

25. Prolongo, S., R. Moriche, A. Jiménez-Suárez, M. Sánchez, and A. Ureña, *Advantages and disadvantages of the addition of graphene nanoplatelets to epoxy resins.* European Polymer Journal, 2014. **61**: p. 206-214.

26. Jayan, J.S., A. Saritha, B. Deeraj, and K. Joseph, *Triblock copolymer grafted Graphene oxide as nanofiller for toughening of epoxy resin.* Materials Chemistry and Physics, 2020. **248**: p. 122930.

27. He, S., N.D. Petkovich, K. Liu, Y. Qian, C.W. Macosko, and A. Stein, *Unsaturated polyester resin toughening with very low loadings of GO derivatives.* Polymer, 2017. **110**: p. 149-157.

28. Li, T., S. He, A. Stein, L.F. Francis, and F.S. Bates, *Synergistic toughening of epoxy modified by graphene and block copolymer micelles.* Macromolecules, 2016. **49**(24): p. 9507-9520.

29. Rafiee, M.A., J. Rafiee, Z. Wang, H. Song, Z.-Z. Yu, and N. Koratkar, *Enhanced mechanical properties of nanocomposites at low graphene content.* ACS nano, 2009. **3**(12): p. 3884-3890.

30. Rafiee, M.A., J. Rafiee, I. Srivastava, Z. Wang, H. Song, Z.Z. Yu, and N. Koratkar, *Fracture and fatigue in graphene nanocomposites.* small, 2010. **6**(2): p. 179-183.

31. Zhang, M., H. Yan, X. Yang, and C. Liu, *Effect of functionalized graphene oxide with a hyperbranched cyclotriphosphazene polymer on mechanical and thermal properties of cyanate ester composites.* Rsc Advances, 2014. **4**(86): p. 45930-45938.

32. Ren, F., G. Zhu, P. Ren, Y. Wang, and X. Cui, *In situ polymerization of graphene oxide and cyanate ester–epoxy with enhanced mechanical and thermal properties.* Applied Surface Science, 2014. **316**: p. 549-557.

33. ASTM, I., *Standard test methods for flexural properties of unreinforced and reinforced plastics and electrical insulating materials.* ASTM D790-07, 2007.

34. ASTM, I., *Standared Test Method for Flexural Properties of Unreinforced and Reinforced Plastics and Electrical Insulating Materialas by Four-Point Bending, ASTM D6272-17*. March 2017.

35. ASTM, I., *Standard Test Method for Mode I Interlaminar Fracture Toughness of Unidirectional Fiber-Reinforced Polymer Matrix Composites. ASTM D 5528-01*. July 2008.

36. Zhu, J., A. Imam, R. Crane, K. Lozano, V.N. Khabashesku, and E.V. Barrera, *Processing a glass fiber reinforced vinyl ester composite with nanotube enhancement of interlaminar shear strength.* Composites Science and Technology, 2007. **67**(7-8): p. 1509-1517.

37. Pal, R., S.L. Goyal, and I. Rawal, *Lightweight graphene encapsulated with polyaniline for excellent electromagnetic shielding performance in X-band (8.2–12.4 GHz).* Materials Science and Engineering: B, 2021. **270**: p. 115227.

38. Upadhyay, J. and A. Kumar, *Structural, thermal and dielectric studies of polypyrrole nanotubes synthesized by reactive self degrade template method.* Materials Science and Engineering: B, 2013. **178**(15): p. 982-989.

39. Ng, H., N.M. Saidi, F.S. Omar, K. Ramesh, S. Ramesh, and S. Bashir, *Thermogravimetric analysis of polymers.* Encyclopedia of polymer science and technology, 2002: p. 1-29.

40. Wang, X., L. Song, H. Yang, W. Xing, B. Kandola, and Y. Hu, *Simultaneous reduction and surface functionalization of graphene oxide with POSS for reducing fire hazards in epoxy composites.* Journal of Materials Chemistry, 2012. **22**(41): p. 22037-22043.

41. Cao, Y., J. Feng, and P. Wu, *Preparation of organically dispersible graphene nanosheet powders through a lyophilization method and their poly (lactic acid) composites.* Carbon, 2010. **48**(13): p. 3834-3839.

42. Mishra, K., K.P. Bastola, R.P. Singh, and R. Vaidyanathan, *Effect of graphene oxide on the interlaminar fracture toughness of carbon fiber/epoxy composites.* Polymer Engineering & Science, 2019. **59**(6): p. 1199-1208.

43. Chan, M.-l., K.-t. Lau, T.-t. Wong, M.-p. Ho, and D. Hui, *Mechanism of reinforcement in a nanoclay/polymer composite.* Composites Part B: Engineering, 2011. **42**(6): p. 1708-1712.

44. Shettar, M., C.S. Kowshik, M. Manjunath, and P. Hiremath, *Experimental investigation on mechanical and wear properties of Nanoclay–epoxy composites.* Journal of Materials Research and Technology, 2020. **9**(4): p. 9108-9116.

45. Mishra, K., G. Pandey, and R.P. Singh, *Enhancing the mechanical properties of an epoxy resin using polyhedral oligomeric silsesquioxane (POSS) as nano-reinforcement.* Polymer Testing, 2017. **62**: p. 210-218.

46. Domun, N., H. Hadavinia, T. Zhang, T. Sainsbury, G. Liaghat, and S. Vahid, *Improving the fracture toughness and the strength of epoxy using nanomaterials–a review of the current status.* Nanoscale, 2015. **7**(23): p. 10294-10329.

47. Mishra, K., L.K. Babu, D. Dhakal, P. Lamichhane, and R.K. Vaidyanathan, *The effect of solvent on the mechanical properties of polyhedral oligomeric silsesquioxane (POSS)–epoxy nanocomposites.* SN Applied Sciences, 2019. **1**(8): p. 1-7.

48. Bilyeu, B., W. Brostow, and K.P. Menard, *Epoxy thermosets and their applications II. Thermal analysis.* Journal of Materials Education, 2000. **22**(4/6): p. 107-130.

49. Zhao, R. and W. Luo, *Fracture surface analysis on nano-SiO2/epoxy composite.* Materials Science and Engineering: A, 2008. **483**: p. 313-315.

50. Liu, K., S. He, Y. Qian, Q. An, A. Stein, and C.W. Macosko, *Nanoparticles in glass fiber-reinforced polyester composites: comparing toughening effects of modified graphene oxide and core-shell rubber.* Polymer Composites, 2019. **40**(S2): p. E1512-E1524.

51. Zheng, N., Y. Huang, H.-Y. Liu, J. Gao, and Y.-W. Mai, *Improvement of interlaminar fracture toughness in carbon fiber/epoxy composites with carbon nanotubes/polysulfone interleaves.* Composites Science and Technology, 2017. **140**: p. 8-15.

52. Wicks, S.S., R.G. de Villoria, and B.L. Wardle, *Interlaminar and intralaminar reinforcement of composite laminates with aligned carbon nanotubes.* Composites Science and Technology, 2010. **70**(1): p. 20-28.

53. Arai, M., Y. Noro, K.-i. Sugimoto, and M. Endo, *Mode I and mode II interlaminar fracture toughness of CFRP laminates toughened by carbon nanofiber interlayer.* Composites Science and Technology, 2008. **68**(2): p. 516-525.

VITA

Dilli Ram Dhakal

Candidate for the Degree of

Doctor of Philosophy

Dissertation: SYNTHESIS AND CHARACTERIZATION OF NANOSIZED HYBRID POLYMER MODIFIER (HPM) FOR IMPROVED MECHANICAL AND THERMAL BEHAVIOUR OF COMPOSITES

Major Field: Materials Science and Engineering

Biographical:

Education:

Completed the requirements for the Doctor of Philosophy in Materials Science and Engineering at Oklahoma State University, Stillwater, Oklahoma in May, 2022.

Completed the requirements for the Master of Science in Materials Science and Engineering at Oklahoma State University, Stillwater, Oklahoma in 2018.

Completed the requirements for the Master of Science in Physics at Tribhuvan University, Kathmandu, Nepal in 2012.

Completed the requirements for the Bachelor of Science in Physics at Tribhuvan University, Kathmandu, Nepal in 2007.

Experience:
Graduate Research/Teaching assistant at Oklahoma State University- Aug 2019 to Present.

R&D Quality Engineer at MITO Material Solutions – May 2018 to Aug 2019

Graduate Research/Teaching assistant at Oklahoma State University – Aug 2016 to May 2018

Professional Memberships:
Society for the Advancement of Material and Process Engineering (SAMPE).